Volume 22
Number 38
14 October 2020
Pages 21553–22118

PCCP

Physical Chemistry Chemical Physics

rsc.li/pccp

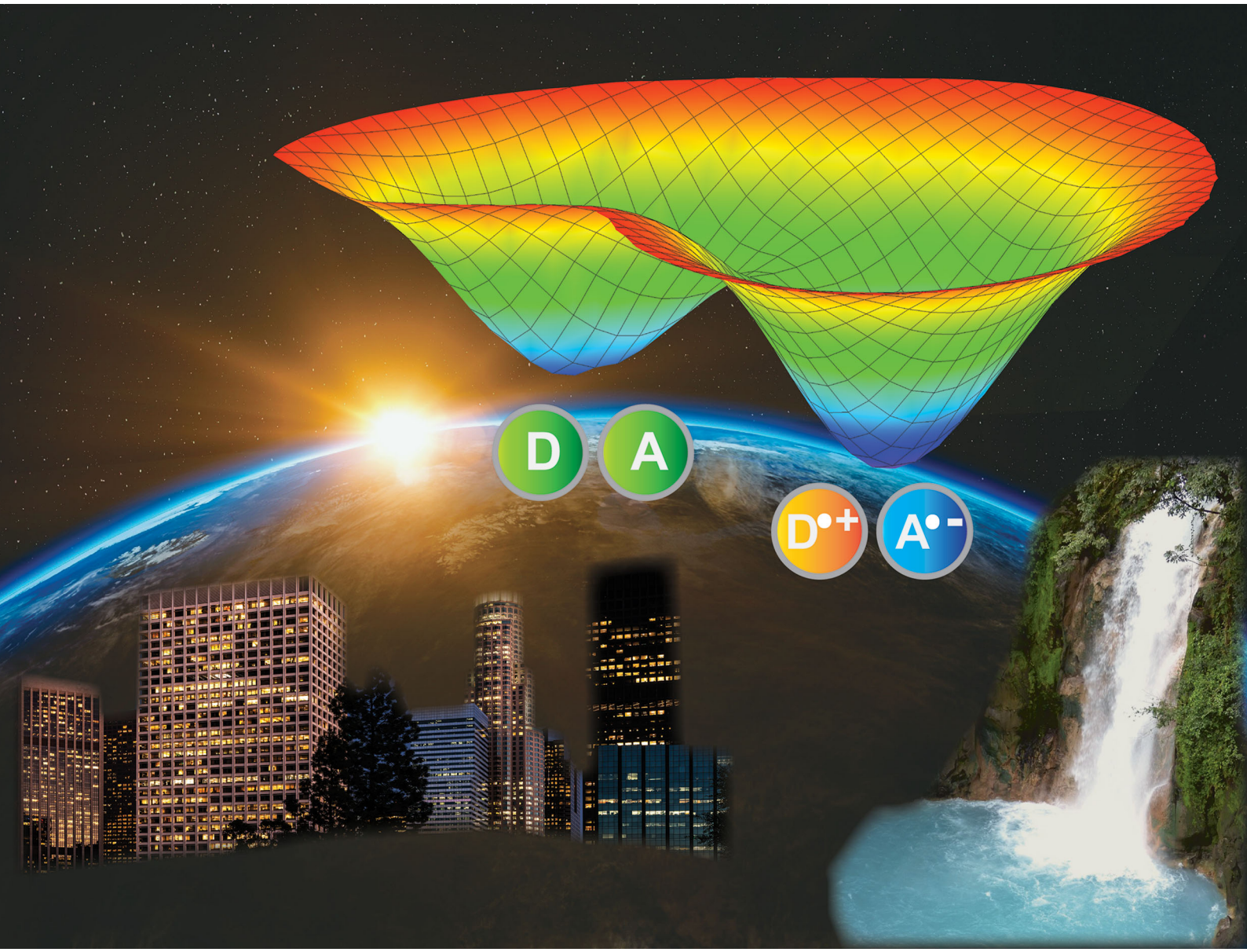

ISSN 1463-9076

ROYAL SOCIETY OF CHEMISTRY

PERSPECTIVE
Valentine I. Vullev *et al.*
Multifaceted aspects of charge transfer

PCCP

ROYAL SOCIETY OF CHEMISTRY

PERSPECTIVE

View Article Online
View Journal | View Issue

Cite this: *Phys. Chem. Chem. Phys.*, 2020, **22**, 21583

Multifaceted aspects of charge transfer

James B. Derr, [a] Jesse Tamayo, [b] John A. Clark, [c] Maryann Morales, [b] Maximillian F. Mayther, [b] Eli M. Espinoza, †[b] Katarzyna Rybicka-Jasińska [c] and Valentine I. Vullev *[abcd]

Charge transfer and charge transport are by far among the most important processes for sustaining life on Earth and for making our modern ways of living possible. Involving multiple electron-transfer steps, photosynthesis and cellular respiration have been principally responsible for managing the energy flow in the biosphere of our planet since the Great Oxygen Event. It is impossible to imagine living organisms without charge transport mediated by ion channels, or electron and proton transfer mediated by redox enzymes. Concurrently, transfer and transport of electrons and holes drive the functionalities of electronic and photonic devices that are intricate for our lives. While fueling advances in engineering, charge-transfer science has established itself as an important independent field, originating from physical chemistry and chemical physics, focusing on paradigms from biology, and gaining momentum from solar-energy research. Here, we review the fundamental concepts of charge transfer, and outline its core role in a broad range of unrelated fields, such as medicine, environmental science, catalysis, electronics and photonics. The ubiquitous nature of dipoles, for example, sets demands on deepening the understanding of how localized electric fields affect charge transfer. Charge-transfer electrets, thus, prove important for advancing the field and for interfacing fundamental science with engineering. Synergy between the vastly different aspects of charge-transfer science sets the stage for the broad global impacts that the advances in this field have.

Received 22nd March 2020,
Accepted 31st July 2020

DOI: 10.1039/d0cp01556c

rsc.li/pccp

[a] *Department of Biochemistry, University of California, Riverside, CA 92521, USA. E-mail: vullev@ucr.edu*
[b] *Department of Chemistry, University of California, Riverside, CA 92521, USA*
[c] *Department of Bioengineering, University of California, Riverside, CA 92521, USA*
[d] *Materials Science and Engineering Program, University of California, Riverside, CA 92521, USA*
† Present address: College of Bioengineering, University of California, Berkeley, CA 94720, USA.

Introduction

This article introduces the fundamental concepts of charge transfer (CT) and charge transport (CTr) in a tutorial style with historic perspectives. This foundation sets the paradigms for understanding and appreciating the common trends in the diverse sets of examples that follow from biology, medicine,

James B. Derr

James Derr is a Biochemistry graduate student at the University of California, Riverside in the group of Prof. V. Vullev. He grew up outside of Philadelphia and attended West Chester University for his BS degree, where as an undergraduate he triple-majored in Biochemistry, Chemistry and Biology. His research focuses on the design and synthesis of bioinspired molecular electrets for emerging charge-transfer phenomena, important for energy science and engineering.

Jesse Tamayo

Jesse Tamayo is a Chemistry graduate student at the University of California, Riverside (UCR), in the group of Prof. V. Vullev. He received his BS degree in Chemistry from the University of California, Davis, in 2015. His research on interfacial charge transfer focuses on the surface chemistry and photophysics of metal-halide perovskites. As a graduate student at UCR, Mr Tamayo was awarded an NSF GRFP Fellowship for his research in nanophotonics.

environmental science, electrosynthesis, photocatalysis, and electronics. CT and CTr make energy conversion, signal transduction and chemical transformations possible. It is no wonder why CT is in at the very core of natural life and modern technologies.

Why is movement of charges so important? Why has life evolved to depend on CT and electric interactions? Why is it impossible to imagine modern technologies without CT? Electromagnetism emerges from the second strongest of the four fundamental forces in the universe. Unlike the strong force, *i.e.*, the strongest of the fundamental forces, electric interactions do not have subatomic distance limitations. Conversely, the gravitational force, which is also long range, is too weak for the masses pertinent for biology and chemistry. Overall, the electric force dominates within the practical dimensions of our everyday lives. The ranges of its effects exceed the short nuclear scales of the strong and weak forces, but they are not deterministic at planetary and galactic distances where gravity dominates by bending space and time. The strength and the range of the electric force, therefore, make it the most important for molecular, nanoscale, cellular and even organism science and engineering.[1,2]

The electric force governs electrostatic and electrodynamic interactions. Magnetic forces are inherently weak, which is consistent with their relativistic origin from electrodynamics. Nevertheless, the impacts of electromagnetism on technology are incomparable. Concurrently, bioelectromagnetism emerges as an intricate component of medicinal physical sciences and bioengineering.[3,4] The importance of spin magnetic interactions not only in chemistry and physics, but also in biology and medicine, is undisputable.[5–8] Fundamentally, charges are

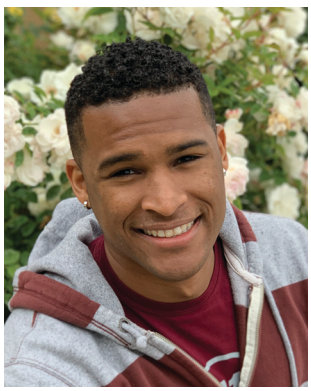

John A. Clark

John Clark is a Bioengineering graduate student at the University of California, Riverside (UCR), in the group of Prof. V. Vullev. He received his BS degree in Bioengineering also from UCR, where as an undergraduate, he was awarded an NSF-funded MYBEST fellowship that supports year-round research. He joined the group of Prof. Vullev to carry out research in biophotonics and microbiology. Currently as a graduate student, John is an AGEP Fellow, supported by NSF. His research interest include the design, synthesis, electrochemistry and photophysics of chromophores for biological and charge-transfer systems.

Maryann Morales

Maryann Morales graduated with BS in Chemistry from the University of California, Riverside (UCR). As Freshman, she joined the group of Prof. V. Vullev as a researcher to work on photo-induced charge transfer and biomedical photophysics. As an undergraduate at UCR, she was awarded an NIH-funded MARC U Star Fellowship for two consecutive years. In 2018, Ms Morales was awarded a Deutscher Akademischer Austauschdienst (DAAD) Fellowship that allowed her to carry out medicinal chemistry research at the Helmholtz Zentrum Dresden Rossendorf. In the Autumn of 2020, she starts her doctoral studies in Chemistry at the California Institute of Technology.

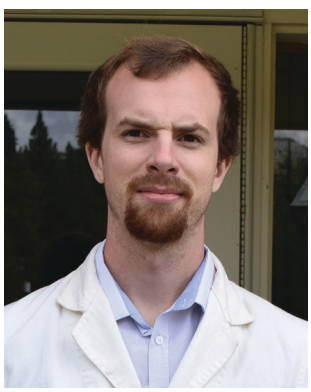

Maximillian F. Mayther

Maximillian Mayther is a Chemistry graduate student at the University of California, Riverside (UCR), in the group of Prof. V. Vullev. He received his BS from Pacific Lutheran University in 2015. His research focuses on the design and synthesis of non-native amino acid for mediating long-range charge transfer, and on emerging Stark effects from localized electric fields.

Eli M. Espinoza

Dr Eli Espinoza is a postdoctoral scholar in Bioengineering at the University of California, Berkeley, in the group of Prof. Niren Murthy, where his research focuses on enzyme-activated probes for point-of-care diagnostics. He received Bachelor's degree in Chemistry from Azusa Pacific University, and was awarded an NIH MORE grant from the California State University, Los Angeles, where he pursued Master's research in the group of Prof. Feimeng Zhou. For his doctoral work in Chemistry, he joined the group of Prof. Valentine Vullev at the University of California, Riverside, where his research was on electron-deficient photosensitizers and on dipole-modulated charge transfer.

the centrepieces of electric interactions. Electric fields, which are the carrier of such interactions, originate and terminate at charged species. Therefore, the diverse forms of transfer and transport of charges are vital for us and for our environment.

Electric fields strongly affect CT. Localized fields originating from electric dipoles are short in range but inherently strong. Therefore, dipole effects on CT are enormous, especially when low-polarity media minimize the screening of the fields.[2,9,10] Despite the nanometer range of these effects, they can prove deterministic for emerging properties of materials and devices at large scales.

Since the last universal common ancestor, transmembrane proton transport and pH gradients are conserved for energy conversion and storage.[11,12] Concurrently, this paradigm from biology, yielding some hints about the origin of life,[11] gives ways to using ion gradients for storing energy. In this respect, lithium-ion batteries represent one of the most impactful examples as acknowledged by the 2019 Nobel Prize in Chemistry.[13] Ion transport drives the propagation of action potentials responsible for the functionality of biological neural circuits.[14] Similarly, electron transport in electronic and photonic devices makes information exchange and storage possible.[15,16] By driving photoinduced charge separation followed by multiple electron-transfer steps, solar light is the main energy source that makes life on Earth possible. The advent of photosynthesis has marginalized the contributions of geothermal to the energy intake of our biosphere.[17–23] While fossil fuels are photosynthetic products,[24] photovoltaics and photoredox catalysis (also driven by photoinduced charge transfer) provide roads to adopting natural paradigms for meeting the global energy-consumption demands of our civilization.[25,26] Conversely, charge transfer in cellular respiration, similar to fuel cells, provides a means for extracting energy stored in the form of covalent bonds.[27–34]

The multifaceted aspects of CT and CTr make life on Earth and the modern human civilization possible. Thus, after introducing the fundamental concepts of the various forms of CT, we present key examples not only of CT and CTr in biology and Earth sciences, but also of their impacts on medicine. Beyond their importance for energy science and technology, preparative electrochemistry and photoredox catalysis illustrate the intricate importance of CT for chemical synthesis. Discussing the same processes in electronics and photonics reveals their broad importance. Understanding the ubiquity of CT and CTr in living and manmade systems advances CT science and transforms energy, materials and device engineering.

Fundamental concepts

Thermodynamic considerations

CT represents a transition between two states with distinctly different spatial distribution of their charged particles, such as electrons and protons. For example, electron transfer (ET) involves the move of n electrons from a donor, D, with an initial charge x, to an acceptor, A, with an initial charge y:

$$[D^{x}\cdots A^{y}] \rightarrow [D^{x+n}\cdots A^{y-n}]\ (ET) \qquad (1a)$$

For thermodynamic feasibility of ET, the reduction potential of D^{x+n} should be more negative than the reduction potential of A^{y}, *i.e.*, $E^{(0)}_{D^{x+n}|D^{x}} < E^{(0)}_{A^{y}|A^{y-n}}$, when estimated for the same solvent medium. It ensures that the energy level of the highest occupied molecular orbital (HOMO) of the donor is above that of the lowest unoccupied molecular orbital (LUMO) of the acceptor (Fig. 1a). Such an arrangement of the orbital energy levels proves favourable driving force, $-\Delta G^{(0)}_{ET}$, for ET in medium with dielectric constant ε:[35,36]

$$\Delta G^{(0)}_{ET}(\varepsilon) = F\left(E^{(0)}_{D^{x+n}|D^{x}}(\varepsilon_D) - E^{(0)}_{A^{y}|A^{y-n}}(\varepsilon_A)\right) + \Delta G_S + W \qquad (1b)$$

where F is the Faraday constant; ε_D and ε_A are the dielectric constants of the media used for determining the reduction

Katarzyna Rybicka-Jasińska

Dr Katarzyna Rybicka-Jasińska was born in Konin, Poland. She joined the research group of Prof. D. Gryko in 2012. In 2014, she graduated from the Warsaw University with Masters in Chemistry. She obtained a PhD from the Institute of Organic Chemistry of the Polish Academy of Sciences in 2018, under supervision of Prof. D. Gryko. Currently she is a postdoctoral scholar in the group of Prof. V. Vullev at the University of California, Riverside. Her research interests include photoredox catalysis in organic chemistry and photochemistry.

Valentine I. Vullev

Dr Valentine Vullev is a professor of bioengineering, chemistry, biochemistry and materials science and engineering at the University of California, Riverside (UCR). He grew up in Bulgaria and moved to the USA for his higher education. Dr Vullev obtained his PhD in Chemistry from Boston University (advisor: Prof. Guilford Jones). After completing his postdoctoral work at Harvard University in the group of Prof. George Whitesides, he moved to UCR where he built a research program in charge transfer, molecular photonics and biological inspiration. For his work on dipole-modulated charge transfer, he developed the concept of molecular electrets. In 2018–2019, Prof. Vullev was a Fulbright US Scholar at the Universidade de São Paulo, São Paulo, Brazil.

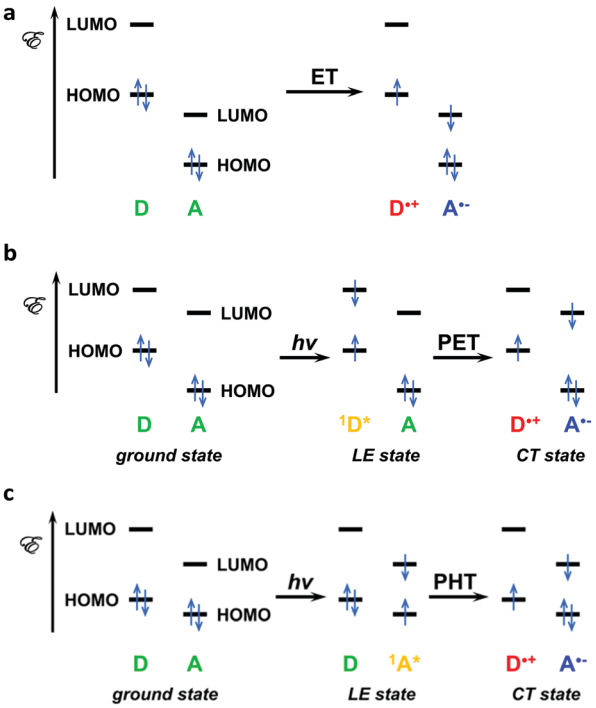

Fig. 1 Molecular-orbital (MO) diagrams depicting examples of: (a) ground-state electron transfer, ET; (b) photoinduced electron transfer, PET; and (c) photoinduced hole transfer, PHT. In these examples, PET and PHT show a transition through locally excited, LE, states. A strong coupling between the ground and the CT states allows for direct photo excitation into the latter. Such MO diagrams provide excellent conceptual representation about the manner in which the electrons move between the orbitals during the various processes. Nevertheless, the depicted assumption that the energy level of each of the orbitals does not change as the electron donor, D, and acceptor, A, transition between their singlet and doublet states is a rough approximation at best. Furthermore, MO diagrams do not capture the dependence of the energies of the various states on (1) the solvating media and (2) permanent dipoles. State and Jabłoński diagrams address this issue.

potentials of the donor and the acceptor, respectively. ΔG_S is the born solvation energy, accounting for electrostatic interactions of the donor and the acceptor with the solvent media, and W is the coulombic work term, accounting for the electrostatic interactions between the donor and the acceptor:[35,36]

$$W = \frac{n(y-x-n)q_e^2}{4\pi\varepsilon_0\varepsilon R_{DA}} \quad (1c)$$

where q_e is the elementary electron charge, ε_0 is the electric permittivity of vacuum, and R_{DA} is the centre-to-centre donor–acceptor distance.

Considering the polarity dependence of the reduction potentials, ΔG_S corrects $E^{(0)}_{D^{x+n}|D^x}(\varepsilon_D)$ and $E^{(0)}_{A^y|A^{y-n}}(\varepsilon_A)$ to values they would assume for a solvent with a dielectric constant ε:[35]

$$E^{(0)}_{D^{x+n}|D^x}(\varepsilon) = E^{(0)}_{D^{x+n}|D^x}(\varepsilon_D) + \frac{nq_e^2(2x+n)}{8\pi\varepsilon_0 F r_D}\left(\frac{1}{\varepsilon}-\frac{1}{\varepsilon_D}\right) \quad (1d)$$

$$E^{(0)}_{A^y|A^{y-n}}(\varepsilon) = E^{(0)}_{A^y|A^{y-n}}(\varepsilon_A) + \frac{nq_e^2(2y-n)}{8\pi\varepsilon_0 F r_A}\left(\frac{1}{\varepsilon}-\frac{1}{\varepsilon_D}\right) \quad (1e)$$

$$\Delta G_S = \frac{nq_e^2}{8\pi\varepsilon_0}\left(\frac{2x+n}{r_D}\left(\frac{1}{\varepsilon}-\frac{1}{\varepsilon_D}\right) - \frac{2y-n}{r_A}\left(\frac{1}{\varepsilon}-\frac{1}{\varepsilon_A}\right)\right) \quad (1f)$$

where r_D and r_A are the radii of the donor and the acceptor, respectively, which, along with ε_D and ε_A tend to present challenges in implementing this formalism.

Because the media for electrochemical measurements require large concentrations of supporting electrolyte, ε_D and ε_A are not always straightforward to estimate. They differ from the dielectric constants of the neat solvents, $\varepsilon_D^{(0)}$ and $\varepsilon_A^{(0)}$.[35,37] Furthermore, possible ion pairing between the electrolyte and the components of the redox couples can result in misleading estimates of the potentials and the ET driving forces.[38] Pulse radiolysis provides a means for estimating the reduction potentials for media that do not contain electrolyte.[38–41]

Pulse radiolysis is a time-resolved technique where MeV electron pulses ionize the sample, predominantly the solvent, saturating it with strongly reducing and oxidizing species, such as solvated electrons and radical cations.[42] The solution composition controls whether the electron pulses generate oxidizing or reducing environment. This ionized environment transfers electrons or holes to the dissolved sample. The low concentration of the sample ensures that it is not the main absorber of the ionization energy from the electron pulses.

Optical detection allows for monitoring the fate of the holes and the electrons on the sample molecules. Roughly, pulse radiolysis is like transient absorption spectroscopy, but employs fast ionization, rather than optical excitation, to initiate CT processes. Similar to laser-flash photolysis,[43] monitoring the changes in the intensity of continuous-wave probe light, transmitted through the ionized sample, allows for attaining nanosecond resolution.[42] Analogously to pump–probe transient-absorption spectroscopy,[44] pulse-probe radiolysis, synchronizing picosecond electron pulses and femtosecond laser probes, pushes the resolution to the low picosecond time domain.[42,45] Unlike optical excitation, ionizing pulse places only an electron or a hole on the sample molecule and allow for monitoring its transfer without interferences from the countercharge. This feature makes pulse radiolysis indispensable for CT mechanistic studies and for probing redox properties of a wide range of samples.[38,45,46]

Despite its power as a tool for mechanistic studies, the prohibitive cost of pulse-radiolysis equipment prevents its broad use. Conversely, recording the dependence of the reduction potentials on the electrolyte concentration, C_{el}, offers a feasibly facile alternative.[35,37] Extrapolation to $C_{el} = 0$ provides the values of the reduction potentials for the neat solvent media with well characterized dielectric constants, $\varepsilon_D^{(0)}$ and $\varepsilon_A^{(0)}$. Such extrapolated $E^{(0)}$ values are convenient for reliable implementation in eqn (1b) and (1f).[47–52] Most ion-pairing dissociation constants are in the mM ranges. Thus, using sub-mM sample concentrations aids decreasing, and even eliminating, the effects of ion pairing on the estimations of the potentials for neat solvents.[53]

Most formalisms for estimating medium effects assume spherical solvation cavities. Many of the molecular electron donors and acceptors, however, do not have spherical shapes. What is the physical meaning of r_D and r_A for such redox

moieties? In CT analysis, the somewhat "soft" interpretation of r_D and r_A still raises questions. Computationally, the van der Waals radii represent radii of spheres in which the analyzed molecule species can fit. Such van der Waals radii, however, can significantly overestimate r_D and r_A when molecular shapes deviate from spherical symmetry.[37] Quite frequently, the treatment involves approximating the shapes of the redox moieties to ellipsoids, and estimating r_D and r_A as half of the averages of the three ellipsoid axes. Extension of solvation theories to non-spherical shapes, however, does not reveal a real physical base for such estimates of the radii, especially when the charge density is not equally distributed throughout the solute.[37] Conversely, generalized Born radii take into account the spatial distribution of the partial charges in redox species. They provide good estimates for r_D and r_A that are implementable in CT analysis.[37]

Resorting to experimentally obtained values, hydrodynamic radii can sometime serve as estimates for r_D and r_A.[35] When it comes to CT systems, electrochemical analysis can provide some of the most pertinent evaluations for r_D and r_A. A two-dimensional analysis for a redox moiety involves:[53] (1) recording its reduction potentials for electrolyte solutions in different solvents at different C_{el}; (2) extrapolating to $C_{el} = 0$ for each solvent; (3) estimating r_D and r_A from linear fits of the extrapolated reduction potentials *vs.* $1/\varepsilon^{(0)}$; and (4) extrapolating values of the reduction potentials for media with different polarities from the same dependence on $1/\varepsilon$.[47,48] Estimating the reduction potentials for the medium with a dielectric constant of interest, *i.e.*, $\varepsilon_D = \varepsilon_A = \varepsilon$, as outlined in (4), eliminates the need for the ΔG_S term in eqn (1b).

This thermodynamic analysis focuses on changes in the charges of the donor and the acceptor during ET, and therefore employs the Born solvation energy. The oxidation of the donor and the reduction of the acceptor, however, can also cause changes in their electric dipole moments.[9] Inherently, the Born formalism cannot quantify the alterations of the solvation energies originating from such dipole changes in the donor and the acceptor. While the contributions of dipole changes to the magnitudes of the reduction potentials tend to be minor, they can have significant effects on evaluating small CT driving forces. Adding an Onsager term (or higher multipole terms) in eqn (1b) can address this issue.

Based on the Born solvation energy, ΔG_q, the ΔG_S term in eqn (1b) accounts for the differences in the contributions to the driving force, $-\Delta G^{(0)}_{CT}$, from the changes in the charges of the donor and the acceptor during CT in different solvent environment. Basically, ΔG_q depicts the energy gained when transferring an ion, with charge q and radius r, from vacuum to medium with dielectric constant ε, *i.e.*, $\Delta G_q \propto -((\varepsilon - 1)/\varepsilon)(q^2/r)$.[54] Taking it a step further, Onsager solvation energy, $\Delta G_{\boldsymbol{\mu}}$, accounts for the medium stabilization of an electric dipole, $\boldsymbol{\mu}$: $\Delta G_{\boldsymbol{\mu}} \propto -((\varepsilon - 1)/(2\varepsilon + 1))(|\boldsymbol{\mu}|^2/r^3)$.[55] Expanding the expressions for ΔG_q and $\Delta G_{\boldsymbol{\mu}}$ provides a means for estimating the solvation energy of any multipole, $\mathbf{Q}^{(i)}$, where i is the order of the tensor describing it. That is, charge is a scalar, *i.e.*, a tensor with order 0, $q = \mathbf{Q}^{(0)}$, and dipole is a vector, *i.e.*, $\boldsymbol{\mu} = \mathbf{Q}^{(1)}$, The tensors with orders 2, 3, and 4 describe quadrupoles, octupoles, and hexadecapoles with solvation energies, $\Delta G_{\mathbf{Q}(i)} \propto -((\varepsilon - 1)/((i + 1)\varepsilon + i))(|\mathbf{Q}^{(i)}|^2/r^{(2i+1)})$.[56] Assuming linear solvent response to the perturbations from the charge distributions in the solute, this Born–Kirkwood–Onsager formalism provides estimates of the total solvation energy of any species by adding the contributions from the solvation of its charge and multipoles, *i.e.*, $\sum_i \Delta G_{\mathbf{Q}(i)}$.[54–58]

When the oxidation of the donor and the reduction of the acceptor alters not only their charges, but also their multipoles, the expression for the ΔG_S term in eqn (1b) warrants modification to include all pertinent $\Delta G_{\mathbf{Q}(i)}$, rather than only ΔG_q. Defining the dipole moment of a charged species and quadrupole of a dipolar one warrants caution. Multipole expansions around the centres of mass shows the CT-induced changes in the electrostatic characteristics of the donor and the acceptor.[9] For most organic molecules, including the solvation energies that account for CT-induced changes in charge and dipole usually suffices. An increase in the symmetry of the donor or the acceptor, however, may warrant considerations of CT-induced changes of higher multipole terms.

When the energy level of the HOMO of the donor lies between the HOMO and the LUMO of the acceptor, *i.e.*, $E^{(0)}_{D^{x+n}|D^x} > E^{(0)}_{A^y|A^{y-n}}$, and the LUMO or the donor is above the LUMO of the acceptor, ET is thermodynamically unfeasible. Conversely, photoexcitation of the donor to its locally excited (LE) electronic state can provide the energy for driving this "uphill" ET. In such photoinduced electron transfer (PET), placing an electron on the LUMO of the donor makes its transfer to the LUMO of the acceptor energetically feasible (Fig. 1b):[35,36]

$$[D^x\cdots A^y] \rightarrow [D^{x*}\cdots A^y] \rightarrow [D^{x+1}\cdots A^{y-1}]\ (\text{PET}) \quad (2a)$$

$$\Delta G^{(0)}_{PET}(\varepsilon) = F\left(E^{(0)}_{D^{x+1}|D^x}(\varepsilon_D) - E^{(0)}_{A^y|A^{y-1}}(\varepsilon_A)\right) - \mathscr{E}_{00}(D) + \Delta G_S + W \quad (2b)$$

where $\mathscr{E}_{00}(D)$ is the zero-to-zero energy difference between the ground and the LE state of the donor from which PET occurs.

Photoexcitation of the acceptor can also provide the energy for ET. In this case, however, an electron from the HOMO of the donor moves to the singly-occupied "HOMO" of the photoexcited acceptor. Analogous to solid-state physics and electronics, this process of electron transfer between HOMOs represents a hole transfer (HT) from the electron acceptor to the electron donor. The driving force of this photoinduced hole transfer (PHT) depends the zero-to-zero energy of the acceptor, $\mathscr{E}_{00}(A)$ (Fig. 1c):[35,36]

$$[D^x\cdots A^y] \rightarrow [D^x\cdots A^{y*}] \rightarrow [D^{x+1}\cdots A^{y-1}]\ (\text{PHT}) \quad (2c)$$

$$\Delta G^{(0)}_{PHT}(\varepsilon) = F\left(E^{(0)}_{D^{x+1}|D^x}(\varepsilon_D) - E^{(0)}_{A^y|A^{y-1}}(\varepsilon_A)\right) - \mathscr{E}_{00}(A) + \Delta G_S + W \quad (2d)$$

For experimental feasibility, the reduction potentials of the donor and the acceptor must be well within the electrochemical windows of the media used for their determination. That is, the solvent and the supporting electrolyte should not undergo CT interactions with the components of the redox couples of the donor and the acceptor. Photoexcitation of the donor, however,

makes it a strong reductant and the photoexcitation of the acceptor – a strong oxidant. Thus, the excited-state reduction potentials can be well outside of the electrochemical windows of the media. It makes PET from the donor to the solvent, or PHT from the acceptor to the solvent, thermodynamically feasible. Solvent-induced emission quenching (that do not follow polarity or viscosity trends) can be an indication for such photoinduced charge transfer (PCT) with the media.[59–61] An examination using eqn (2b) and (2d) can aid avoiding solvents for which $\Delta G^{(0)}_{PCT}$ with the donor or the acceptor is negative.

While selective excitation of the donor or the acceptor leads to PET or PHT, respectively, efficient Förster or other resonance energy transfer (EnT) can ensure that one of these processes dominates the CT pathways:[62–64]

$$[D^{x}\cdots A^{y}] \rightarrow [D^{x}\cdots A^{y*}] \rightarrow [D^{x*}\cdots A^{y}] \rightarrow [D^{x+1}\cdots A^{y-1}] \quad (\mathscr{E}_{00}(D) < \mathscr{E}_{00}(A), \text{EnT}-\text{PET}) \tag{3a}$$

$$[D^{x}\cdots A^{y}] \rightarrow [D^{x*}\cdots A^{y}] \rightarrow [D^{x}\cdots A^{y*}] \rightarrow [D^{x+1}\cdots A^{y-1}] \quad (\mathscr{E}_{00}(D) > \mathscr{E}_{00}(A), \text{EnT}-\text{PET}) \tag{3b}$$

When the LUMO of the donor lies above the LUMO of the acceptor, while the HOMO of the donor is below the HOMO of the acceptor, photoexcitation of the donor allows for ET from its LUMO to the LUMO of the acceptor with concurrent HT from its HOMO to the HOMO of the acceptor. This bidirectional ET leads to transferring of the excitation energy of the donor to the acceptor and illustrates electron-exchange, or Dexter, EnT.[63] Such electron-exchange EnT is crucial for energy upconversion and optical imaging.[65–73]

These thermodynamic considerations are readily applicable to other CT processes, such as proton transfer (PT). In addition, consideration of the Fermi levels, ionization energies, electron affinities and optical band gaps of solid materials, allows for expanding this formalism (eqn (1)–(3)) to heterogeneous CT processes, which demonstrates the broad utility of this analysis.

Kinetic considerations

An electronic coupling between a donor and an acceptor is necessary for CT between them to occur, regardless if they are components of the same molecule or physically separated from each other. Even if a donor and an acceptor are not in van der Waals contact with each other, an overlap between the evanescent components of the wavefunctions of their frontier orbitals is essential for ET between them to occur. Such diabatic ET between weakly coupled moieties, involves quantum tunnelling of electrons and represents most CT processes in biological and organic systems. Frequently used as its double negative "nonadiabatic," the term "diabatic" originates from the Geek word for "passable,"διαβατος. It refers to a behaviour of moving back and forth along the potential-energy surface of initial state, i, and passing over the transition state without transferring to a final state, f (Fig. 2a). In adiabatic CT, on the other hand, strong donor–acceptor electronic coupling leads to mixing of i and f that splits the potential-energy surfaces enough to prevent such passing over. It makes the transition from i to f a highly probable outcome (Fig. 2b).

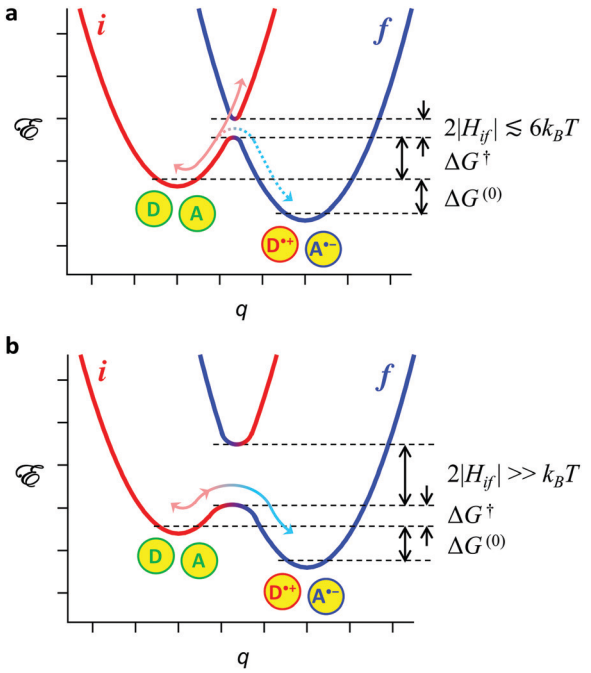

Fig. 2 State diagrams, *i.e.*, energy, $\mathscr{E}$, *vs.* generalized coordinates, *q*, of (a) diabatic and (b) adiabatic electron transfer, depicting transitions between an initial, i, ground state and a final, f, charge-transfer state.

Fermi's Second Golden Rule, originating from Dirac's work, provides a good description for the kinetics of such diabatic CT. As the Born–Oppenheimer approximation implements, this kinetic expression separates the electronic from the nuclear, or Franck–Condon (FC), contribution to the rate constant:

$$k_{ET} = \frac{2\pi}{\hbar}|H_{if}|^2\rho(h\nu_f) \tag{4a}$$

where the inverse of the Planck's constant, $2\pi/\hbar$, represents the fundamental frequency, H_{if} embodies the electronic coupling between the donor and the acceptor, H_{DA}, and the density of vibrational states, $\rho(h\nu_f)$, at energy $h\nu_f$ of the final electronic state represents the FC contribution to the kinetics.

The rate constants of tunnelling fall off exponentially with the lengths of the potential barriers and with the square roots of their heights. For diabatic processes, therefore, considering the edge-to-edge distance between the donor and the acceptor along the CT pathways, r_{DA}, and introducing an empirical parameter, β, accounting for the nature of the tunnelling medium, provides a broadly used means for fast CT analysis:

$$|H_{if}|^2 \approx |H_{DA}(r_{DA} = 0)|^2 \exp(-\beta r_{DA}) \tag{4b}$$

where $H_{AD}(r_{DA} = 0)$ represents the electronic coupling when the donor and the acceptor are in direct contact with each other. The parameter β depends on the CT media between donor and the acceptor. The dependence of CT rates on r_{DA} provide a means for computational or experimental estimations of β.

Employing electronic states described by symmetric parabolic potentials and implementing Gaussian distribution of low-frequency vibrational modes, Marcus transition state

theory provides an excellent and broadly used description of the FC contributions to the CT rate constants:[74–78]

$$\rho(h\nu_f) = \frac{\exp\left(-\frac{\Delta G^\dagger}{k_B T}\right)}{\sqrt{4\pi\lambda k_B T}} \quad (4c)$$

where the transition-state (or activation) energy, $\Delta G^\dagger$, can be expressed in terms of the thermodynamic CT driving force (eqn (1b), (2b) and (2d)) and the reorganization energy, λ:[74–80]

$$\Delta G^\dagger = \frac{\left(\Delta G_{CT}^{(0)} + \lambda\right)^2}{4\lambda} \quad (4d)$$

Overall, λ represents the energy needed for rearranging ions and dipoles to compensate for the changes of the electric fields around the donor and the acceptor during the CT step. Specifically, λ encompasses the energy for reorganizing (1) the solvent media, λ_m, *i.e.*, outer reorganization energy, and (2) the molecular structures of the donor and the acceptor, λ_ν, *i.e.*, inner reorganization energy:

$$\lambda = \lambda_m + \lambda_\nu \quad (5a)$$

The spring constants of the initial and final states, $k^{(i)}$ and $k^{(f)}$, respectively, of the vibrational and bending modes important for the CT process, and the change in the general coordinates, q, along those modes, provide estimates for the inner reorganization energy:

$$\lambda_\nu = \sum_j \frac{k_j^{(i)} k_j^{(f)}}{k_j^{(i)} + k_j^{(f)}} \left(q_j^{(f)} - q_j^{(i)}\right)^2 \quad (5b)$$

Conversely, Born model, encompassing the solvation energy originating from the orientational, $\mathbf{P_\mu}$, and nuclear, $\mathbf{P}_\nu$, polarization of the media, *i.e.*, the Pekar factor $\gamma = (n_m^{-2} - \varepsilon_m^{-1})$,[81] can describe λ_m in terms of the optical refractive index, n_m, and the static dielectric constant, ε_m, of the solvent. For transferring n electron charges from the donor to the acceptor or between solid surface and a redox moiety with radius, r_R, therefore, the expressions for λ_m are:[74,76,77]

$$\lambda_m = \frac{\gamma n^2 q_e^2}{4\pi\varepsilon_0}\left(\frac{1}{2r_D} + \frac{1}{2r_A} - \frac{1}{R_{DA}}\right) \text{ homogeneous CT} \quad (5c)$$

$$\lambda_m = \frac{\gamma n^2 q_e^2}{8\pi\varepsilon_0}\left(\frac{1}{r_R} - \frac{1}{R_{R\text{-electrode}}}\right) \text{ heterogeneous CT} \quad (5d)$$

Marcus' work, based on statistical-mechanics approaches for the development of this theory,[74,76,77] was acknowledged by the 1992 Nobel Prize in Chemistry.[82] Employing quantum-mechanical tools on harmonic oscillators, Hush derived the same expression for rates of CT (eqn (4)), and broadened the applicability of the theory.[83,84] Concurrently, Levich and Dogonadze reported a quantum-mechanical formalism for diabatic CT that also shows quadratic expression for the transition-state energy.[85–90] Based on these developments, along with some earlier work, *e.g.*, from Kubo and Toyozawa,[91] combining eqn (4a)–(4d) encompasses the Marcus–Hush (MH) formalism for treating CT kinetics.[92]

Solvent dynamics, along with vibronic modes of the donor and the acceptor during the transfer through the transition state, can impact the CT kinetics leading to rates that deviate from what the MH formalism predicts under the continuous-dielectric approximation of the media. Recurrently observed femtosecond oscillation of the electron while moving away from the donor during coherent PCT appear crucially important for the operation of photovoltaic (PV) devices.[93,94]

Focusing on high-frequency vibrational modes, the work of Jortner reveals the importance of quantum-mechanical nuclear tunnelling that can be prevalent for processes with large driving forces, most often falling in the Marcus inverted region.[95,96] It led to the Marcus–Levich–Jortner (MLJ) formalism. A simplified expression, accounting for one of these high frequencies, ν_C—which also can represent an average of high frequencies—illustrates the MLJ approach:[97–102]

$$k_{ET} = \frac{2\pi}{\hbar}|H_{if}|^2 \frac{\exp\left(-\frac{\lambda_\nu}{h\nu_C}\right)}{\sqrt{4\pi\lambda_m k_B T}} \times \sum_{j=0}^{\infty} \frac{\left(\frac{\lambda_\nu}{h\nu_C}\right)^j}{j!} \exp\left(-\frac{\left(\Delta G_{CT}^{(0)} + \lambda_m + jh\nu_C\right)^2}{4\lambda_m k_B T}\right) \quad (6)$$

The MH and MLJ formalisms describe well diabatic processes that represent moving back and forth along the potential surface of the initial state and passing over the transition state, with low probability for transferring to the final state, *i.e.*, cases where $H_{if} \leq 3k_B T$ (Fig. 2a). Conversely, relatively large donor–acceptor electronic coupling considerably separates the bottom surfaces of the potential wells of the initial and the final states, from the upper ones (Fig. 2b). This separation precludes passing over the transition state without transferring to the final state. Eyring transition-state theory can provide classical description of such adiabatic CT processes:[103,104]

$$k_{ET} = \kappa \frac{k_B T}{h} \exp\left(-\frac{\Delta G^\dagger}{k_B T}\right) \quad (7)$$

where in this Eyring–Evans–Polanyi equation the transmission coefficient, κ, is set to unity for most cases, and the preexponential factor, *i.e.*, the natural frequency, is temperature dependent, which deviates from the Arrhenius model. Also, the transition-state energy, $\Delta G^\dagger$, is smaller than the estimates that the Marcus formalisms provides (eqn (4d) and (6)).

Multiple faces of charge transfer

When the donor and the acceptor are noncharged (*i.e.*, $x = y = 0$ in eqn (1a), (2a) and (2c)), CT leads to charge separation (CS) or photoinduced charge separation (PCS):[2]

$$[D\cdots A] \rightarrow [D^{\bullet+}\cdots A^{\bullet-}] \text{ (CS)} \quad (8a)$$

$$[D\cdots A] \rightarrow [D^{*}\cdots A] \rightarrow [D^{\bullet+}\cdots A^{\bullet-}] \text{ (PCS } \textit{via} \text{ PET)} \quad (8b)$$

$$[D\cdots A] \rightarrow [D\cdots A^{*}] \rightarrow [D^{\bullet+}\cdots A^{\bullet-}] \text{ (PCS } \textit{via} \text{ PHT)} \quad (8c)$$

where for one-electron CT, radicals form when the donor and the acceptor have closed-shell initial states.

CS also encompasses cases involving positively charged donors or negatively charged acceptors, *i.e.*, cases where CT leads to increases in the positive charges of the donor and the negative charges of the acceptor. Referred to as ''exciton dissociation'' in solid-state physics, PCS (eqn (8b) and (8c)) represents a crucially important step for solar-energy conversion in PVs and in photosynthesis. Transitions from photogenerated CS states back to the ground state undergoes *via* charge recombination (CR), which is often an undesired outcome:

$$[D^{\bullet+}\cdots A^{\bullet-}] \rightarrow [D\cdots A]\ (CR) \quad (8d)$$

When the donor is positively charged and the acceptor is negatively charged, CT eliminates charges from the donor and acceptor leading to charge annihilation (CA) or photoinduced charge annihilation (PCA):[2]

$$[D^{-}\cdots A^{+}] \rightarrow [D^{\bullet}\cdots A^{\bullet}]\ (CA) \quad (9a)$$

$$[D^{-}\cdots A^{+}] \rightarrow [(D^{-})^{*}\cdots A^{+}] \rightarrow [D^{\bullet}\cdots A^{\bullet}]\ (PCA\ \textit{via}\ PET) \quad (9b)$$

$$[D^{-}\cdots A^{+}] \rightarrow [D^{-}\cdots (A^{+})^{*}] \rightarrow [D^{\bullet}\cdots A^{\bullet}]\ (PCA\ \textit{via}\ PHT) \quad (9c)$$

Despite the resemblance between PCA and CR, they represent different processes. While CR leads from a CT state to a ground state, PCA involves the transition from a locally excited state to a CT state comprising a noncharged oxidized donor and a noncharged reduced acceptor.

Charge shift (CSh) and photoinduced charge shift (PCSh) represent another set of CT processes involving: (1) a negatively charged donor and a nonchanged acceptor, or (2) a noncharged donor and a positively charged acceptor. In the former case, CSh and PCSh lead to electron shift (ESh) and photoinduced electron shift (PESh) from the donor to the acceptor, while in the latter – to hole shift (HSh) and photoinduced hole shift (PHSh) from the acceptor to the donor:[105,106]

$$[D^{-}\cdots A] \rightarrow [D^{\bullet}\cdots A^{\bullet-}]\ (ESh) \quad (10a)$$

$$[D\cdots A^{+}] \rightarrow [D^{\bullet+}\cdots A^{\bullet}]\ (HSh) \quad (10b)$$

$$[D^{-}\cdots A] \rightarrow [(D^{-})^{*}\cdots A] \rightarrow [D^{\bullet}\cdots A^{\bullet-}]\ (PESh\ \textit{via}\ PET) \quad (10c)$$

$$[D^{-}\cdots A] \rightarrow [D^{-}\cdots A^{*}] \rightarrow [D^{\bullet}\cdots A^{\bullet-}]\ (PESh\ \textit{via}\ PHT) \quad (10d)$$

$$[D\cdots A^{+}] \rightarrow [D^{*}\cdots A^{+}] \rightarrow [D^{\bullet+}\cdots A^{\bullet}]\ (PHSh\ \textit{via}\ PET) \quad (10e)$$

$$[D\cdots A^{+}] \rightarrow [D\cdots (A^{+})^{*}] \rightarrow [D^{\bullet+}\cdots A^{\bullet}]\ (PHSh\ \textit{via}\ PHT) \quad (10f)$$

The strict requirement for electroneutrality poses a question on the true nature of the CSh processes. The definition of CSh focuses on the charges of the donor and the acceptor before and after CT. Charged species, however, cannot exist freely without counterions around them, especially when in nonpolar media. When the counterion is immobilized next to the charged donor or acceptor in rigid or viscous media, the rates of CSh can considerably exceed the rates of ion movement. In such a case, the shift of the negative charge from the donor to the acceptor (or of the positive charge from the acceptor to the donor) involves its separation from the counterion nearby. Therefore, such CSh processes represent cases of CS. Conversely, if the counter ion moves fast enough, the ion transfer (or ion transport) can couple with the ET (or HT) of the CSh step and conserve the overall neutrality of both the donor and the acceptor before and after the CT.

Pulse radiolysis provides some of the best means for studying CSh processes,[107–110] where (1) the dynamics of placing charges on donor–acceptor conjugates and dissipating the countercharges can be quite faster than the induced CSh processes; and (2) the distances between the charged donor–acceptor conjugates and potential countercharges can readily exceed the Onsager radii.

The CSh processes represent the discreet steps of charge hopping mechanisms, which govern long-range CT in biological systems, conducting polymers and overall in organic and bio-organic CT materials. The crucial importance of CSh with all its complexity, therefore, is undisputable.

While the examples in eqn (8)–(10) focus on single-electron processes, they can readily be extended to multielectron CT characterized with the same features.

''Anomalies'' originating from the Marcus transition-state theory

One of the most important outcomes of the Marcus theory is the quadratic expression for the activation energy (eqn (4d)) that challenged the established ways of thinking at the time. Because $\lambda > 0$ and $\Delta G^{(0)}_{CT} < 0$, the quadratic features in the expression for the transition-state energy (eqn (4d)) reveals an important trend that Marcus described in the 1950s.[74,76,77,111] Miller *et al.* experimentally proved it 30 years later,[112–114] and Wasielewski *et al.* also confirmed closely afterwards.[115]

Intuitively, increasing the thermodynamic driving force, *i.e.*, making $\Delta G^{(0)}_{CT}$ more negative, increases the rate of the reaction, k_{ET}, and it is exactly what eqn (4d) shows as long as $-\lambda < \Delta G^{(0)}_{CT} < 0$ (Fig. 3a). When $\Delta G^{(0)}_{CT} = -\lambda$, the reaction is activationless and its rate depends only on the donor–acceptor electronic coupling (Fig. 3b). As $\Delta G^{(0)}_{CT}$ becomes more negative than $-\lambda$, however, another activation-energy barrier builds up and the reaction slows down with an increase in $-\Delta G^{(0)}_{CT}$. This state configuration represents the Marcus inverted region for the relationship between the CT kinetics and thermodynamics (Fig. 3c).[111] Conversely, $-\lambda < \Delta G^{(0)}_{CT} < 0$ corresponds the Marcus normal region; and $\Delta G^{(0)}_{CT} = -\lambda$—the tip of the Marcus curves, where the FC contribution to the kinetics is negligible and processes are activationless (Fig. 3d).[111] An important feature that the quantum nuclear tunnelling introduces is diminishing the effects of the driving force on the rates in the deep inverted region, as revealed with the implementation of the MLJ formalism (Fig. 3d).

In a classical sense, a counterintuitive feature of the inverted region is the ''sudden'' change of the direction of the reaction. That is, the initial state must move along the generalized reaction coordinates away from the equilibrium minimum of the final state to get to the transition state (Fig. 3c). After the transition, the system moves back along the final state beyond the coordinates of the starting point. Nevertheless, the most prevalent examples of the inverted region involve the movement of small particles, such as electrons, and not of heavy substituents as in S_N2 reactions. Also, this representation is oversimplified and

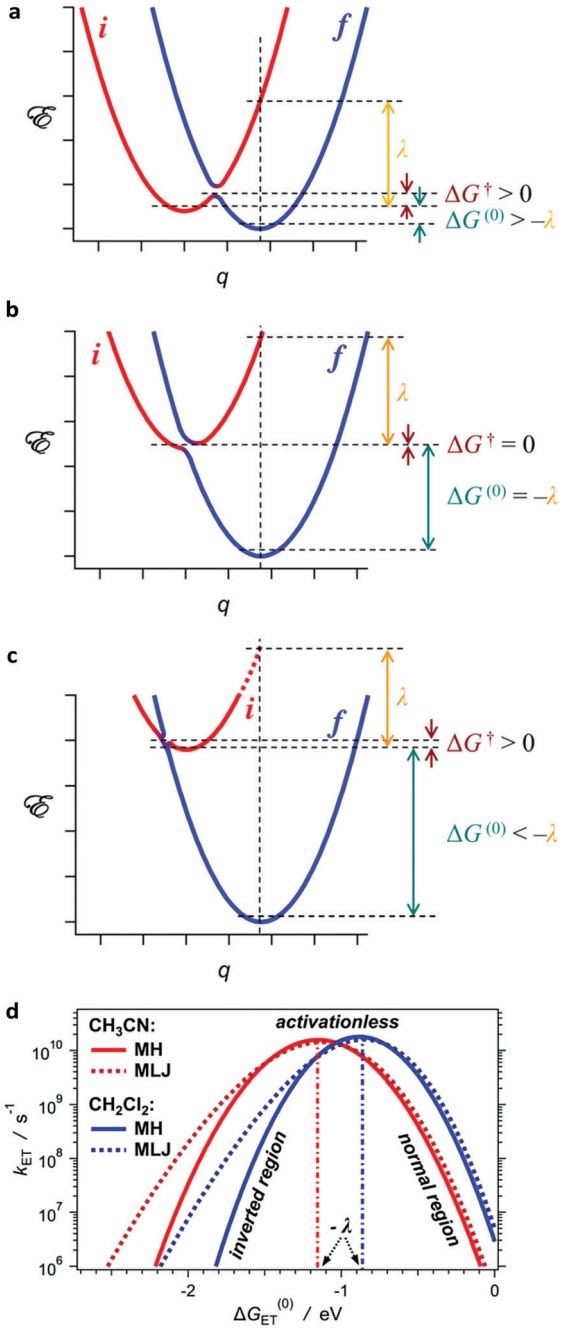

Fig. 3 State diagrams showing diabatic transitions between initial, i, and final, f, states: (a) in the Marcus normal region, (b) under activationless regime, and (c) in the Marcus inverted region, as depicted by varying the driving force, $\Delta G^{(0)}$, while keeping the reorganization energy, λ, constant. (d) Marcus curves for solvents with different polarity, *i.e.*, CH_3CN and CH_2Cl_2, obtained using MH (eqn (4)) and MLJ (eqn (6)) formalisms, where H_{if} = 1 meV, λ_ν = 0.1 eV, $h\nu_C$ = 0.2 eV, r_D = r_A = 4 Å, and R_{DA} = 9 Å.

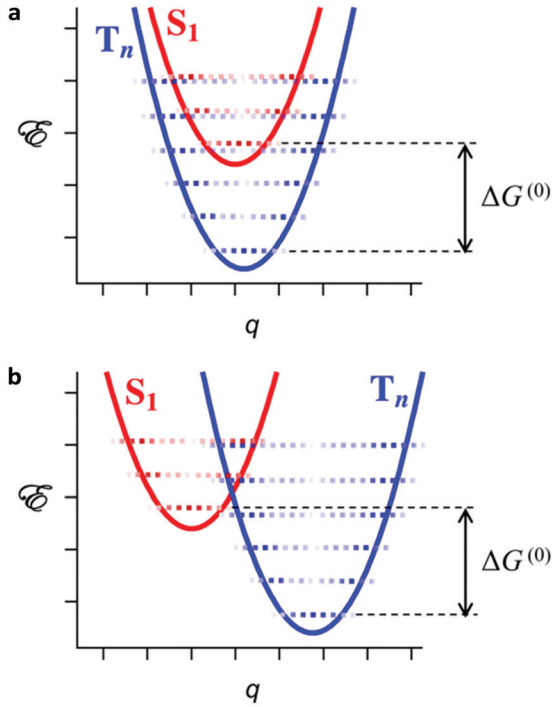

Fig. 4 State diagrams depicting ISC under: (a) weak vibronic coupling, where the nested geometry leads to an overlap between the lowest-energy vibrational wavefunction of the S_1 electronic state with the central region of the upper vibrational wavefunctions of the triplet state. In each electronic state, inherently, the density of the wavefunctions in the middle decreases with an increase in the vibrational energy. That is, for nested states, the vibronic overlap decreases with an increase of the ISC driving force. (b) Strong vibronic coupling, where vibrational wave functions from the S_1 and T_n electronic sates overlap at the crossings of the potential-energy surfaces of the electronic states. The densities of the vibrational wavefunctions is, indeed, the highest at the potential-energy surfaces of the wells.

does not illustrate the multidimensional nature of the potential-energy surfaces of the electronic states.

In analogy to the Marcus formalism, intersystem crossing (ISC) for weak-coupling limits shows inverted-region-like kinetic behaviour for triplet formation.[116] For transitions between singlet and triplet states with almost the same geometry and polarity, the reorganization energy is minute. The potential wells of the two states have practically the same shapes and their minima are at similar reaction coordinates, *i.e.*, the upper state, S_1, is nested in the lower one, T_n, (Fig. 4a). This arrangement prevents crossing of the potential-energy surfaces of the wells and forming of transition states. Nevertheless, an increase in the driving force increases the vertical displacement between the wells along the energy coordinate. Such displacement decreases the vibrionic coupling between the two states and slows down ISC. This behaviour is characteristic for the Marcus inverted region.[116] Conversely, when the structures of the singlet and triplet states are significantly different, the displacement between their potential wells lead to the formation of a transition state (Fig. 4b), and in normal-region behaviour for relatively small driving forces.[116]

Despite the unimolecular nature of the processes that eqn (4)–(7) describe, Marcus initially developed the theory for CT between two ions. Also, many of the initial CT reports focus on biomolecular reactions. These quests illustrate a principal reason why the inverted region had evaded the experimentalists for three decades. As the increase in the driving-force enhances k_{ET} in the normal region, the diffusion processes, bringing the

donor and the acceptor together, become rate-limiting steps prior to reaching the tip of the Marcus curve at $\Delta G^{(0)}_{ET} = -\lambda$.

About a decade prior to the first experimental demonstrations of the inverted region, Rehm and Weller developed empirical expressions for $\Delta G^{\dagger}$ and the rate constant, k_q, for analysis of CT-induced bimolecular emission quenching. They depict ET as the rate-limiting steps at small driving forces and the diffusion—at large $-\Delta G^{(0)}_{ET}$:[36]

$$\Delta G^{\dagger} = \frac{\Delta G^{(0)}_{CT}}{2} + \sqrt{\left(\frac{\Delta G^{(0)}_{CT}}{2}\right)^2 + \left(\frac{\lambda}{4}\right)^2} \quad (11a)$$

$$k_q = \frac{k_d}{1 + \frac{k_{-d}}{Z}\left(\exp\left(\frac{\Delta G^{\dagger}}{k_B T}\right) + \exp\left(\frac{\Delta G^{(0)}_{CT}}{k_B T}\right)\right)} \quad (11b)$$

where k_d and k_{-d} are the rate constants of formation and dissociation, respectively, of the donor–acceptor complex, and Z is the universal collision frequency factor.

The Agmon–Levine equation presents an alternative for treating bimolecular CT kinetics where diffusion becomes the rate-limiting process at large driving forces:

$$\Delta G^{\dagger} = \Delta G^{(0)}_{CT} + \frac{\lambda}{4\ln(2)}\ln\left(1 + \exp\left(-4\frac{\Delta G^{(0)}_{CT}}{\lambda}\ln(2)\right)\right) \quad (12)$$

Eqn (11b), along with (11a), is called Rehm–Weller equation. It is not to be confused with the expression for estimating the driving force of PCT from the excitation energy and the reductions potentials of the donor and the acceptor (eqn (2b) and (2d)).[35,36,117] For the latter, the introduction of the coulombic term is a principal contribution from Rehm and Weller.[36]

Considering the challenges introduced by diffusion-limited kinetics, it was not serendipitous that the first experimental demonstrations of the Marcus inverted region involved intermolecular CT in solid media[112,114] and intramolecular CT mediated in donor–bridge–acceptor (DBA) conjugates.[113,115]

Despite the limits diffusion imposes, reports of bimolecular CT systems exhibiting inverted-region behaviour in liquid media followed the breakthroughs from the early 1980s.[118–128] For observing the inverted region in such systems, Guldi and Asmus point out the importance of (1) increasing the biomolecular diffusion rates by using donors and acceptors with widely deferent sizes, as illustrated by the Smoluchowski and Einstein–Stokes equations, and (2) lowering the reorganization energy, so that the tip of the Marcus curve shifts to less negative $\Delta G^{(0)}_{CT}$.[122,123] Employing these consideration produces complete Marcus curves when k_{CT} of the donor–acceptor complex at the tip does not exceed 10^{10} or 10^{11} s^{-1}.[122] Employing solvated electrons with high mobility as ''electron donors'' increases the diffusion rates even further allowing CT to be the rate limiting step for k_{CT} as high as 10^{13} s^{-1}.[127] Even when the diffusion becomes the rate-limiting step, analysis with Rehm–Weller equation (eqn (11b)) allows for eliminating the contribution of the bimolecular rates to k_q and for constructing all regions of the Marcus curve.[126] This example is quite amazing: it shows the use of a formalism, which was developed to address the growing at that time doubts if the Marcus inverted region existed, for actually demonstrating the Marcus inverted region.

(Mis)interpretation of $\Delta G^{(0)}_{CT}$ presents another reason for missing inverted-region behaviour in experimentally obtained kinetic trends. When CT leads to excited-state radical ions, or CR leads to triplets lying above the ground states, the values for the driving forces, $-\Delta G^{(0)}_{CT}$, are overestimated.[112,119] In fact, most of the first demonstrations of the inverted region involved ground-state CSh processes (eqn (10a) and (10b)).[112–114] Quantifying for the losses in the driving force originating from the formation of excited-state CT products moves the ''deeply inverted'' systems toward the tip of the Marcus curve and account for the observed ''anomalies'' with such strongly exergonic reactions.[119,127,129]

When considering high-frequency modes (eqn (6)), the steepness of the Marcus curve in the inverted region decreases. That is, for the same driving forces, the CT rates in the inverted region predicted using MLJ formalism for $\nu_C \neq 0$ (eqn (6)) are larger than those obtained from the MH analysis (Fig. 3d). This feature presents additional experimental challenges. The increased rates for $-\Delta G^{(0)}_{CT} < -\lambda$ require stronger donors and acceptors to observe the trends of the Marcus inverted region. Making $E^{(0)}_{D^{x+1}|D^x}$ more negative and $E^{(0)}_{A^y|A^{y-1}}$ more positive, while keeping $\mathscr{E}_{00}$ as large as possible, indeed increases $-\Delta G^{(0)}_{CT}$. It also makes the excited-state donor and acceptor strong enough reductant and oxidant, respectively, to readily undergo PCT with the solvent. Hence, the selections of media for attaining the inverted region, especially for bimolecular reactions, can prove limited.

The usually strong exergonicity of CR has made it a preferred process for demonstrating the Marcus inverted region.[115,130] Furthermore, placing PCS near the tip of the Marcus curve ensures the CR is in the inverted region and $k_{CR} \ll k_{PCS}$, which is of pragmatic importance.[131] This way of thinking, however, is based on an erroneous assumption that the electronic coupling between the LE and the CT sate is the same as the electronic coupling between the CT and the ground state. In fact, differences in the electronic coupling for the CS and CR processes can be a principal reason for $k_{CR} < k_{CS}$.[132]

The reorganization energy for CT depends on the medium polarity (eqn (5)). Therefore, changing the polarity affects not only the CT driving force but also the shape of the Marcus curve, which reveals some of the complexity of the solvent effects on the CT kinetics.

Another ''anomaly'' originating from the Marcus transition-state theory encompasses cases where increasing the donor–acceptor distance increases the rates of CT. An overview of the CT analysis shows a non-trivial dependence of k_{ET} on the donor–acceptor distance. The electronic contribution to the kinetics for diabatic processes (eqn (4b)) manifests a linear relationship between $\ln(k_{ET})$ and the edge-to-edge donor acceptor distance, r_{DA}, which provides an important means for estimating the β parameter for various media. Changes in the centre-to-centre distance, R_{DA}, however, affects the medium reorganization energy (eqn (5c)) and the coulombic term of the driving force (eqn (1c)).

These effects of donor–acceptor distance on the ET kinetics can oppose one another.[133] Specifically, an increase in R_{DA} leads to an increase in λ_m (eqn (5c)) and in k_{CT} when $\Delta G_{CT}^{(0)} < -\lambda$ (eqn (4d) and (6)). This "counterintuitive" dependence of k_{CT} in the inverted region on R_{DA} becomes especially prevalent when $-\Delta G/\lambda$ exceeds 1.5 or 2 and when nuclear tunnelling (eqn (6)) has negligible contributions to the ET kinetics.[133] Therefore, to study electronic-coupling pathways, it is essential to focus on systems with $-\Delta G/\lambda \approx 1$ as Gray, Winkler *et al.* emphasize, for example.[129,134,135]

Understanding bimolecular PCT and CT is fundamentally important for advancing photocatalysis.[136,137] In addition to the abovementioned challenges, it is not truly straightforward to define donor–acceptor distances and the media between the donor and the acceptor (if any) during the CT steps, which are essential for quantifying the kinetics of such processes.[138] Hence, the new advanced tools, emerging from developments in computational methods and optical spectroscopy, are essential for driving charge-transfer science forward.

Long-range charge transfer and charge transport

As the donor–acceptor distance increases, the electronic coupling between them decreases and eventually CT becomes highly unlikely. The medium that bridges the donor and the acceptor plays a crucial role for such long-range processes. Even when the energy levels of the HOMOs and the LUMOs of the donor and the acceptor lie above the HOMOs and below the LUMOs of the bridging moieties (Fig. 5), coupling between all these frontier orbitals provides pathways for long-range CT. In other words, H_{if} includes coupling between the frontier orbitals of the donor with those of the bridge, and the frontier orbitals of the bridge with those of the acceptor. The energy differences between the orbitals of the bridge and the orbital of the donor from where CT

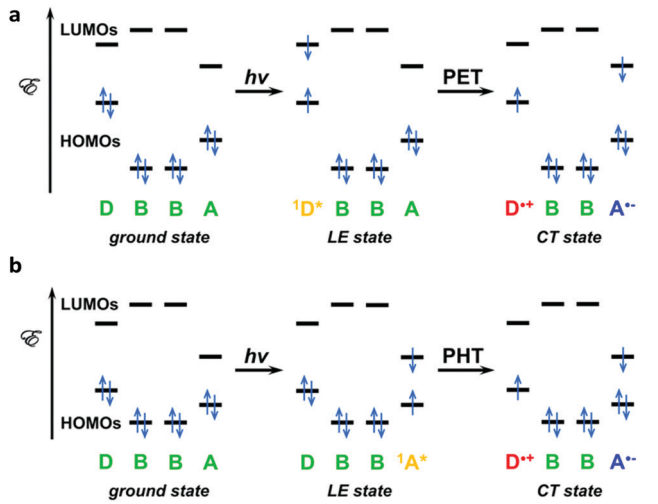

Fig. 5 MO diagrams depicting examples of long-range (a) photoinduced electron transfer, PET, and (b) photoinduced hole transfer, PHT, proceeding *via* superexchange mechanism with the electron transferring directly from the donor, D, to the acceptor, A, without residing on the bridging units, B. The state diagrams depict improved representation of the energetics of these processes (Fig. 6a and c).

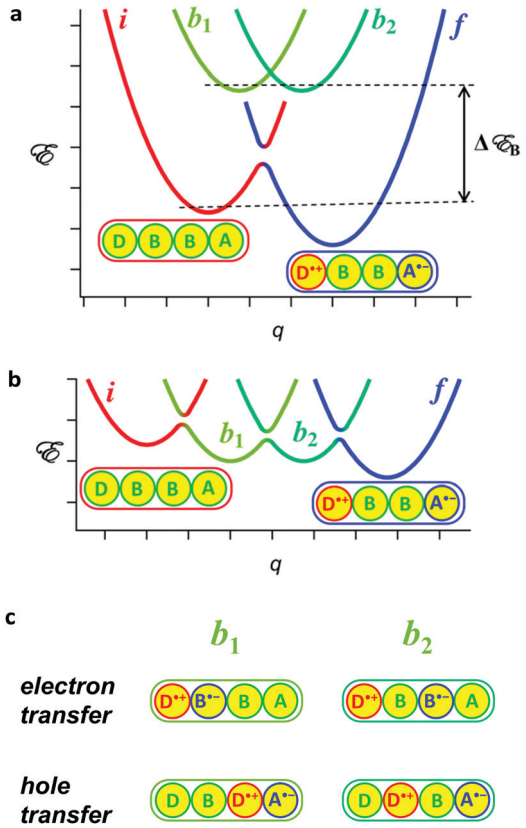

Fig. 6 State diagrams depicting long-range CT *via*: (a) superexchange mechanism; and (b) hopping mechanism. For simplicity, we show DBA systems with only two bridging units that have identical states when oxidized or reduced. (c) Charge distribution in the bridging states, b_1 and b_2, where the transferred electron is on the LUMOs, or the transferred hole is on the HOMOs, of the bridging unites.

commences, modulate the strength of the electronic coupling. This superexchange mechanism provides a means for CT at distances that can significantly exceeds the sizes of the donor and the acceptor.[139] That is, superexchange ET and HT involves electron tunnelling where the bridge mediates the electronic coupling between the donor and the acceptor. In effect, the bridge lowers the tunnelling barrier along the CT pathways.[140,141] For DBA mediating long-range electron tunnelling from the donor to the acceptor along n identical bridging units, the superexchange electronic coupling relates to the coupling between the donor and the bridge, H_{DB}, between neighbouring bridging unit, H_{BB}, and between the bridge and the acceptor, H_{BA} (Fig. 6a and c):[140,142,143]

$$H_{if} = \frac{H_{DB}(H_{BB})^{n-1}H_{BA}}{\Delta\mathscr{E}_B{}^n} \quad (13)$$

where $\Delta\mathscr{E}_B$ is the energy difference between the initial state and the high-lying virtual CT state where the transferred electron or hole is on the bridge (Fig. 5a and c).[140,142,143]

It should be emphasized that the superexchange CT mechanism describes long-range electron tunnelling. It does not involve charge hopping where electrons or holes reside on sites along the CT pathway. Erroneous statements in the literature describe superexchange through polypeptides and proteins as hopping of

holes along the backbone amides. Such CT states where h^+ charge carriers reside on the bridge, however, have energy levels above those of the transition states (Fig. 5a), *i.e.*, they represent virtual states. When $\Delta\mathscr{E}_B > 3k_BT$ for such virtual states, they are likely inaccessible. Furthermore, placing a hole on amides (at about 1.5 V *vs.* SCE) inevitably leads to their irreversible degradation and to decomposition of the polypeptide.[144] The capabilities of proteins and polypeptides to mediate long-range CT without prevalently breaking apart renders hopping along the amides as an unfeasible mechanism.

Empirical values of β (eqn (4b)) allow for facile evaluation of the kinetics of long-range CT through various types of structures, such as proteins, alkanes and polyenes.[143,145] For each media, β represents an average value for the r_{DA}-induced attenuation of the tunnelling propensity along the electronic-coupling pathways. For a number of cases, however, such average values of β cannot provide acceptable quantification of the CT kinetics.[146–149] For two systems with identical r_{DA}, the coupling pathways can have different segments. That is, even in the same protein, depending where the donor and the acceptor is, the pathways with the same r_{DA} can encompass different numbers of covalent bonds, hydrogen bonds, and through-space jumps across van der Waals contacts. To address such inconsistencies, Beratan, Betts and Onuchic developed the Pathway model.[150] It accounts for the specific bonding patterns of the media between the donor and the acceptor. The long-range electronic coupling is proportional to the product of the rate decreases caused by the individual covalent bonds, $\varepsilon^{(C)}$, hydrogen bonds, $\varepsilon^{(H)}$, and through-space jumps, $\varepsilon^{(S)}$, along each CT pathway:[150,151]

$$|H_{if}| \approx |H_{DA}(r_{DA}=0)| \prod_i \varepsilon_i^{(C)} \prod_i \varepsilon_i^{(H)} \prod_i \varepsilon_i^{(S)} \quad (14a)$$

$$\varepsilon_i^{(C)} = 0.6 \quad (14b)$$

$$\varepsilon_i^{(H)} = 0.36 \exp(-1.7(r_i^{(H)} - 2.8)) \quad (14c)$$

$$\varepsilon_i^{(S)} = 0.6 \exp(-1.7(r_i^{(S)} - 1.4)) \quad (14d)$$

where $r_i^{(H)}$ and $r_i^{(S)}$ represent the tunnelling distances, respectively, along the ith hydrogen bond and the ith through-space jump.

In addition to providing meaningful descriptions of the spatial features of long-range donor–acceptor coupling, the pathway analyses reveals the emergence of quantum effects that frequently govern the CT kinetics. For example, quantum interference between multiple parallel electronic-coupling pathways, mediating CT coherently, can profoundly affect the kinetics of charge transduction.[152–155] While constructive interference makes the system robustly insensitive to conformational fluctuations, destructive interference can completely shut down the CT processes.[154] In the latter case, vibrational modes and out-of-equilibrium transient conformations, which remove the symmetry responsible for the distractive interference between the parallel pathways, become immensely important for mediating the observed long-range CT.[154,155] Alternatively, when destructive interference makes CT along parallel through-bond pathways unfeasibly improbable and somewhat ''unlikely'' routes through van der Waals contacts and solvent molecules can take precedence.[156] Overall, the kinetics of long-range CT tends to be quite susceptible to non-Condon effects.[157–160]

Conformational dynamics provides finite probability for attaining resonance between the frontier orbitals of the donor, the bridging moieties and the acceptor, resulting in CT rates that are larger than the rates expected for long-range tunneling.[161] This flickering resonance is especially pronounced for PET when the energy levels of the LUMOs of the bridging moieties are situated only slightly above the LUMOs of the donor; and for PHT when the bridge HOMOs are only slightly below the HOMOs of the acceptor.[162]

As important as coherent quantum tunnelling is for long-range CT, it still has inherent distance limitations and can hardly account for the myriad of processes vital for the living systems, energy materials and electronic devices. Conversely, charge hopping (CH), which involves multiple efficient short tunnelling steps, provides a means for transducing charges with negligible distance limitations (Fig. 5b). While CH is an incoherent process, it is responsible for the highly efficient long-range CT mediated by biological systems and organic materials.[17,163–177] At distances beyond the Onsager radius, *i.e.*, beyond the coulombic traps of the initially formed CS states, the rates of CH have an inverse power dependence on the number of the hopping sites, N, *i.e.*, $k_{CH} \propto N^{-\eta}$.[163] For unbiased cases of diffusive hopping, η assumes a value of 2, and for biased random walk, η ranges between 1 and 2.[163] Indeed, biased directionality of CT, induced, for example, by electric fields originating from molecular dipoles, further suppresses the distance dependence of k_{CH}.

The LUMOs of the CH sites provide pathways for electron hopping (EH) when their energy levels are above that of the LUMO of the acceptor and below the energy of the transferred electron on the donor (Fig. 7a).[2] EH is vital for a wide range of biological processes, such as photosynthesis and cellular respiration.[17,178,179] Conversely, the HOMOs of the CH sites provide routes for hole hopping (HH) when their energy levels are between those of the HOMO of the donor and a singly-occupied orbital of the acceptor (Fig. 7b).[2] HH governs the efficient long-range CT along DNA and PNA strands.[174]

Indeed, a hole, h^+, is a ''virtual'' entity representing a vacancy in a singly occupied orbital. Physically, both, ET and HT, involve transferring of electrons. The nature of the transduced particles, however, is distinctly different for EH and HH. In EH, an electron from the donor hops along the LUMOs of the bridging moieties to reach the LUMO of the acceptor *via* a series of ESh steps. In contrast, HH does not involve a transfer of an electron from the donor to the acceptor. That is, an electron from the HOMO of a bridging moiety moves to a vacancy of a low-lying orbital of the acceptor. Then another electron from the HOMO of the next bridging site hops onto the singly occupied orbital of the moiety oxidized by the acceptor. Through such a series of hops, the vacancy on the HOMOs of the bridging moieties migrates toward the donor and extracts an electron from its HOMO (Fig. 7b). Overall, HH involves a sequence of transfers of different electrons along the HOMOs of the bridge, *i.e.*, a series of HSh steps, that results in an incoherent migration of a hole from the acceptor to the donor.[2]

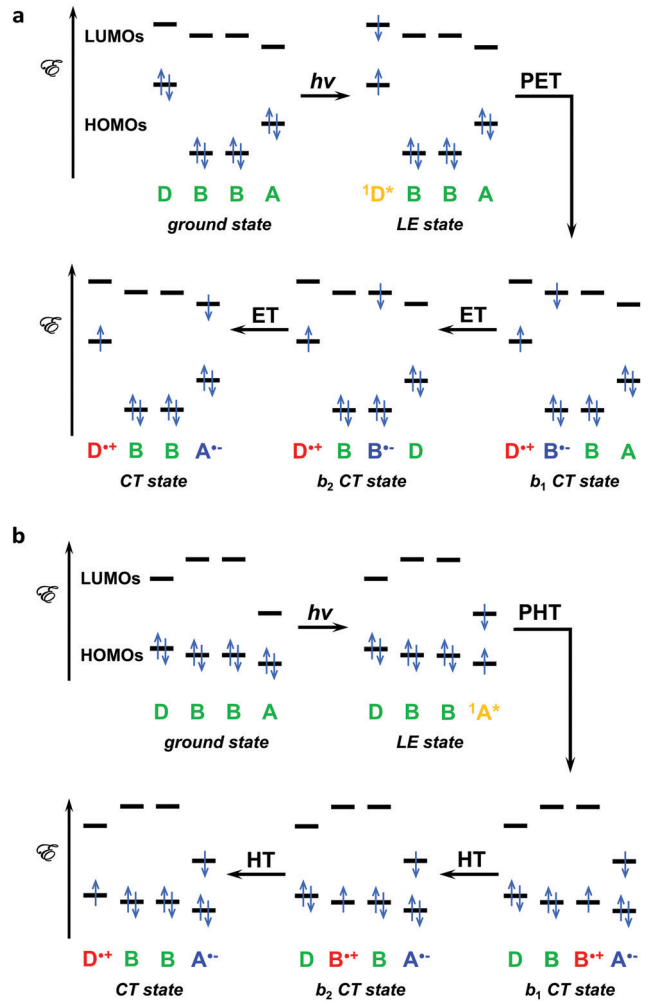

Fig. 7 MO diagrams depicting examples of long-range (a) photoinduced electron transfer, PET, and (b) photoinduced hole transfer, PHT, proceeding *via* charge hopping mechanism where the transferred electron and hole reside, respectively, on the LUMOs and HOMOs of the bridging units. The MO diagrams do not capture all nuances of the energetics of the charge-hopping steps. For example, the coulombic term, W (eqn (1c)), in the $\Delta G^{(0)}$ expressions (eqn (1) and (2)) reveals that if the two bridging units, B, are identical the b_1 states will be energetically more favourable that b_2 ones, especially for low-polarity media. It can make CR transition from the b_1 to the ground state more likely that the ET or HT transition from the b_1 to the b_2 state. State and Jabłoński diagrams depict these energy-level nuances, such as on Fig. 6b, where $\mathscr{E}(b_1) \approx \mathscr{E}(b_2)$, consistent with B units that are different or negligible coulombic contributions, W, due to polar media or to large distances between the bridging units and the donor or acceptor.

Similarly, long-range PT involves a sequence of short transfers of different protons between protonatable sights of a sequence of moieties, which is key for the design of proton wires.[180,181] Often coupled with ET, PT is essential for biology and for energy conversion.[182–185]

Donor–sensitizer–acceptor (DSA) conjugates represent an important family of systems that allow for attaining long-range CT states following two relatively short coherent CT steps. Selective photoexcitation of the sensitizer induces HT with the acceptor and ET with the donor. The back CT between the oxidized donor and the reduced acceptor requires a relatively long-range tunnelling through the sensitizer, which suppresses this undesired CR. DSA constructs prove important for light-energy conversion and for demonstrations of systems approach to mimicking photosynthesis.[186–189]

The examples illustrating long-range CT focus on systems comprising donors and acceptors with well-defined states. When the same bridging media spans between conducing electrodes with continuous distributions of electronic states (described by bands rather than molecular orbitals), application of a potential bias induces charge transport, CTr.[177,190–196] When the bias is small enough to ensure that the Fermi energy levels, $\mathscr{E}_F$, of the two electrodes are above the HOMOs and below the LUMOs of the bridge, CTr occurs *via* tunnelling, *i.e.*, nonresonant or off-resonance CTr (Fig. 8a).[197,198] Application of a bias that places the energy levels of the LUMOs of the bridge between the Fermi

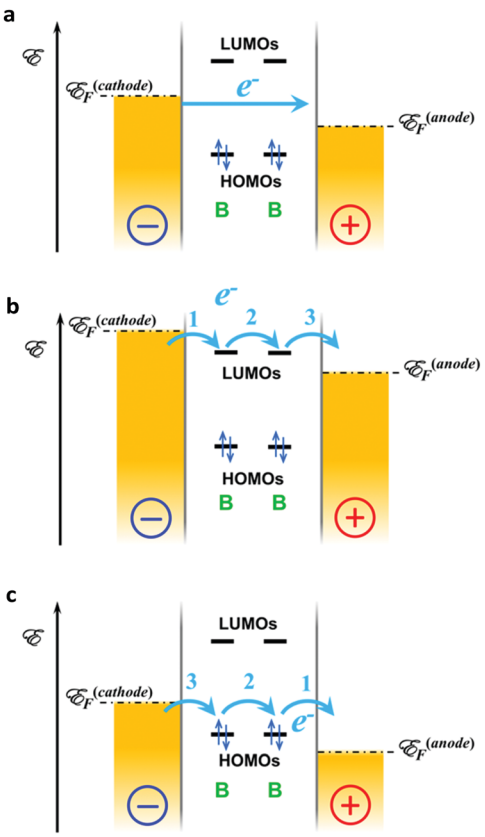

Fig. 8 MO/band diagram of charge transport through metal–molecule–metal junction where the molecule comprises two bridging units connecting the two electrodes. Along with the electronic coupling between the electrodes and the molecule, the alignment between the Fermi energies, $\mathscr{E}_F$, and the energy levels of the frontier orbitals determines the mechanism of CTr. (a) Off-resonance (nonresonant) CTr involving electron tunnelling from the cathode to the anode. (b) On-resonance (resonant) electron transport involving (1) electron injection from the cathode to the first bridging unit; (2) hopping along the bridging units; and (3) an electron hop from the reduced bridge to the anode. (c) On-resonance (resonant) hole transport involving (1) an electron hop from the bridge to the anode, *i.e.*, hole injection in the bridge; (2) hole hopping along the HOMOs of the bridging units, *i.e.*, electron transfer from a HOMO of one bridging unit to the vacancy on the HOMO of a neighbouring unit; (3) an electron hop from the cathode to bridge HOMO with a vacancy.

levels of the two electrodes, induces resonant or on-resonance electron transport (Fig. 8b).[2,199,200] Similarly, a bias placing the HOMOs of the bridge between the Fermi levels of the electrodes induces resonant or on-resonance hole transport (Fig. 8c).[2,201–203] While rate constants characterize the dynamics of CT, electric currents quantify CTr.

During CH the charges must tunnel to hop at each discreet step, and the CT rates strongly depend on the electronic coupling between the neighbouring hopping sites. Strengthening the electronic coupling between identical hopping sites leads to mixing and delocalization of their frontier orbitals. It can lead to the formation of band type electronic configurations that can span over the whole CT pathway. On-resonance CTr through such structures shows ohmic behaviour.

As an intermediate case, such mixing can lead to delocalization of the frontier orbitals over only a few hopping site, rather than the whole CT pathway.[204,205] Because the delocalization decreases the number of hopping steps, the rates of CT through such partially delocalized system are larger than the rates of CH along discreet localized sites. Because of conformational dynamics for organic conjugates, CH along partially delocalized sites is more common than CT through conduction or valence bands spanning between the donor and the acceptor. Tightly packed defect-free crystalline phases or other means of strong rigid bonding between the hopping sites is essential for attaining band electronic structures manifesting metallic or semiconducting behaviour.

Mobility of charge carriers exceeding 1 $cm^2\ V^{-1}\ s^{-1}$ and anti-correlating with temperature is consistent with band conductivity in solids. Conversely, hopping of localized holes and electrons is another important mechanism of CTr through semiconductor media.[206–209] In the 1930s Landau introduced the concept of self-trapped electrons that Pekar further developed.[81,210,211] The electric field from an electron (or a hole) perturbs the vibrational modes of the lattice around it and distorts it. This lattice distortion generates a reaction field that traps the charge, which induced it. Strong coupling with the lattice localizes the charge to form a small polaron, or a Holstein polaron. It features large lattice distortions that do not extend much beyond a single unit cell. Weak coupling results in small perturbations over a number of unit cells, forming a large polaron, or a Fröhlich polaron. As the vibrational distortions in the lattice of a small polaron extend over to another site to induce an electric-field trap there, the charge moves along.[209] Such hopping of small polarons can proceed under a diabatic or adiabatic regime, which determines the charge mobility and the conductivity of the material.[206,207,209] Hopping of small polarons is especially important for describing CTr through tightly packed ionic materials such as metal oxides.[206] In materials with somewhat plastic structures, such as metal-halide perovskites, polarons stabilize the holes and the electrons, keep them spatially separated, and thus suppresses the undesired CR.[208]

With $\Delta G^{(0)} \approx 0$, considering the transition-state energy, $\Delta G^{\dagger}$, the electronic coupling, H_{if}, and the reorganization energy, λ (eqn (4)–(6)), allows for employing the Marcus theory for characterization of the kinetics of diabatic polaron hopping.[212–214] In fact, in its high-temperature limit Holstein's small-polaron theory converges into Marcus' transition-state theory. Unlike charge mobility in bands, an increase in temperature increases the conductivity originating from hopping of small polarons.[207]

The commonalities of long-range CT and CTr illustrate the important relations between the molecular-level understanding of biological processes and targeted functionalities in molecular and nanoelectronics, as well as in energy conversion.

Dipole effects on charge transfer and charge transport

Electric dipoles are ubiquitous, and their effects on CT can be enormous.[2,9] Discussions of the idea about dipole effects on CT commenced in the 1960s.[215–218] In the 1990s, the first experimental evidence demonstrated the key importance of localized electric fields and of molecular dipoles for controlling the directionality of CT.[219–222]

The dipole-generated localized electric fields induce Stark effects and modulate the electronic properties of the molecular systems in their vicinity.[223] The notion for such effects on CT focuses on dipole-induced changes in the reduction potentials of the donor and the acceptor. These dipole effects on $E^{(0)}$ affect the CT driving forces and thus, the FC contributions to the CT kinetics:[9]

$$\Delta G^{(0)}_{CT} = F\left(\left(E^{(0)}_{D^{x+n}|D^{x}} + \phi^{(D)}_{\boldsymbol{\mu}}\right) - \left(E^{(0)}_{A^{y}|A^{y-n}} + \phi^{(A)}_{\boldsymbol{\mu}}\right)\right) + \Delta G_S + W \tag{15a}$$

$$\Delta G^{(0)}_{PCT} = F\left(\left(E^{(0)}_{D^{x+1}|D^{x}} + \phi^{(D)}_{\boldsymbol{\mu}}\right) - \left(E^{(0)}_{A^{y}|A^{y-1}} + \phi^{(A)}_{\boldsymbol{\mu}}\right)\right) + \mathscr{E}_{00} + \Delta G_S + W \tag{15b}$$

where $\phi^{(D)}_{\boldsymbol{\mu}}$ and $\phi^{(A)}_{\boldsymbol{\mu}}$ are the dipole-field potentials in the space that the donor and the acceptor, respectively, occupy.

Containing ordered electric dipoles, electrets are an excellent choice for localized-field sources.[1] While electrets are the electrostatic analogues of magnets,[224] the design of electrets and magnets present completely opposite challenges. Inherently limited by the Curie temperature, decreasing the sizes of isolated magnetic domains and making molecular magnets is nontrivial at all.[225,226] In contrast, increasing the sizes of the electrets poses challenges due to the inherent strength of the electric forces. Enlarging domains with ordered electric dipoles increases the propensity for extracting changes from the surrounding environment. This charge extraction screens the dipole effects. Therefore, while molecular magnets are still challenging, molecular electrets are relatively attainable.

Biology offers the best examples of molecular electrets. Protein α-helices have intrinsic dipole moments that amount to about 5 D per residue, oriented from the negatively polarized C-termini to the positively polarized N-termini.[227–231] (Despite some discrepancies in the literature, the vectoral direction of electric dipoles is from their negative to their positive poles.[232]) Each peptide bond, *i.e.*, a secondary aliphatic amide, contributes about 3.5 D to the helix macrodipole.[230,233] Upon the formation of the hydrogen bonding network, essential for stabilization of

the secondary conformation, the electrons from the carbonyl oxygens of one peptide bond move toward the hydrogen and nitrogen of the other. The polarization due to this collective shift of the electron density from the N- to the C-termini, provides a further enhancement of the helix macrodipole by 1.5–1.7 D per hydrogen bond.[230,231,234]

Similar to the α-helix, the tightly folded conformer, 3_{10}-helix, has a dipole of 4.6 D per residue.[231] The nomenclature 3_{10} indicates three residues per a turn with 10 bonds making the complete loop between two neighbouring hydrogen bonds connecting the helix turns. Following the same nomenclature, the α-helix is, in fact, a 3.6_{13}-helix.

The polyprolines do not have hydrogen-bonding networks because they contain only tertiary amides along their backbones. Isomerization of the peptide bonds in polyprolines between *E* and *Z* alters the type of helical conformation and changes the magnitude and the direction of the macrodipole. Specifically, comprising peptide bonds in their *E*-conformations, polyproline type I (PPI) has a dipole of 4.1 D per residue that points from its C- to its N-terminus, which is opposite to α- and 3_{10}-helices containing all *Z*-amides.[231,235] Conversely, polyproline type II (PPII) contains *Z*-amides and has a dipole ranging between 0 and 1.5 D per residue, pointing from its N- to its C-terminus.[231,235] Because of this difference in the magnitude of the macrodipole, changes in solvent polarity induce transitions between PPI and PPII conformations,[236] which can serve as an electret switch.

As one of the most common secondary structures of proteins, β-sheets do not possess a significant dipole moment. Each residue contributes about 0.25 D to the macrodipole of a single strand.[231] In a sheet containing multiple β-strands, however, the opposing orientation of the dipoles from the amide and hydrogen bonds cancels out their net contribution to a macrodipole.[231]

Helix dipoles play a key role for defining the structures and the functions of proteins.[237] Protein helix dipoles have immense physiological importance with making transmembrane CTr (of ions) possible and ion channels functional.[238,239] A particular class of enzymes rely on the vast network of dipoles for inducing double stranded breaks in DNA sequences.[240,241] Localized fields from electric dipoles play an important role in governing enzymatic activity as illustrated, for example, by Stark effects on the rates of the catalysed reactions.[242]

Polypeptide helices have enormous dipole moments and they are easy to prepare by using automated solid-phase peptide synthesis.[243–248] Therefore, they have been the principal structural motif in systems for investigating dipole effects on long-range CT and CTr since the first reports by Galoppini and Fox.[220,221] Since then, every few years new sets of publications testify for waves of growing interest in dipole effects on CT.[231,249–270] While much work focuses on small polar molecules at interfaces,[259–270] with a few exceptions, all reports on long-range CT utilize polypeptide helices as dipole sources.[231,249–258]

Polypeptide helices have been the centrepiece not only for investigating CT mediated by biomolecular systems,[271–281] but also for understanding self-assembly of dipolar species and the supramolecular structures that they compose.[282–284] A key challenge for self-assembling of polar conjugates is the assurance that their dipole moments point in the same direction. The electrostatically unfavourable co-directional orientation is essential for maximizing the dipole effects on CT in such structures. Important work in the 1990s provided the key design principles for leucine zippers, hydrogen-bonding and cofactor inclusion that allow for rational control of the formation of helix bundles.[282,283] Each helix turn in the leucine zipper contributes only 40 to 50 meV to the binding energy.[285,286] Still, *de novo* engineered molecular recognitions can drive with amazing specificity the formation of (1) dimers, trimers and tetramers of co-directionally oriented helices,[282] and (2) tightly packed helix bundles.[283,287,288] Others and we have extensively used such leucine-zipper motifs for designing CT-mediating helix dimers.[250,274,276,285,289–292]

In addition to their propensity for forming quaternary bundle structures, polypeptide α-helices can readily self-assemble in ordered monolayers on solid substrates.[293] It has allowed the demonstration of dipole effects on interfacial CT and CTr,[249,250,294–298] and of the effects of the macrodipoles on the (semi)conductive substrate.[258,299]

Polypeptides composed of aliphatic helix-forming α-amino acids, however, mediate CT along their backbones *via* superexchange mechanism. It limits the feasible efficiency of long-range CT to about 2 nm.[143] For example, the shortest electronic-coupling pathway through a single turn of a polypeptide α-helix comprises one hydrogen and two covalent bonds. Therefore, placing a donor and an acceptor on an α-helix about 2 nm apart, which is about four helix turns, decreases the CT rates by more than 7 orders of magnitude in comparison to the rates for $r_{DA} = 0$ (eqn (14)). Considering interference between multiple pathways and non-Condon effects may alter this estimate, but not to an extent that makes such biomimetic systems practical for CT spans exceeding 2 nm. In addition to the challenges with mediating long-range CT and CTr, polypeptide helices are quite sensitive to the microenvironment and susceptible to denaturation. It leads to losses of their macrodipoles.

Placing redox moieties on the sidechains of the residues comprising the polypeptide helices may provide hopping sites for long-range CT. The 5 Å increment of the α-helix loops, however, poses a demand on the minimum dimensions of such redox moieties. "Regular-size" redox moieties tend to be too small and too far from one another along the helix to ensure sufficient electronic coupling between them. As a result, the electronic-coupling pathways along the polypeptide backbone, which mediates coherent tunnelling, become considerably more probable than the incoherent hopping along the redox moieties on the side chains.[300–302] Increasing the size of the redox moieties can increase probability for van der Waals contacts between them and improve the electronic coupling. Attaching π-conjugates DBA derivatives to the polypeptide helices presents an alternative approach for attaining long-range CT in the presence of macrodipole-generated fields.[303] This approach, however, relies on colinear arrangements of the helices and the DBA conjugates. Co-assembly of the polypeptide helices with CT π-extended conjugates on conducting surfaces can lead to such colinear arrangements.[258]

Employing small polar molecules for coating conductive substrates, ensuring short tunnelling distances, offers an alternative

for facile materials processing. Layers of benzene derivatives with different dipole moments demonstrate the values of dipole effects on CT in device settings.[259,265] Small push–pull moieties, intercalated in the CT pathways, introduce dipole effects to such systems.[263,265,269] While the short tunnelling distances across the layers of small molecules are advantageous for the desired forward CT steps, they are not long enough to sufficiently suppress the undesired CR. Also, their small sizes limit how large their dipoles can be.

In addition to the need for dipolar molecules to efficiently mediate long-range CT along their dimensions exceeding one or two nanometre, electrets must be electric insulators. Free mobile charge carriers can readily screen any dipole-generated fields.

Again, biology offers the best paradigms of insulating materials that efficiently mediate long-range CT. In photosynthetic reaction centres, for example, the alignment of cofactors within the protein environment provides pathways for picosecond EH across the lipid membrane.[17] In addition to cofactors, amino acids with redox-accessible side chains, such as tryptophan,[304] can also provide hopping sites for increasing the distances of efficient CT in proteins.[172] The π-stacked arrangement of electron rich bases in DNA and PNA strands allows for efficient HH over distances of many nanometres,[174,305] which brings the chemistry and biochemistry of CT to the realms of nanotechnology.

Considering the best of the two worlds, we developed the concept of bioinspired molecular electrets, which are polypeptides composed of non-native aromatic β-amino acids, *i.e.*, derivatives of anthranilic acid (Fig. 9).[9,10,47,48,306–314] (1) Similar to polynucleotides, these electrets possess arrays of aromatic moieties for mediating long-range CT *via* hopping mechanism (Fig. 9). (2) Similar to protein helices, the ordered amide and hydrogen bonds in the molecular electrets generate large macrodipoles. Each amide contributes about 2 D to the electric macrodipole.[306] Due to the angular arrangement of the amide dipoles, only a part of their vectors is projected on the backbone axes.[306,315] Similar to protein α- and 3_{10}-helices, the polarization induced by the hydrogen-bond formation causes a cumulative shift of electron density from the carbonyl oxygens to the amide hydrogens. It enhances the dipole moment by about 1 D per hydrogen bond.[306]

With the extended π-conjugation along their backbones, the anthranilamide (Aa) molecular electrets offer pathways for

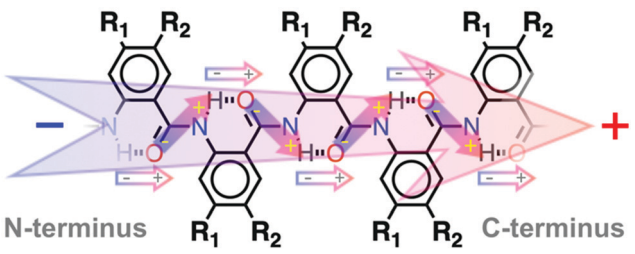

Fig. 9 Bioinspired molecular electret, based on an oligomer of anthranilamide, Aa, residues, along with its permanent electric dipole originating from ordered amide bonds and from the polarization due to the hydrogen-boned formation leading to a collective shift of electron density from the carbonyl oxygens to the amide hydrogens.

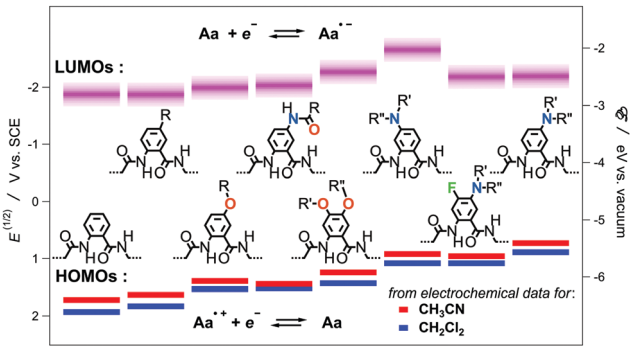

Fig. 10 Relative energy levels of the frontier orbitals of electron-rich electret Aa residues comprising different side chains, R_1 and R_2 (Fig. 9), as estimated from their reduction potentials for acetonitrile and dichloromethane. The energy levels of the HOMOs are estimated from the half-wave reduction potentials of the oxidized residues, $E^{(1/2)}_{Aa^{\bullet+}|Aa}$, *i.e.*, $\mathscr{E}(\text{eV } vs. \text{ vacuum}) = -4.68 - FE^{(1/2)}_{Aa^{\bullet+}|Aa}$ (V *vs.* SCE), where F is the Faraday constant. The optical HOMO–LUMO gap, $\mathscr{E}_{00}$, allowed for estimating the energy levels of the LUMOs, *i.e.*, $\mathscr{E}(\text{eV } vs. \text{ vacuum}) = \mathscr{E}_{00} - 4.68 - FE^{(1/2)}_{Aa^{\bullet+}|Aa}$ (V *vs.* SCE).

efficient long-range CT, which sets them apart from the biological and biomimetic electrets based on polypeptide helical structures. Most importantly, the aromatic rings along the backbone of these electrets, can provide sites for mediating long-range HH or EH. Unlike the native amino acids, the Aa residues have two side chains (R_1 and R_2, Fig. 9) that provide immense flexibility for adjusting their electronic and optical properties (Fig. 10).[47,308] This feature allows for developing proteomic approaches toward the design and development of systems with widely diverse electronic and photonic properties.[310,311]

The π-conjugation character of the polar Aa residues leads to important synergy between the dipole effects on the FC contributions to the CT kinetics (eqn (15)) and the donor–acceptor electronic coupling.[10,132] Furthermore, the Aa residues not only are dipole sources but also can participate in the CT steps as electron donors or acceptors. This feature allows for exploring and establishing the factors important for harnessing the dipole effects on CT.[9]

The dipole effects on CT are inherently enormous. How do we harness them? Lowering solvent polarity destabilizes CS states and not only decreases the CT driving forces, but also can make $\Delta G^{(0)}_{CT}$ positive and completely shut down the process.[316] At the same time, decreasing solvent polarity substantially improves the permittivity of the dipole-generated electric fields. Therefore, media with low polarity actually enhances the dipole effects on CT.[9,10] As counterintuitive as it may seem, lowering the solvent polarity can substantially increase the rates of ET along the dipole.[9] That is the dipole effects on CT can be quite stronger than the solvation-induced destabilization of CS states. Furthermore, the same lowering of the medium polarity, can completely shut down the ET against the dipole.[9]

Electric fields from dipoles fall off substantially with distance, *e.g.*, r^{-6} for point-dipole approximation. Therefore, placing the donor and the acceptor as close as possible to the solvation cavities of the dipoles is essential for harnessing their effects on CT. The Aa electrets present an ideal case where the donor

(and the acceptor) can be in the same solvation cavity with the dipoles. Such co-solvation provides an incomparable means for exploring, for example, enhancement of the dipole effects on CT resulting from the Onsager fields.[55,315] That is, an increase in the solvent polarity screens the fields outside the solvation cavities of dipoles. Concurrently, the same polarity increase enhances the fields inside solvation cavities of dipolar species.[55,315] This feature has direct implications on the functionalities of solid-state organic materials and devices.

Another important requirement for attaining substantial dipole effects on CT is to select donor–acceptor systems that inherently have as small as possible driving forces in the absence of external electric fields, *i.e.*, $\Delta G_{CT}^{(0)} \rightarrow 0$ for $\phi_{\boldsymbol{\mu}}^{(D)} = \phi_{\boldsymbol{\mu}}^{(A)} = 0$ (eqn (15)).[9,10] When the driving forces are large, relatively small perturbations from the dipole-generated fields can hardly affect the CT kinetics. Conversely, when the driving forces are small, dipoles can substantially enhance the CT rates or completely shut down the CS processes.[9]

Selecting small driving forces, $-\lambda < \Delta G_{CT}^{(0)} \leq 0$, places the CT kinetics in less than optimal regime of operation. Therefore, dipole effects that bring $\Delta G_{CT}^{(0)}$ close to $-\lambda$, *i.e.*, close to the tip of the Marcus curve, can induce substantial beneficial effects on the CT kinetics. Lowering the medium polarity decreases the reorganization energy. It can further enhance this effect by ensuring that even small dipole fields can bring $\Delta G_{CT}^{(0)}$ to the tip of the Marcus curve and make the reaction activationless.

Although the ideas about dipole effects on CT have evolved since the middle of the 20th century, this field still remains unexplored. The numerous examples demonstrating the importance of such effects place demands for improved understanding of how dipoles affect CT.

Charge transfer in biology

Charge transfer processes are the principal drive for the flows of energy that sustain the life on our planet. Photosynthesis harvests the energy from the solar radiation reaching the Earth's surface and stores it in the form of high-energy covalent bonds, *i.e.*, as fuels.[24,317,318] Cellular respiration and other processes release that harvested energy to propel the vital functions in the living systems.[179,319,320] In parallel, a minute percentage of the energy input for the life on Earth comes from chemical sources at geothermal sites where thermophilic organisms strive.[321–325]

Photosynthesis: light harvesting and energy storage

Following the initial PET from the porphyrin special pair (SP) in the bacterial photosynthetic reaction centre, a series of ET steps drive proton transport across the lipid membrane to generate a pH gradient.[326] The sequence of ET steps in the anaerobic photosynthetic bacteria forms a closed cycle. An electron leaves the photoexcited SP to hop along the LUMOs of a series of moieties. It reaches the quinone responsible for the transmembrane proton transport *via* double reduction and oxidation. At the end, the electron recombines with the hole left on the HOMO of the SP. This light-driven proton pump converts the absorbed solar energy into a pH gradient.

Proton motive force principally propels energy conversion and storage in living cells. Transmembrane pH gradients are the most conserved means for storing energy in living organisms and define the current thinking about the origin of life.[327] In a similar manner, lithium-ion batteries store energy by generating Li^+ gradients, without faradaic conversion to metal Li.[328]

As such energy-storage media in the living cells is similar to capacitors, the generated transmembrane pH gradients do not have too high energy density. Furthermore, the lipid bilayers cannot maintain large pH differences across them for extended periods of time. Therefore, the pH gradient drives the synthesis of adenosine triphosphate (ATP) from adenosine diphosphate (ADP), to store the harvested energy in the form of covalent bonds, *i.e.*, a biochemical fuel.

Long range electron hopping with quantitative quantum efficiency drives the natural photosynthesis. It includes diffusive transport of electrons (along with the protons) across the membranes by quinone shuttles. Such shuttles, which mediate diffusive transport of charges, are crucial for energy engineering. In the dye-sensitized solar cells, for example, redox mediating shuttles bring electrons from the cathode to the oxidized dye.[326] In heterophasic redox reactions for organic synthesis, such charge shuttles bring electrons between aqueous and organic phases.[329]

Mimicking the CT processes of photosynthetic bacteria demonstrates that these light driven ion pumps can have wide applicability. Modifying the quinone shuttle, for example, permits it to mediate transmembrane transport of divalent ions, such as Ca^{2+}, against their concertation gradient.[330]

The photosynthesis in plants and other aerobic organisms has evolved to utilize the harvested solar energy for water splitting (Fig. 11), in addition to pumping protons across the thylakoid membrane.[326] Two photosynthetic reaction centres work in sequence to ensure that photoexcitation in the red/near infrared (NIR) spectral region provides sufficient driving force for: (1) water oxidation and oxygen release at the "anodic" site, *i.e.*, at the thylakoid lumen side the photosystem II (PSII); and (2) water reduction to a hydride, *i.e.*, NADPH, at the "cathodic" side, *i.e.*, at the ferredoxins at the chloroplast stroma side of photosystem I (PSI) (Fig. 11).[326] The sequence of ET steps from PSII to PSI also mediates proton transport from the chloroplast stroma to the thylakoid lumen.

Indeed, ATP has a vital importance for storing energy and transferring it to other enzymes, regulating biochemical pathways, and building biomolecules such as DNA, RNA, proteins, fats, and sugars. ATP, however, is quite unstable and not a truly feasible for long-term energy storage. Therefore, ATP and NADPH drive the Calvin Cycle. The Calvin Cycle takes CO_2, a highly oxidized form of carbon, and reduces it to glyceraldehyde 3-phosphate (G3P). The carbohydrates produced from CO_2 reduction are kinetically considerably more stable than ATP. This stability makes them feasible for long-term energy storage.

Fats are not only key building blocks in living organisms, but also a biological fuel with high energy density. That is, fats store energy with density of about 9 kcal g^{-1}. In comparison,

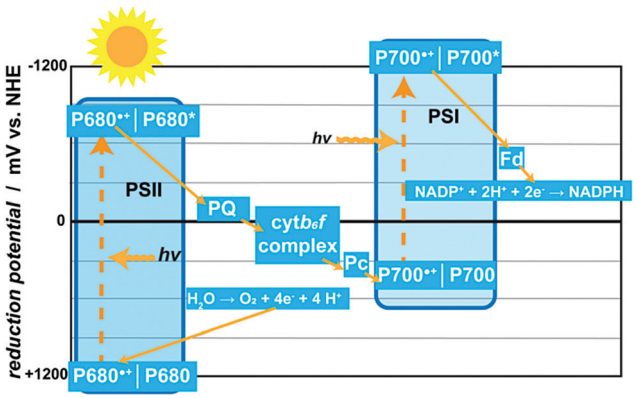

Fig. 11 Electron-transfer diagram of natural aerobic photosynthesis. Photosystem I (PSI) and photosystem II (PSII) utilize solar energy to drive water splitting. The oxygen-evolving complex of PSII represents the anodic side of this natural photoelectrochemical cell, and the ferredoxin (Fd) of PSI represents the cathodic side that catalyses the production of a hydride, NADPH, from nicotinamide adenine dinucleotide phosphate ($NADP^+$). The diagram depicts only some of the key moieties that mediate the sequence of ET steps: P700 and P680 are the special pairs of PSI and PSII, respectively; PQ is a plastoquinone responsible not only for diffusive electron transport, but also for pumping protons across the membrane; *cyt*b_6f is the cytochrome b_6f complex; and Pc is a copper-containing protein, plastocyanin.[331]

ethanol carries about 7 kcal g^{-1}, and carbohydrates and proteins – about 4 kcal g^{-1}. *Via* a series of CT steps and substrate shuttling, fatty acid synthase (a class of multienzymes) mediates formation of carbon–carbon bonds and reduction of carbonyls to yield highly reduced products, *i.e.*, fatty acids.[332] The substrates for the fatty acid synthases include (1) acetyl coenzyme A (CoA), a product of carbohydrate glycolysis and pyruvate dehydrogenase complex; (2) malonyl CoA, a product of ATP-driven enzymatic carboxylation of acetyl CoA; and (3) NADPH, a potent hydride donor and a reducing agent.

Natural photosynthesis and the formation of highly reduced kinetically stable biomolecules provide a broad learning platform for energy science and solar-fuel engineering. In the photosynthetic organisms, the light-harvesting absorbers, the CS and CT cofactors, and the catalysts driving the water splitting, are different. This feature reflects on an important lesson for energy engineering. Good catalysts often are terrible photosensitizers due to their short excited-state lifetimes or lack of strong absorptivity of visible light. Concurrently, good chromophores tend to have unimpressive catalytic properties, especially when it comes to multi-electron transformations.

"All-in-one" designs, where the same species harvest solar light, induces CT and drive chemical conversions to store the absorbed energy, have beneficial values and their pursuit should be encouraged. A decrease in the lengths of CT pathways and the number of conversion steps can eliminate significant losses. On the other hand, the natural paradigms suggest for parallel strives for high-power-conversion photovoltaics and for efficient energy-storage systems, such as electrocatalytic synthesizers of fuels.

The Calvin cycle points to another important set of paradigms for energy engineering. Despite the great advances for direct electrochemical reduction of CO_2,[333–340] such approaches to carbon solar fuels still present a variety of key challenges. Inherently, CO_2 is quite inert and not readily susceptible to reduction.[341] The need for concentrating the atmospheric CO_2 in the vicinity of the catalyst presents another hurdle. The RuBisCO-catalysed initial reduction step of CO_2 is one of the slowest enzymatic reactions in biology.[342] As an alternative to direct photoreduction of CO_2, the natural systems outline a paradigm that involves channelling solar energy into producing electron-rich agents that consequently reduce CO_2. Photocatalytically or electrocatalytically generated hydride nucleophiles, for example, can prove immensely beneficial for reducing CO_2. While such an approach adds extra steps in the conversion of solar energy to reduced carbon, it offers promising bioinspired roads for pursuing some of the hardest conversions in biology.

As important as the natural light harvesting and energy storage are, they represent only a small subset of biological processes where CT is vitally crucial for sustaining life on Earth.

Cellular respiration: extracting energy from fuels

Glycolysis and gluconeogenesis are arguably the two most important biological pathways in any organism. Glucose is the major energy source in living cells. In addition, it is a key structural component. Encompassing degradation (catabolism) and synthesis (anabolism), metabolisms usually involve efficient ET from and to the substrates. Both, catabolism and anabolism, are truly vital and heavily depend on each other not only for substrates, but also for regulation. Catabolism is a multistep oxidative process from the substrate point of view, requiring hole inputs. Anabolism is quite the opposite, involving reductive process and consumption of electrons to convert fundamental building blocks into a variety of macromolecules. The electrons and the energy released during the catabolism of glucose drive the formation of, *e.g.*, NADH and ATP from NAD^+ and ADP, respectively, which are crucial for sustaining multiple cellular pathways and body functions.

In aerobic organisms, the Krebs cycle, is a single-direction cyclic pathway transferring electrons from citrate to NAD^+, FAD and GDP to produce NADH, $FADH_2$, and GTP. The NADH and $FADH_2$ cofactors are major e^- sources for the electron transport chain (ETC), which for accuracy should be named electron-transfer chain. It involves a series of CT reactions between the electron donors, NADH and $FADH_2$, and the final electron acceptor, O_2. The ETC generates a transmembrane pH gradient that drives the production of ATP, using ATP synthase. Similar to photosynthesis, the ETC involves ET throughout various cofactors and quinones to facilitate the proton pumping from a media with high to low pH, *i.e.*, from low to high activity of proton ions.[326,343]

In cellular respiration, therefore, the Krebs cycle and the ETC serve as a fuel cell that aids the oxidation of (1) products from the catabolism of kinetically stable carbohydrates, (2) fats to produce different biological fuels, and (3) reducing agents with relatively small kinetic stability that are active enough to drive a range of cellular processes. For example, β-oxidation is the process of catabolic degradation of fatty acids, two carbons at a time, to produce: (1) intermediates that can enter the Krebs Cycle, and (2) $FADH_2$ and NADH, which can enter the *etc.*[344]

Reactive oxygen species (ROS) play an important role in the immune system, for example. Beyond the immune defences, CT processes under aerobic conditions generate ROS as side products that are damaging for the cells. Enzymes, such as catalase and superoxide dismutase, as well as the reduced or sulfhydryl form of glutathione, can scavenge ROS by reducing them to water. In its oxidized form, glutathione is a dimer, *i.e.*, as glutathione disulphide. Glutathione reductase utilizes the reducing power of NADPH and mediates ET to the disulphide bond dissociating the dimer into the two ROS-scavenging monomers. That is, multistep CT delivers electrons and protons from NADPH to the ROS as a protective measure against oxidative stress to keep cells alive and tissues intact.

Cellular respiration gives important lessons for bioinspired design and engineering of fuel cells. In addition, biology reveals key paradigms of how to protect such devise from oxidative damages, showing unique ways for diminishing their susceptibility to aerobic deterioration.

Vision and phototaxis: it is not all about energy management

Photoinduced triplet formation, leading to generation of singlet oxygen and consequently to ROS, is detrimental for living organisms. Conversely, PCS leading to the formation of triplet CT states is essential for the survival of migrant birds.[345] The triplet CT states act as sensors of the Earth's magnetic field, that is, CT makes the light driven compasses of birds functional.[6,346]

In addition to harvesting solar energy for sustaining life on Earth, light absorption, inducing CT, has a crucial sensory importance in biology, which is essential for vision and phototaxis.[347]

The G-protein-coupled photoreceptor, rhodopsin, contains retinal, *i.e.*, the aldehyde of vitamin A, as a principal chromophore embedded in a bundle of α-helices spanning across the membrane. The aldehyde functionality of the retinal provides a means for covalent bonding, as an imine, to an ε-amine of a lysine. It forms a Schiff base with pK_a immensely sensitive to the conformation of the chromophore and the surrounding protein microenvironment. A photoinduced *cis–trans* isomerization of the retinal initiates a series of proton-transfer steps that are coupling to the cell signalling pathways.

In the rod cells of the eye retina, these multistep CT processes govern the detection of the level of brightness similar to the function of a pixel element of charge coupled device (CCD) or complementary metal oxide semiconductor (CMOS) imaging chips.[348] In prokaryotic organisms, however, in addition to serving as a photosensor, microbial rhodopsins can also act as proton pumps, chloride pumps or light-gated ion channels.[349,350]

Ion transport drives the circuitry of the nervous system

In multicellular organisms, electrical impulses represent a principal means for propagating information and controlling body functions. Unlike electronic circuits where transport of electrons and holes drives signal transduction, in the circuitry of the nervous system tightly regulated ion transport is responsible for the propagation of action potentials. Along with neurotransmitters, this electric-potential propagation carries the flow of information.

The resting potential across a neuron membrane is more positive at the exterior than in the interior of the cell. Because the potential of the surrounding media serves as a reference, the conventional values for the resting potential are negative, amounting typically to about −70 mV. It corresponds to about 7 GV/m transmembrane field strength.[351] During depolarization, fast Na^+ voltage-gated ion channels open allowing for the diffusion-driven influx of ions leading to positive trans-membrane potentials. Repolarization occurs when slow K^+ voltage-gated channels open and allow for the efflux of the ions to return to resting potential. Because the slow-responding K^+ ion channels take relatively long time to close, the cell becomes hyperpolarized reaching potentials more negative than the resting potential. While at such negative potentials the voltage-gated Na^+ and K^+ ion channels are closed, ion pumps transport the Na^+ and K^+ in opposite directions across the membrane to restore their distribution and the resting potential.[352]

This dynamics of transmembrane ion transport provides a unique means for unidirectional spatial propagation of the action potential. The positive shift in the electric fields during depolarization activates the ion channels in the direction of the propagation of the action potential, *i.e.*, in the regions at resting potential. Conversely, the ion channels in hyperpolarized membrane in the opposite direction (from where the action potential arrives) remain inactive. Coupling these changes in the polarization patterns with release and sensing of neurotransmitters allows for transferring action-potential waves between neurons. It also drives: (1) the induction of signals into other types of cells, such as myocytes, and (2) the reception of signals from a wide variety of receptors crucially important for interfacing an organism with its environment.

Indeed, the mechanisms of electric transduction mediated by the nervous system for sustaining the life of multicellular organisms drastically differ from the principles employed in electronic circuits. Nevertheless, biology offers numerous examples where long-range ET and HT are crucial for the welfare of cells. These ET and HT paradigms, and the logic of the circuitry of the nervous system, offer unique invaluable lessons for device engineering.

"Rock breathing" bacteria redefine long-range charge transfer

In the 1980s the "rock breathing" microorganism, *Geobacter metallireducens*, observed and discovered by Lovley *et al.* in samples from Potomac River,[353–361] has presented the scientific community with unprecedented paradigms for biomolecular "wires" that efficiently mediate long-range CT. Nealson *et al.* shortly followed with the discoveries of similar organisms: *Shewanella oneidensis*, isolated from Lake Oneida,[362,363] and *Shewanella putrefacie*, isolated from the Black Sea.[363–365]

"Rock breathing" is cellular respiration under anaerobic conditions where the organisms transfer electrons to reducible inorganic minerals rather than to molecular oxygen. It represents metabolic pathways that were vital for sustaining the primordial life on Earth, prior the Great Oxygen Event and the advent of photosynthesis.[366] Since the beginning of the 20th century reports for ion-reducing modes of operation have documented this metabolic behaviour for a range of prokaryotes.[367–370] The discoveries in

the last three decades, on the other hand, brought the attention to the long-range electric connectivity that these cells establish between themselves and with the redox active substrates.

Under anaerobic conditions, bacteria such as *Geobacter* and *Shewanella* use metal ions at high state of oxidation, *e.g.*, iron(III) and manganese(IV), as a source of holes to drive their cellular respiration.[371–374] Because the metal ions are not internalized by the cells, the microorganisms grow extensions, such as pili, for electric contacts with the oxidizing minerals.[375–377] The extensions can exceed the micrometre size of the cells several times. These organisms have truly redefined the notion of how long ''long-range'' HT and ET along biomolecular structures can be.

Due to their communal nature, these microorganisms readily form intercellular electric connectivity.[377–379] In cultures and biofilms, therefore, cells that are away from the oxidizing minerals or the organic nutrients can still receive holes or electrons, respectively, vital for their survival. Intercellular electric connectivity, for example, is vital for symbiotic co-existence of ''rock breathers'' and anoxygenic photosynthetic organisms. This symbiosis provides: (1) the ''rock breathers'' with access to solar energy, and (2) the photosynthetic cells with access to respiration oxidants.[380]

In addition to maintaining cellular respiration, the long CT pili play an important defence role. Sulphur-reducing *Geobacter* and *Desulfovibrio* organisms readily convert uranium(VI) compounds into less soluble uranium(IV) ones. Keeping the remote contact with the oxidant, prevents the internalization and accumulation of this radioactive element in the cells.[381–383] The pili not only ensure efficient CT for this conversion, but also keep the site of reduction away from the cell wall preventing cell-damaging periplasmic mineralization.[381] Indeed, this unique ability of such ''rock breathers'' offers key paradigms for biological remediation of nuclear waste.

Despite the extensive amount of work on these microorganisms for the last 30 years, the questions about the mechanism for the pilus-mediated long-range CT still remain open. The electrical conductivity of the extracellular extensions of *S. oneidensis*, for example, strongly depends on the presence of c-type multi-haem cytochromes along them, showing CT behaviour consistent with long-range hopping.[376,384,385] Reduced expression of the haem-rich cytochromes results in the formation of ''wires'' with the same morphology but compromised electric conductivity.[376] Along with the other evidence, the reported p-conductance for such organisms suggest that hole hopping along the haems likely accounts for the observed incoherent long-range CT[377] It is consistent not only with ''wires'' comprising haems predominantly in their reduced state of oxidation, Fe(II), but also with tryptophan hole-hopping channels within the proteins.[386]

The CT and CTr mechanisms mediated in *S. oneidensis* colonies, however, are more complex than a model resembling charge transduction in p-conducting polymers. Unlike *G. sulfurreducens*, the ''wires'' maintaining the electrical conductivity of *S. oneidensis* do not have pilus-type structures. Instead, they are extensions of the cell membrane, *i.e.*, outer-membrane vesicles[387] connected with tether structures.[388–390] These vesicles with a network of tubular channels provide a means for diffusive transport of charges by non-bound cytochromes, *i.e.*, a CTr mechanism that functions in parallel with the hopping between the immobilized heme proteins.[388] In addition, secretion of flavin and the presence of flavin-binding sites on the cytochromes further enhances the extracellular electron transport in *S. oneidensis* colonies.[391–393]

Conversely, the ''wires'' *G. sulfurreducens* have pilus structures and studies manifest the importance of the presence of aromatic amino acids in these pili for their ability to mediate long-range CT.[375,394–397] While evidence show that outer-membrane cytochromes have a contribution to the CT properties of *G. sulfurreducens*,[378,394,398] pili enriched with aromatic residues define the electrical characteristics of these species. Mutations substituting the aromatic residues in the pili with alanines compromise the electrical conductivity.[399] In addition, pilus-deficient mutants still attach to mineral surfaces but cannot reduce them.[394] The induction of charge propagation upon application of positive potentials, rather than negative,[375] is consistent with prevalent hole-transfer mechanisms. Studies on pili of *G. sulfurreducens* reveal that their electric conductivity resemble that of metallic carbon nanotubes, rather than of conductive polymers.[375,395] Neither purely coherent mechanism, nor purely incoherent CT, involving hole hopping between the individual aromatic side chains of the residues comprising the pili, can account for rates that are representative of the measured conductivities.[397] On the other hand, an intermediate CT mechanism, involving holes delocalized over a range of residues, can quantify the experimental findings.[397,400] It is a mechanism that also accounts for the immensely long-range CT along double stranded DNA.[305,401]

The archaella of *Methanospirillum hungatei* mediate long-range CTr more efficiently than the filaments of *G. sulfurreducens*.[402] The known high-resolution structural details of the *M. hungatei* archaella[403] underlines the importance of this finding. Specifically, arrays of the aromatic side chains of phenylalanines define the structure of the archaella of *M. hungatei*.[402,403] The importance of establishing the relationships between atomistic-level structures and CT functionality cannot be overstated.

The drastic differences between the bacterial ''wires'' illustrate evolutionary convergence important for the adaptation of these organisms. Different structures, *i.e.*, pili enriched with aromatic amino acids and membrane tethers loaded with cytochrome cites for charge hopping, evolved to have the same CT functionalities.

Employing the paradigms of biological ''wires'' to the design and development of synthetic structures provides the platforms for important tests of the understanding of the features that govern their electronic properties. Biomimetic fibers, composed of phenylalanine-rich synthetic polypeptide helices, manifest CTr properties similar to those of the filaments of ''rock breathing'' microorganisms.[404,405]

Biology offers a myriad of paradigm for structures that efficiently mediate CT. Testing these lessons from nature by biomimicry and biomimesis sets the foundation of invaluable bioinspired drives for advancing science and engineering.[1]

Charge transfer and charge transport in medicine

Charge-transfer-induced pathology

Well synchronized sequential and parallel CT and CTr processes in multiple temporal and spatial scales are responsible for keeping the human body alive. Even the slightest disturbance of this fine balance between the multiscale charge transductions can lead to grave pathological outcomes.[406] For example, disruptions in ETC worsens the effects of neurodegenerative diseases, such as Parkinson's. It affects neurons by shutting down NADH:ubiquinone oxidoreductase.[407] Concurrently, malfunctions in the pentose phosphate pathway (PPP) allows an increase in the accumulation of ROS, which in their turn lead to oxidative stress and cancer.[408–410]

The PPP serves two major functions within biological systems. (1) It produces a reducing agent, NADPH, acting as an electron and proton donor in the catabolism of important molecular species, such as fatty acids and various cofactors.[411] (2) The PPP-formed NADPH acts as a reducing agent for ROS that are produced naturally as side products from the ETC and unnaturally from ultraviolet (UV) radiation. As discussed in the previous section, NADPH reduces the oxidized dimer of glutathione producing the reduced monomers that act as electron donors in the ROS scavenging.[411]

G6P-dehydrogenase deficiency is a well-known and classified disorder commonly found in people of African, Indian, Southeast Asian, or South American decent,[412] due to the lack of function in the oxidative phase of the PPP.[413] This mutation is evolutionary linked to these ethnicities due to the high outbreak of falciparum malaria in those regions of the world. This deficiency leads to high oxidative stress because of the increased amount of ROS in the cells, specifically, in the red blood cell in this case. An erythrocyte typically has a lifetime of 120 days, but with this deficiency, the lifetime decreases drastically. The malaria parasite requires healthy and long-lived erythrocytes to "prosper," and this disorder lowers the individuals' susceptibility to such an infection.

Fields originating from ion transport open windows to the brain and the heart

At a macroscale, monitoring the "electrical circuits" of the body is a key component of medical diagnosis and prevention. The collective propagation of all active potentials in the central nervous system (CNS) generates alternating electric fields that are readily detectable outside of the skull.[414] By recording these brainwaves with sufficiently sensitive equipment, electroencephalography (EEG) provides access to the functionality of CNS.[415] Indeed, EEG cannot detect every single action potential, and it does not have molecular and even cellular spatial resolution. The facile and non-invasive nature of EEG, however, makes it a promising medical tool for observing CNS that complements pricier alternatives, such as MRI, fMRI and optogenetics.[416–419]

Similar to neurons, myocytes have a negative resting potential. Their depolarization leads to a rapid positive shift in the cell potential due to the influx of Na^+ and Ca^{2+} ions that induce the muscle contraction. Opening of the K^+ channels leads to repolarization, returning the cell to its resting potential. As synchronized action of such CTr events in the cardiac muscle, the sinoatrial node is the natural pacemaker of the heart. It sends electrical signal down the atrioventricular node causing the atria and the ventricles to contract and pump the blood throughout the body.[420,421] These collective back-and-forth transport of ions throughout the heart generates alternating electric field that propagates outside of the body. The heart-generated electric field is an order of magnitude stronger than the magnitude of the brainwaves. Recording the temporal alterations of these relatively strong electric signals outside the chest is the foundation of electrocardiography (EKG or ECG) (Fig. 12). It is an indispensable well-established technique for non-invasive monitoring of heart health.[416–418]

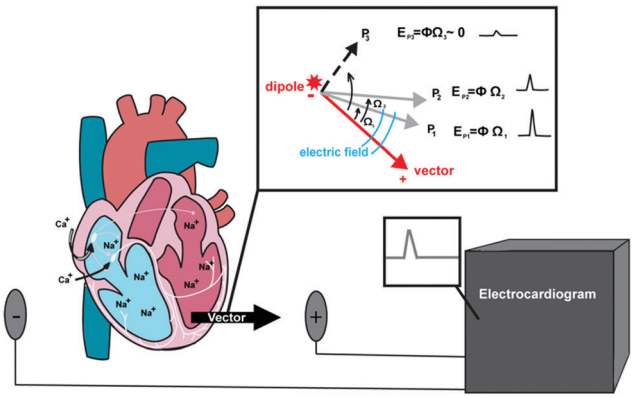

Fig. 12 Principles of electrocardiography, EKG. Ion transport processes, resulting in collective charge shifts within the heart, lead to polarization and depolarization, depicted by the vector of a cumulative electric dipole moment. Changes in the angle and the magnitude of this vector yields measurable signals.

Electroceuticals: from ancient acupuncture to pacemakers and the brain revolution

Monitoring techniques, such as EEG and EKG, are indispensable diagnostic medical tools. It is logical that application of such tools in reverse can have important treatment and healing implications. That is, employing electric fields in regulated manner for inducing and controlling CT and CTr processes, can address a range of serious health disorders.[422–426] Advancing such ideas has led to the evolution of electroceuticals, which complement pharmaceuticals that inherently aim at addressing medical problems by changing chemical balances in the body.[427,428]

The term "electroceuticals" was only recently coined.[428,429] Nevertheless, the idea of using external electric stimulation for medical therapy and treatment is not new at all. The ancient art of acupuncture,[430,431] for example, involves the selective application of electric-field concentrators, *i.e.*, metal needles, that can affect the CT and CTr process in the human body.[432–439] These effects remain long after the removal of the field concentrators.

While EKG provides an electric means for monitoring the cardiac function, the pacemakers regulate it. They exert electrical signals to induce heart contractions if heart rate is

irregular or retarded. Pacemakers comprise small battery-operated generators of electric pulses that stimulate the myocytes to contract when ''out of rhythm.''[440–442]

The vagus nerve (VN) runs across the face and the thorax to the abdomen, and plays a key role in the regulation of the metabolic homeostasis and the neuroendocrine-immune axis. One of the most important functions of the VN encompasses transmitting sensory information from the body to the brain.[443] Vagus nerve stimulation (VNS) encompasses electrical or manual techniques for its activation. In the past, manual VNS provided a means for suppressing seizures.[443,444] Electrical VNS studies began in the 1930's and 1940s to further understand the autonomic nervous system. These studies show that VNS affects the brains electrical activity and prove to have anticonvulsant effects.[444] FDA-approved implantable VNS devices hit the market in 1997.[445,446] Similar to heart pacemakers, these devices are implantable pulse generators attached to the VN, and their functions stimulate its activity.[447] By stimulating the activity of the VN, the device can treat a variety of conditions such as seizures, epilepsy, depression headaches and migraines.[443,447]

While acupuncture is an ancient technique, electroacupuncture (EAP) is a fairly new field of electroceuticals. It involves the application of electric potentials to the inserted needles inducing currents in the body for nerve stimulation and treating inflammatory diseases, for example.[430,439,448] A recent discovery reveals that the use of EAP for reducing inflammation can treat severe cases of sepsis.[448] The nerve stimulation *via* EAP opens doors for much more simpler procedures than VNS. As a minimally invasive technique, EAP removes the need for implanting an electrical pulse generator in the patient.[449] Rather, EAP allows for external nerve stimulation through small cutaneous punctures.

Electrical stimulations for wound healing imitate the natural mechanism of the endogenous electric fields that aid the skin growth. Such stimulation can decrease edema around the electrode, lyse necrotic tissue, increase blood flow and stimulate production of collagen, all of which are important for wound healing.[450]

The current focus of electroceuticals is on the brain.[451–453] Emerging electroceuticals such as focal brain stimulation or deep brain stimulation (DBS) provide access to improved understanding of the central nervous system.[454] Applying external potentials and changing the voltage gradients that neuron network maintains alters the CT and CTr behaviour of the cells.[454] In DBS, permanently implanted electrodes can exert pulses that results in similar outcomes to that from healthy tissues where lesions to the brain are. Similarly, implantable electronic chips that process and propagate signals through damaged or missing sections of the brain can preserve the overall functionality of this delicate organ.[455] These electroceutical approaches offer improved control, reversible effects, and diminished deterioration of brain tissue.[451–453,456]

Degradation of neurons relying on dopamine as a neurotransmitter in the substantia nigra pars compacta, which is responsible for coordinating purposeful motions, causes Parkinson's disease. FDA-approved DBS with implantable devices provides an important means for alleviating Parkinson's symptoms.[433,448]

Taking the understanding of the neural circuitry (and the CT and CTr processes that drive it) to the next level opens countless doors for the brain revolution. Electronic chips implanted in the brains of rats, can provide a means for remote control of the outcomes from probabilistic CT and CTr events that have deterministic impacts.[457–459] Such demonstrations of how to remotely control the decision making and the ''free will'' of an animal illustrate the power of electroceuticals and of CT science.[460] Ethical consideration, indeed, prevents the use of such electroceuticals for human subjects, except for extreme cases.[461]

The electroceuticals do not need to be truly invasive and the devices do not need to be implanted inside the brain in order to control its circuitries. External cutaneous application of electric signals can significantly impact the decision making and the behaviour of humans.[462]

Powering implanted medical devices

Despite the power of all the marvels that bioengineering and artificial intelligence may offer in the pursuit of bionic cures and ''immortality,'' they are all less than useless without energy to drive them. For all practical purposes, batteries are the principal energy source for powering implantable medical devices.[463] Inductive powering of implanted devices, along with recharging of implanted batteries from external remote sources, provides an alternative.[463]

Piezoelectric effects offer access to electrical energy harnessed from mechanical displacements, such as body movements.[464] The charging from such energy sources can be sufficient for running low-power devices.[465] Systems employing such effects can provide sufficient energy to power medical devices for electrical-stimulation and other implantable or cutaneous ones.[466] Flexible bandage-shaped devices comprising layers of Cu/PTFE and Cu placed on different sides of polyethylene terephthalate sheets can generate electric potentials from bending motions. Using rats as animal models demonstrates the possibility for building up electrical potentials from breathing motion.[157,467,468] The alternating amplitudes of the generated potentials reflect the breathing patterns. Such mechanically produced electric power is sufficient for speeding up the healing of wounds. The electric signals enhance skin regeneration by promoting fibroblast migration, proliferation and trans differentiation. Such advances demonstrate the utility and the potential benefits of such CT and CTr technologies.[469]

Fuel cells present one of the most attractive means for powering implantable medical devices.[470,471] The bodies of multicellular organisms circulate sufficient amounts of high-energy molecules, such as glucose, that can provide the electrons for such power devices, bioinspired from the cellular respiration and the functionality of the mitochondria.[472–475]

The human body is driven by a complex electric circuit comprising finely tuned and intricately synchronized CT systems. Understanding how these CT systems function and how their individual characteristics lead to the emergence of vital properties of the body, along with careful and responsible implementation of such knowledge, offers countless possibilities to medicine for improving the quality of life.

Charge transfer in nature outside living systems

While biology offers some of the best examples of life sustaining electron tunnelling, electron hopping and ion transport, inorganic nature provides a wealth of information about CT and CTr processes vital for the environmental balance of ecosystems. Iron and manganese are, respectively, the 4th and the 12th most abundant elements in the Earth's crust. The CT and CTr properties of their compounds have a principal impact on the redox dynamics that shapes formation and dissolution of minerals, processing of environmental contaminants, and sequestration of trace elements.[476–480] The electrochemical potentials of the various Fe(III)|Fe(II) redox couples are comparable to the potentials induced by the oxidizing atmosphere of our planet. Concurrently, manganese is the only element that has eight stable states of oxidation, ranging from 0 to 7+. They cover a broad range of reduction potentials, and allow facile multielectron redox processes and charge storage. The manganese water oxidation complex in photosystem II illustrates an important impact from the unique redox properties of this element.[481–489]

Iron and manganese oxides compose a wide range of minerals and particulates in soils and sediments that are insulators or semiconductors with poor electroconductive properties.[490,491] Nevertheless, many of them mediate CT and CTr, important for maintaining redox processes with key environmental impacts.[480]

Named for its blood-red colour and having a bandgap ranging from 1.9 eV to 2.3 eV, hematite, α-Fe_2O_3, is one of the most abundant minerals on Earth and its particles are spread throughout the lithosphere and the hydrosphere. It manifests anisotropic resistivity ranging from about 10^{-3} to 10^{7} Ω m, defined by weak n-conductance.[480,491] For example, the presence of Fe^{2+} in the surrounding aqueous media leads to deposition of Fe_2O_3 on (001) surfaces of hematite due to oxidation of the ferrous ions.[480] Concurrently, the other (*hk*0) surfaces dissolve due to reduction of Fe^{3+} of the hematite mineral. That is, the (001) surface acts as an anode and the (*hk*0) surfaces – as a cathode. As determined indirectly though ion exchange and directly though isotope monitoring, redox processes occurring on different sides of the particles build potential differences driving efficient long-range CT and CTr through the Fe_2O_3 medium.[480] These natural bipolar electrodes[492–494] are essential for mediating a wide range of environmentally important redox processes that benefit from the catalytic properties of the hematite surfaces.[477,495–503]

Similar to hematite, a large number of other oxides such as pyrolusite (β-MnO_2), goethite (FeO(OH)) and birnessite ($Na_{0.3}Ca_{0.1}K_{0.1}(Mn^{4+},Mn^{3+})_2O_4{\cdot}1.5H_2O$) show CT capabilities of environmental importance.[478,479,504] With resistivity exceeding 10^{7} Ω m, birnessite is practically an insulator.[490] Nevertheless, it plays a key role in detoxification of As(III) by converting it to As(V).[478,505] Bacteria, such as *Shewanella* sp. can utilize the oxidative strength of As(V) for their metabolic activity. By releasing Mn^{2+}, birnessite can serve as a source of holes for biooxidation of lactate where As(V)|As(III) redox couple acts as an electron shuttle,[504] instead of hole-transducing pili that many "rock breathing" bacteria develop for direct contact with the mineral surfaces (Fig. 13).[370,379]

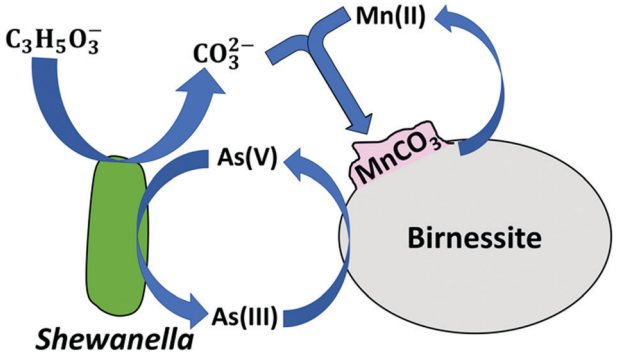

Fig. 13 CT with birnessite minerals drives the anaerobic respiration of *Shawanella* sp. As(III)|As(V) redox couple acts as a shuttle to carry holes from Mn(IV) from the birnessite to the bacterial cell respiratory oxidation of lactate, $C_3H_5O_3^-$. The CO_2 produced from the respiration forms carbonic acid and leads to the precipitation of the Mn^{2+} ions released in the aqueous media from the reduction of Mn(IV) from the mineral.

Such bacterial–inorganic interfaces show promising results for biotic-abiotic hybrid systems. For example, arrays of TiO_2 nanowires under irradiation can serve as an electron source for acetogenic bacteria.[506] Such setups allow for CO_2 fixation producing acetate that can be further used through genetically engineered *E. coli* for synthesizing a variety of chemicals. Such interfacing of non-photosynthesizing living prokaryotes with inorganic materials of PV devices allows for utilizing cellular metabolism for light-driven production of complex organic compounds from CO_2 and H_2O.[506] A complementary approach employs "rock breathing" species, *G. sulfurreducens*, in hybrid fuel cells. The bacteria drive the transduction of electrons from liquid fuels to electrodes, to which the cells are attached.[507] Such biotic-abiotic devices demonstrate an important means for benefiting from some key properties of living systems, such as damage management and self-repair, for which no viable technology is yet available.

Synthetic benefits from charge transfer. What's light got to do with it?

Electrosynthesis

Much of CT in nature leads to chemical transformations. Therefore, it is not surprising that since the advent of electrochemistry, its value as a synthetic tool has become quite apparent.[508,509] Production of high-purity electrolytic copper and chloralkali electrolysis, essential for NaOH and HCl synthesis, are just a couple of examples for mature technologies that implement interfacial CT and are intricate parts of our modern industrial lives.

One of the most attractive features of electrochemistry involves the capabilities to drive certain anodic and cathodic transformations by selective application of the external voltage. That is, the applied potential regulates the Fermi level, $\mathscr{E}_F$, of an electrode, allowing it to selectively oxidize or reduce

molecules in the vicinity of its surface, *i.e.*, extract electrons from occupied orbitals with energy levels above $\mathscr{E}_F$, and push electrons into unoccupied orbitals lying below $\mathscr{E}_F$. This thermodynamic view on interfacial CT, however, is quite oversimplified and warrants extreme caution when designing electrochemical synthetic procedures. While the thermodynamic considerations are crucial for interfacial CT, ultimately the kinetic features govern if the chemical transformations on electrode surfaces are feasibly fast. Interfacial CT is, indeed, heterogeneous in nature. Nevertheless, the kinetic considerations developed for monomolecular homogeneous reactions can extend to describing the CT processes on electrode surfaces.[510]

Overpotentials, η, reflect the lack of thermodynamic ideality of interfacial CT. Pragmatically, η represents the extra voltage, required in addition to the thermodynamic potential, for driving interfacial CT and chemical transformations at electrode surfaces. CT activation energy, diffusion of redox species to and from electrode surfaces, and interfacial energy (*i.e.*, surface tension) for the formation of new phases are some of the reasons for overpotentials. As bad as overpotentials may sound, they can serve as key design features in preparative electrochemistry. The overpotential for water oxidation to molecular oxygen ensures the anodic production of chlorine from NaCl aqueous solution. It is the working principle of chloralkali electrolysis that is at the heart of chemical industry. On the cathodic side, the water reduction to hydrogen presents its own challenges. Similar to chloride oxidation, the formation of H_2 is a two-electron process. Affinity of the electrode material for hydrogen and protons aids the process immensely. The proximity between formed hydrogen atoms on the surface is key for them to combine into H_2. In addition, energetically feasible collection of sufficient amounts of hydrogen molecules on the cathode is essential for nucleating a bubble to remove the product. For example, the atomically flat surface of mercury, when employed as a cathode in chloralkali electrolysis, prevents the evolution of H_2. Instead, mercury favours the reduction of Na^+ from the aqueous NaCl solution. By amalgamating the formed metal sodium, Hg stabilizes it as a product. On the other side of the spectrum, the enormous affinity of palladium and platinum for hydrogen has made them the preferred catalyst materials for hydrogenation in organic chemistry, water reduction in electrochemistry and H_2 oxidation in fuel cells. Cost, however, is a principal challenge for large-scale synthesis and energy conversion that use such materials as catalysts.

Despite the maturity of electrochemistry and electrosynthesis, the search for catalysts, which improve the electronic coupling or lower the energy of the transition states of interfacial CT, is still very much ongoing.[511–517] Bioinspired and rational molecular designs yield promising catalysts for chemical transformations. "Wiring" such catalysts to electrodes presents additional challenges. The electronic-coupling pathways between the electrode substrate and the catalytic active sites are essential. It is especially important for non-conducting macromolecules, such as enzymes, where efficient CT with the electrode and access for mass transport to (from) the active sites from (to) the bulk solution are paramount. Nanoscale assemblies of catalytically active molecules or metal clusters, which are arranged in microstructures on electrode surfaces with areas of square centimeters and even square meters, presents dimensional hierarchies that are essential for advancing electrosynthesis.[518,519] The pursuit of efficiency for CT-driven chemical transformations has boosted the growth of this field of metamaterials engineering. Concurrently, the emergence of new properties from such hierarchical structures, which are not inherent to the individual comprising components, provide important feedbacks for advancing the frontiers of CT catalysis.

The importance of the atomistic and multiscale surface structures has been acknowledged since the advent of nanotechnology and heterogeneous catalysis, as recognized by the 1912 Nobel Prize in Chemistry awarded to Paul Sabatier for his pioneering work on metal-aided chemical transformations.[520] He shared it with Victor Grignard for his breakthroughs in synthetic chemistry.[521] Through the 20th century, the needs of the chemical industry fueled the development of nanotechnology and heterogeneous catalysis. In fact, catalytic conversions are responsible for more than 90% of the products from the chemical industry. Nowadays we have amazing synthetic tools for advanced materials, which complement the improving means for monitoring their structures from sub-atomic resolution to mesoscales. These resources boost the renaissance in nanotechnology, which we have witnessed for the last few decades.

The benefits from hierarchical catalyst designs goes beyond meeting the needs for densely packing surfaces with active cites. For multistep oxidative or reductive transformations requiring different catalyst, nanoscale arrangements of active sites in proximity to one another on electrode surfaces aid driving the reactions.[522–524] Such electrocatalytic cascades are especially invaluable for transformations proceeding through unstable intermediates that cannot survive long-range diffusion.

In electrosynthesis, as important as the chemical composition of the electrode is, the morphology of its surface plays a crucial role. It is a key feature of heterogeneous catalysts. Platinum electrodes with rough surfaces perform superiorly in comparison to polished Pt. When CT on such rough surfaces drives the formation of gaseous products, however, the formed bubbles can mechanically damage the nano- and microstructures on the electrode, causing an increase in the overpotentials.

This lack of durability of the electrode surfaces illustrates an important challenge for heterogeneous catalysis, which sets it apart from CT-driven chemical transformations in living systems. In biology, most of the important CT-driven chemical transformations are at membrane interfaces. This heterogeneity closely resembles the settings in electrosynthesis. Enzymatic electrocatalysis, employing redox-active biomolecules attached to electrodes, has led to key advances in biomimetic and bioinspired synthesis.[525–529] Nevertheless, living systems evolved with well-regulated damage management. That is, damages of biomolecules and degradation of self-assemblies during metabolic and catabolic processes are an intricate part of life. Instead of preventing them, living cells have mechanisms for repairing the damages or replacing the whole biomolecular assemblies. Conversely, overengineering of manmade systems aims at damage prevention. For hierarchical photocatalysts with precisely arranged multiscale structural designs,

however, such overengineering is challenging. Self-repairing, or self-healing, paradigms present the ideal alternatives for over-engineering. Despite the recent advances in self-repairing heterogeneous designs,[530–534] electrosynthesis still awaits for the breakthroughs that will lead to electrodes with self-healing capability close to those of living systems.

Overall, the catalytic activity can be an inherent property of materials surfaces. Concurrently, modifying inactive surfaces with other materials, synthetic molecules or enzymes can activate them and modulate their catalytic properties.[535–539]

As important as the electrode surface is for electrocatalytic transformations, alternative approaches allow for addressing some of the key challenges. Hybridization between heterogeneous CT and homogeneous catalysis allows "ordinary" electrodes and diverse sets of catalysts to drive a wide range of chemical transformation.[540–544] At the cathode of such mediated electrolysis, a catalyst shuttles electrons from the electrode surface to a substrate in the bulk of the solution, and diffuses back to get re-reduced again for the next turnover cycle. In a similar manner, a catalyst shuttles holes from the anode to a substrate in the bulk that needs to be oxidized. Using heterogeneous systems with multiple liquid phases provides further possibilities.

Taking this hybrid paradigm of mediated electrode reactions a step further, transforms electrosynthesis to photoredox catalysis. Electrodes apply the necessary potentials for driving the CT steps. A photoredox catalyst can serve the same function.[136,137] Specifically, selective photoexcitation of a small molecule increases its oxidizing or reducing propensity allowing it to shuttle electrons from a weak reductant to a weak oxidants that do not directly react with each other.

Photoredox catalysis

The field of photocatalysis provides incomparable opportunities for broadening the potentials of synthetic organic chemistry.[136,545] The term photocatalyst (PC) refers to a light-absorbing moiety that, upon photoexcitation, aids to overcome large activation-energy barriers of exergonic reactions, *i.e.*, "classic" catalysis.[546,547] For the last two decades, the definition of this term has broaden to encompass photosensitizers for endergonic reactions where light drives the transformation to products with higher energy than the starting materials.[117,548,549]

Overall photochemical reactions involve electronic states that can initiate transformation to organic compounds that are inaccessible using thermal activation. Chemists recognized this potential of light-driven transformations in the early days of organic synthesis. For years, however, synthetic photochemistry has remained a somewhat specialized branch of physical organic chemistry. The need for UV illumination hindered its practicality. Because most organic compounds do not absorb in the visible spectral region, ultraviolet A (UVA) or ultraviolet B (UVB) illumination is necessary for direct optical excitation of their n–π* and π–π* transition, *i.e.*, for direct photochemistry. In addition, many organic solvents absorb in this spectral region between 280 and 400 nm.

The introduction of coloured photosensitizers, *i.e.*, PCs, which absorb visible or NIR light and activate UV-absorbing substrates *via* CT or EnT, drastically improved the possibilities for synthetic photochemistry. Similar to CT in electrosynthesis, in photoredox catalysis, PCT drives the chemical transformations by oxidizing or reducing the substrate. The increased internal energy of an excited-state PC influences its capability to donate or accept electrons, making it a better reductant or oxidant, respectively, than its ground state. Although an excited-state PC can use different bimolecular mechanisms to activate substrates, such as, EnT and atom transfer, PCT triggers a great portion of photocatalytic transformations. For nearly fifty years, photoredox catalysis has found widespread application in the areas of solar-energy science,[550] including water splitting,[551] and carbon dioxide reduction.[552] Only recently, these principles have been translated to radical generation for chemical synthesis and photo-activation of organic molecules, which enables a large number of organic transformations including oxidations,[553,554] reductions,[555] formation of carbon–carbon[556–558] and carbon–heteroatom bonds,[559,560] and functionalization of inactivated C–H bonds.[561,562]

Having their pros and cons, both, homogeneous and heterogeneous PCs can successfully drive CT-induced transformations. Commonly used photoredox catalysts under homogeneous settings include metal complexes, with Ru, Ir, Cu, and Fe chelates among the most popular,[137,563] and organic dyes.[136] The modus operandi for such PCs follows one of the two mechanistic pathways: oxidative or reductive catalytic cycle. In an oxidative quenching cycle, the excited-state catalyst, PC*, undergoes PET to reduce an oxidant in the reaction mixture and form $PC^{\bullet+}$. A reductant donates a hole to $PC^{\bullet+}$ to reduce it and bring it back to its ground state, in order to close the turnover cycle. That is, in an oxidative cycle, light drives an electron from a reductant to an oxidant, mediated by photoexcitation of a PC, followed by a PET and an HT step (Fig. 14a). Conversely, in a reductive quenching cycle, PC* first undergoes PHT with a reductant to form $PC^{\bullet-}$ and then ET with an oxidant to complete the turnover cycle (Fig. 14b). In a multistep transformation, if the substrate is the oxidant, a reaction intermediate can be the reductant, and *vice versa*. If the reaction mechanism does not involve a second CT step that can close the turnover cycle, adding equimolar amounts of sacrificial donors or acceptors ensure the required reduction of $PC^{\bullet+}$ or oxidation of $PC^{\bullet-}$, respectively.

While favourable thermodynamics is crucial, the successful implementation of a reaction design requires the proper kinetics for the various CT steps, to ensure that they are sufficiently faster than the competing undesired processes.[138,549] Overall, any closed photoredox catalytic cycle involves at least two CT steps: (1) PCT to quench the excited state, PC*, and (2) subsequent CT to regenerate the ground-state catalyst. Estimates of the CT driving forces and rates from electrotechnical and optical-spectroscopy analyses provide the crucial guidelines in the photoredox reaction designs. The bimolecular nature of many of the CT steps in photoredox catalysis, however, present formidable challenges. The donor–acceptor distances strongly affect the driving force (eqn (1c) and (2)) and the medium reorganization energy (eqn (5c)). In addition to the distance, the media between the

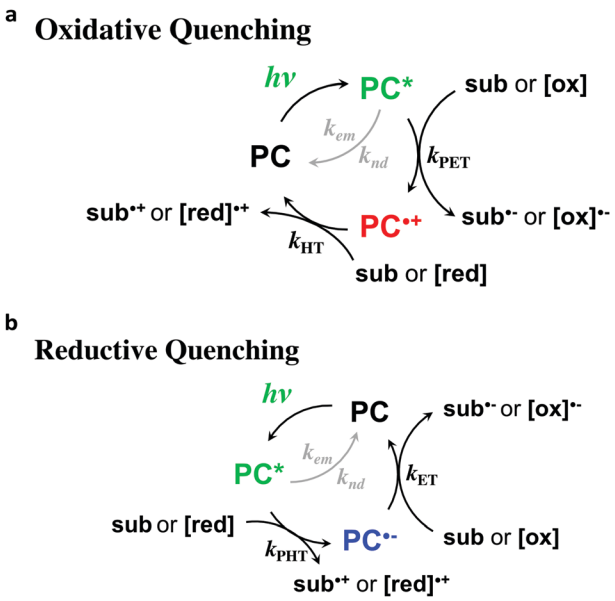

Fig. 14 Photoredox catalysis proceeding *via* (a) an oxidative quenching cycle, and (b) a reductive quenching cycle. The rate constants, k_{em} and k_{nd}, depict the photoemission (radiative) and non-radiative decays of the excited photocatalyst, PC*: sub represents a substrate or a key intermediate; [red] and [ox] represent a sacrificial electron donor and acceptor, respectively, if needed.

donor and the acceptor govern the electronic coupling between them. This deficiency warrants improved understanding of the nature of the bimolecular collisional complexes that mediate the various CT steps. Such a tasks is not trivial for dynamic mechanisms where an enormous variety of collision geometries is possible. For static quenching, where the lifetime of the collision complex is much longer than the timescales of the CT processes, computational methods developed for biomedical molecular engineering to study docking, recognition and binding may prove immensely invaluable.

As biomimetics of some of the most widely spread cofactors in living systems, porphyrins have gained enormous popularity as photosensitizes and PCs due to their versatility and tunability of optical and redox properties.[564,565] In fact, some of the highest power-conversion efficiencies of dye-sensitized solar cells are for devices employing porphyrin sensitizers.[566,567]

In its various forms, vitamin B_{12} is another widespread catalytic agent with vital importance for living systems.[568] Unlike porphyrins, the chemistry of vitamin B_{12} presents formidable challenges,[569,570] which seems to cool down the enthusiasm for a wide pursuit of biomimetics based on such corrinoid cycles. Furthermore, the short excited-state lifetimes of cobalamins renders them unfeasible for photosensitizers. Photocleavage of a Co–C bond, leading to structural changes, represents some of the limited number of examples for optical application of such bioderived compounds.[571–573] S_N2-Type reactions largely dominate vitamin B_{12} catalysis.[574] Nevertheless, in the recent years cobalamin (vitamin B_{12}) has proven its utility for catalyzing other nucleophilic reactions such as S_N2',[575,576] addition/elimination,[577] atom-transfer reactions[578] and Giese-type addition.[579] While most of the studies for electrochemical control of the cobalamin redox reactions involve solution-phase settings, electrodes coated with derivatives of vitamin B_{12} have spurred a recent interest.[580] Cobalt chemistry determines the catalytic properties of vitamin B_{12}. Analogues of the cobalamins with other metals, however, can broaden their utility for catalytic applications.[581]

Metal and semiconductor nanoparticles are an important class of heterogeneous catalysts with enormous surface-to-volume ratios. They can serve as components of hierarchical structures, immobilized on electrode surfaces, or as molecular-type catalysts suspended in liquid solutions. Despite the three-dimensional quantum confinement that induces molecule-like behaviour, these nanomaterials are solids with huge reservoirs of charge carriers. This features makes multi-exciton and multi-electron processes quite readily attainable for quantum dots (QDs) and other nanomaterials.[582–587] It does not come as a surprise, therefore, that for the first demonstration of photocatalytic water splitting, Fujishima and Honda used particles of a broad-band semiconductor, TiO_2.[588] In spite of its UV absorptivity, TiO_2 is among the most popular and reliable material for such applications due to its low cost, photostability and high activity.[589,590] Modifying TiO_2 with co-catalysts and photosensitizers allows for addressing some of its shortcomings.[591,592] TiO_2 photoanodes with catalytic activity of dye- and QD-sensitized solar cells provide key paths toward artificial photosynthesis.

Beyond energy science, the utility of semiconductor QDs as redox PCs offer amazing new possibilities for organic synthesis.[593–595] Broad optical absorption through the visible spectrum with impressively high molar extinction coefficients, susceptibility to multiexciton formation and multielectron CT, and size-induced tunability of electronic properties, are some of the unique features that QDs and other nanocrystalline materials offer. Despite their notorious lack of stability, perovskites with $A^+B^{2+}X^-_3$ composition have exerted some of the strongest impacts in photovoltaics for the last decade.[596] These unprecedented rates of development also fueled the exploration of the utility of perovskite nanocrystals for photocatalysis,[597] with significant efforts on addressing their inherent instability in polar and humid environments.[598]

Metallic clusters and nanoparticles present another set of benefits for photocatalysis. In addition to the enormous field enhancement in the vicinity of metal nanoparticles, the quantum confinement of the free charge carriers in them results in emergence of plasmonic features.[599] The generated hot charge carriers upon photoexcitation of the plasmons with visible light are an extremely attractive characteristic that drives the ever-growing interests in plasmonic photocatalysts.[600–603] CT from photoexcited metallic nanoparticles to organic substrates,[604] or to broad-band semiconductors for enhancing their redox activity,[601] are some of the promising possibilities for plasmonic nanomaterials. The short plasmon lifetimes resulting from femtosecond dephasing and picosecond thermal relaxation, however, impose high demands on the rates of interfacial CT kinetics for indirect ET or HT from the metal. Direct CT, involving optical transitions of an electron or a hole from the metal to the conduction or the valence band of the semiconductor, presents

promising possibilities. Conversely, the Schottky junction with the semiconductor affects the plasmonic characteristics in the metal nanoparticle, which raises new fundamental questions in the pursuit of direct CT. Overall, the CT efficiencies of about 1% warrant deeper understanding of the plasmon-induced charge transduction.[601]

Photoredox catalysis *vs.* electrosynthesis

These two fields are built on the same fundamental principles of CT thermodynamics and kinetics. Unfortunately, they appear to have grown independently with minimal interfacing. A practical consideration that sets apart the electrosynthesis from photoredox catalysis is the requirement for electrolyte in the former and the frequent need for sacrificial donors or acceptors in the latter.

If the substrate or the solvent does not provide the required ionic conductivity, supporting electrolyte is essential for electrochemical cells to function properly. In organic solvents, the large amounts of supporting electrolyte, *i.e.*, hundreds of mM, readily exceed the concentration of the formed products. Such solutions with large concentrations of organic-soluble electrolytes can pose grave challenges for the isolation and purifications of the products. With light illumination, on the other hand, less than 0.001 molar equivalents of PCs can drive the same redox transformations without the need of supporting electrolyte. This feature illustrates a clear practical advantage for a wide range of synthetic applications.

A range of photoredox catalytic transformations require equimolar amounts of auxiliary reductants and oxidants. Fortunately, the products from oxidation and reduction of commonly used sacrificial donors and acceptors are gasses, volatile compounds, or water-soluble salts,[605] all of which are readily removed from the reaction mixtures by evaporation or aqueous washes. For example, single-electron oxidation of tertiary amines, commonly used sacrificial donors, induces abstraction of an α-proton or a hydrogen-atom, as well as carbon–carbon bond cleavage, leading to the formation of volatile or other easy-to-separate products.[606]

An argument against mediated electrosynthesis points to the need for the catalyst to diffuse to and from the electrode surfaces in order to carry the charges to the substrates in the bulk of the solution. Photocatalysis, on the other hand, provides the means for optical excitation and initiation of the CT processes anywhere in the illuminated solution volume. Scaling up, however, invalidates this advantageous notion for photocatalysis. Increases in the concentrations of substrates and PCs increase the optical density of the reaction mixtures. It limits the light penetration to the surface layers of the photoreactors. The industrial needs for large reactors with increased thickness further aggravates this problem. That is, photocatalysis takes a shape of mediated electrosynthesis, where the PC has to diffuse to and from the wall layers of the reactor to drive the substrate transformations in the solution bulk. Fluid-mechanics engineering allows for implementing microfluidics and thin reactors for addressing this issue in photocatalysis and electrosynthesis.[607–617]

Overall, photochemistry and electrochemistry provide powerful tools for organic synthesis as reflected by the recent renaissance of these research areas. Despite the impressive advances achieved so far, both synthetic technologies suffer from some shortcomings. Thus, merging electrochemistry and photochemistry offers the potential to overcome the distinct flaws of one method through the advantages of the other, so that novel reaction pathways that are unachievable with either of the individual approaches can be envisioned.[618,619]

How to translate what we have learned about charge transfer from nature to materials and devices?

Incorporating molecular and supramolecular species as a bridge in a DBA conjugate offer some of the best means for experimental characterization of their CT properties. The bridges can vary from small molecular moieties to large macromolecular and biomolecular assemblies. Placing the same bridging molecules and macromolecules in an electrical junction allows for characterizing their CTr properties and sets key foundations for device engineering.[194]

The electrical molecular junctions are DBA systems with electrodes acting as a donor and an acceptor. Varying the potential difference between the electrodes varies the CTr driving forces, and the measured current flowing through it reveals the CTr efficiency. Furthermore, flipping the polarity of the applied voltage changes the position of the "donor" and the "acceptor" and the direction of the current. Therefore, the current–voltage (*I–V*) characteristics of a junction provides information about the CTr properties of the molecules incorporated in it. Such integration of organic and bioorganic conjugates in circuits and exploration of their CTr features has spun out the field of molecular electronics that has over 40 years of history.[620–623]

Single-molecule junctions

In the 1970s, the cornerstone report by Aviram and Ratner, describing the theoretical design of a *molecular rectifier*,[624] set the quest for single-molecule junctions and for deterministic effects that emerge from quantum phenomena.[625–628] Like all single-molecule experiments, such electric junctions unveil the stochastic nature of nanoscale phenomena, which makes them unique tools for the CT and CTr science. The evolution of different experimental designs has allowed to address principal challenges with wiring of a molecule to two electrodes simultaneously.[628–630]

Commonly, a molecule in a junction is orders of magnitude smaller than the electrodes to which it is attached,[631] making the formation of single-molecule junctions quite challenging. In break junctions, for example, freshly formed metal surfaces slowly recede from each other in a controllable manner while immersed in a diluted solution of the examined molecule, which is usually bifunctional.[632–635]

For imaging, scanning tunnelling microscopy (STM) utilizes the horizontal movement of a metal tip over a conducting

surface with potential applied between them. Mapping the measured currents *vs.* the coordinates of the tip provides ångström-resolution images of the surface topology and thus, of the molecules adsorbed on it.[636] In addition, STM has introduced the capabilities for mechanical manipulation of surface structures.[637] These features of STM provide an excellent means for formation of single-molecule junctions between the tip and the surface, and for interrogation of their *I–V* characteristics.[636]

The electrical contacts of a molecule in a junction can have deterministic effects on its *I–V* performance.[638] Some of the best means for incorporating a bifunctional molecule in a junction involves rapid formation of coordinate and covalent bonds with the conductive substrates of the two electrodes. Sulphur functional groups, such as thiols, thioethers and thioester, provides the most popular approach for attaching a molecule to gold electrodes in a junction.[639] The large affinity of sulphur for coinage metals ensure that such covalent bonds not only are stable, but also provide strong electronic coupling.[640,641] The strength of the sulphur–gold bond is about 2 eV.[642]

The sulphur chemistry for surface attachment has certain drawbacks. The reduced forms of the sulphur in such organic compounds is susceptible to oxidation, which not only changes the electronic coupling, but also weakens and breaks bond with the metal. Concurrently, the high motility of gold atoms in strong electric fields can induce the growth of metal spikes, leading to shortening of the circuit across the junction. This phenomenon places limits on the magnitude of the potentials applied across the electrodes. Constructing junctions comprising symmetric molecules that are not covalently attached to the electrodes offers a means for addressing some of these challenges, especially when the conductive substrates are not composed of motile metal atoms.[643]

In typical metal–molecule–metal junctions (Fig. 8), not only the electrodes are considerably larger than the wired molecules, but also the metal atoms of the electrodes are larger than the carbons and the other atoms composing the organic conjugates. Conductive carbon nanotubes can serve as relatively thin electrodes for junctions, in which the incorporation of the molecules employs strong covalent bonds.[644] Conversely, quantum dots and other nanocrystals provide alternative approaches for electrical wiring of molecules in junctions.[625,645–647]

The advances in the electrode designs and the junction setups have opened doors for molecular-level understanding of CTr.[648,649] Concurrently, they have fuelled the evolution of molecular designs in the search for a wide range of CTr phenomena. For example, junctions comprising inorganic metal clusters, coated with organic ligands, manifest Coulomb-blockade type of *I–V* behaviour at room temperature.[650] The relatively long distance between the electrodes, maintained by the ligand-coated clusters, results in minute off-resonance CTr currents. Conversely, changes in the charging of the metal clusters at increased voltage biases modulates the on-resonance CTr behaviour.[650]

Biomolecular junctions

Expanding the applications of molecular junctions to biological systems provides opportunities not only for characterizing their CTr properties, but also for sequencing and structural analysis.[651–656] While DNA is an insulator, its unique ability to mediate long-range HT[174,657,658] has allowed it to gain considerable traction in molecular electronics.[659] Like with many organic molecular "wires," the process of understanding CTr through DNA involves anchoring both ends of a strand to electrodes to form molecular circuits.[653,654] Unlike most organic polymers, however, a single DNA molecule and the DNA double strands can readily extend over several micrometres, permitting the use of facile optical imaging for monitoring the separation between the electrodes to which the molecular termini are attached.[660] Indeed, the thickness of DNA strands is considerably below the optical diffraction limits.

The research inquiries on the DNA electrical properties began in the early 1990s with the work of Barton and Turro.[661–664] It was not until the advent of the break-junction techniques, however, when the demonstrations of CTr through single-molecule DNA and of the effects of base sequences on the *I–V* behaviour, started making serious advances in the field.[653]

The molecular dynamics of DNA has profound effects on its CTr properties. The conductance of a single-strand DNA is several orders of magnitude lower than that of its counterpart double strand.[665] The π-stacking of the based in double-stranded structures provides the electronic coupling essential for long-range CT and CTr.[664] The lack of such electronic coupling in single strands of DNA, due to its flexibility and random orientation of the bases, outlines the reason for their low electrical conductance.[666] Mismatching between base pairs also affects the electronic coupling along the DNA double strands, altering their conductance by an order of magnitude.[667]

The backbone of DNA, however, is a polymeric phosphate salt. Therefore, the translational dynamics of the counterions coupled with the hole transport along the bases, and the ionic conductivity of the polymer microenvironment, can overwhelmingly impact the measured electrical characteristics. Some of the early experimental findings have led to interpretations declaring that DNA acts as a conductor, a semiconductor, a superconductor and an insulator.[668–672] Through the years, the synergy between experiment and theory has allowed the field to converge away from these discrepancies.[174] The ionic nature of the DNA backbone brings ambiguity to interpretation of experimentally observed CT and CTr behaviour. Conversely, PNA structures offer alternative to DNA strands without the charged backbones.[174]

Globular structures of proteins provide certain advantages in the engineering of molecular junctions.[673–675] The redox sites forming the electronic-coupling pathways for mediating CTr are frequently within well-defined microenvironment in the interior of the proteins. This cofactor microenvironment is practically the same for protein bridges in DBA conjugates and in electrical junctions, setting an excellent foundation for comparisons between CT kinetics and CTr *I–V* behaviour.

Multiple factors, such as protein structure, electronic coupling, and alignment of the frontier-molecular-orbital energies with the Fermi levels of the electrodes, govern CTr through a junction comprising proteins sandwiched between two electrodes.[676] Connection of a protein to the electrodes can be the deciding factor in the capability of a junction to maintain electric

currents at low biases, which can be a basis for bioanalytical methodologies.[677]

When it comes to molecular junctions, mutations of surface residues (to cysteines, for example) provides the needed functionality for wiring the proteins to the electrodes of gold and other noble metals.[678] Conversely, functionalizing the electrode surfaces with peptide ligands, to which the selected proteins have a binding affinity, allows for introducing such biomolecules into electrical junctions in their native form without the need for mutations and extra protein engineering.[676,677] Alternatively, introducing proteins between electrodes without linkers can often yield similar junctions that manifest switching between off- and on-resonance CTr mechanisms.[679]

Introducing polypeptides into molecular junctions eases the experimental approach for gaining understanding of some of the CTr properties governed by specific protein sequences and secondary conformations.[680,681] The well-established automated solid-phase peptide synthesis offers a wealth of opportunities for realization of countless biomolecular designs for engineering of such electrical junctions.[682–685]

A principal challenge for molecular junctions comprising proteins is the inherent conformational instability of these biomolecules when taken out of their native environment. Electrode coatings that prevent denaturation of the proteins attached to them is essential.[686–692] Such coating layers, however, can add a few nanometres in the CTr pathways and significantly decrease the electronic coupling with the conductive substrate.[693,694]

A range of the unique properties of proteins and polypeptides define the functionalities of the molecular junctions they compose. Macrodipoles of polypeptide α-helices induce current rectification to electrical junctions.[250] Introduction of ferritin to molecular junctions induces *I–V* behaviour consistent with negative differential resistance.[675,695]

Junctions based on self-assembled monolayers

Translation from single-molecule setups to molecular ensembles illustrates an important path of evolution toward applied science and technology development.[696] Some of the initial work in molecular electronics involved electrical junctions comprising self-assembled monolayers (SAMs) sandwiched between flat metal electrodes.[621,622] Such metal–insulator–metal (MIM) junctions have the architecture of capacitors with dielectric layers that are nanometre-thick, allowing for efficient CTr (Fig. 8). These devices bring molecular CTr to the realm of organic electronics.

One way to picture SAM devices is as a superposition of a large-number of parallel single-molecule junctions. Conversely, the molecules in such SAM junctions are closely packed together and the intermolecular electronic coupling provides parallel CTr pathways, especially when the SAM molecules assume large tilt angles on the conductive surfaces. Such CTr involving multiple pathways can lead to emergence of new properties of the molecular ensamples that are not inherent to the individual molecules. Furthermore, incorporating π-conjugated CTr molecules in SAMs of alkyl conjugates allows for probing specifically the CTr moieties without interference from lateral intermolecular CT steps.[697,698] Indeed, it is essential to prevent phase separation during the SAM formation, *i.e.*, to ensure that the π-conjugated molecules do not cluster together forming isles in the alkyl SAM.

Attaining nanometre-thick layers extending throughout the large areas of the MIM junctions presents grave challenges for the fidelity of the SAMs and the electrode surfaces. While well-packed SAMs on atomically flat substrates are not too demanding to attain, the edges and the tips of the grains of many electrode materials are sites for defects in the surface coatings. Mercury is a liquid conductor with sufficient surface energy to always form atomically flat surfaces over areas of square millimetres and larger. Therefore, mercury has been a metal of choice for designs of MIM junctions.[699–702]

The chemical inertness of gold has made it one of the most popular materials for electrodes in molecular electronics. The grainy nature of gold surfaces, however, presents inherent challenges for SAM MIM junctions. Depositing gold films on naturally flat substrates, such as mica, allows for overcoming the grainy nature of the metal surfaces. Lifting the mica off, exposes gold surfaces that, while composed of packed grains, adopt the topology of the flat substrates.[703] Such flat metal surfaces are superior electrodes for MIM junctions.[704]

Any pinhole defect can serve as a point of a short circuit and thoroughly compromise the performance of the device. Nevertheless, the balance of the interaction forces between the self-assembling molecules, the substrate surface and the solvent can drive the formation of SAMs with high fidelity. Many SAMs of long molecules can even assume two-dimensional crystalline structures.[705–708] The SAM molecules possesses functional group at one of their termini that can quickly form bonds with the substrate. In the initial phase, the molecules adsorb flat on the surface. Inherently, the intermolecular van der Waals interactions are always stronger than the interactions between these organic conjugates and the inorganic surfaces or the solvent, as the Hamaker constants can readily reveal (after all, like prefers like).[709,710] In alkyl SAMs, each methylene contributes about 0.07 eV to the heat of formation.[711] Therefore, as the surface density of the adsorbed species increases this balance between the van der Waals interactions drives the molecules to pack against each other (each molecule stretching nearly orthogonally to the surface) with their functional groups anchored to the substrate. The energetically favorable minimization of the contact area of each organic moiety with the inorganic surface and the solvent, while increasing the intermolecular contact area, drives the formation of such SAMs. Heating and occasional sonication during the self-assembly process aid the improvement of the quality of the molecular packing and the removal of the potential defects in the formed SAM.[712,713]

The ease of self-assembly of organic thiols into tightly packed layer on gold and other coinage metals, has made these surface structures the most widely used SAMs in chemistry, physics, and biology, in the last three decades.[641,642,714–717] The facile preparation of thiol SAMs has also impacted the field of molecular electronics.[718–720] Bringing a hanging mercury drop, coated with thiol SAM, into contact with another metal surface, coated with the same or different SAM, forms a MIM junction

that allows for characterizing the CTr properties of the molecular assemblies sandwiched between the conductive interfaces.[699–702,721] Instead of using a liquid metal, bringing in contact two orthogonally oriented SAM-coated metal wires also leads to the formation of a MIM junction.[722,723] The curvature of the wires, that are usually micrometre thick, determines the area of such crossed-wire junctions and even allows attainment of single-molecule contacts.[724,725]

Despite their immense popularity, however, SAMs of thiols on gold possess inherent properties that make them less than optimal for electronic applications. The susceptibility to oxidation of the sulphurs anchoring the organic molecules to the metal makes the SAMs vulnerable to damage and desorption. Under ambient conditions (even when immersed in protective liquid) their lack of durability sets major limitations. Therefore, using only freshly prepared thiol SAMs for the MIM junctions is essential for obtaining reliable and reproducible results.

On the other hand, silanization of silicon and metal oxides yields SAMs that are pronouncedly stable. SAMs of silanes, however, do not have the molecular order that thiol SAMs can achieve. Nevertheless, the immense durability of silane SAMs has made silanization a popular approach for introducing molecules into electrical junctions.[726–728]

Silanization anchors the organic molecules to silicon *via* C–Si–O–Si bonding patterns. Hence, the presence of a thin insulating layer of SiO_2 between the organic moieties and the Si semiconducting phase is usually unavoidable.[611,614,729–731] Attaching organic moieties directly to silicon *via* carbon–silicon bonds is the way to address this issue.[732,733] The C–Si bonds are immensely stable and the use of such organic coatings for passivating silicon surfaces is well established.[733,734] Similar to alkylthiols on coinage metals and mercury, alkyls on silicon can form densely packed and ordered SAMs.[735–738] Binding organic moieties to silicon directly *via* C–Si bonds is considerably more difficult and more involved than attaching thiols to gold. As a result, thiol SAMs on metals and chalcogenides have gained incomparable popularity for surface design and materials engineering.

Organic electronics offers countless functionalities that are easily attainable *via* established synthetic procedures. Electroconductive carbon materials provide excellent platforms not only for interfacing organic molecules in devices, but also for pursuing unprecedented possibilities for energy storage and energy conversion.[516,517,739–744] Silicon electronics, on the other hand, is mature and responsible for countless technological breakthroughs of the 20th and 21st centuries. Silicon electronic, therefore, is here to stay. To take advantage of the countless functionalities of that organic electronics can offer, it is essential to interface it with silicon. Placing efforts and resources on developing C–Si interfaces will set the stage for unprecedented technological advances driven by the unique features of the carbon, organic and biomolecular electronics.

Junctions with multiscale architectures

In many electrical junctions, it suffices to attach the molecule to only one of the electrodes. Liquid solution, which is conductive or containing an electron shuttle, establishes a "remote" electrical contact with the other electrode. That is, the junction comprises molecules sandwiched between a solid electrode and a liquid. Such liquid junctions have made enormous impacts on energy science and engineering, encompassing devices such as dye-sensitized solar cells (DSSCs), and other photoelectrochemical cells (PECs), along with various architectures for artificial photosynthesis and an "artificial leaf" (Fig. 15).[745–747] In fact, in the 19th century the first demonstration of the photovoltaic effect employed a liquid-junction device.[748]

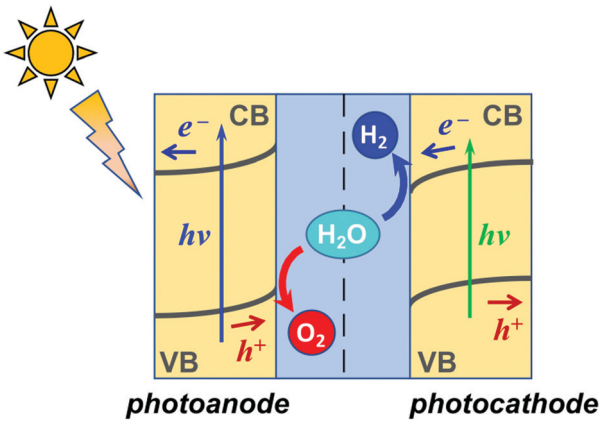

Fig. 15 Photoelectrochemical cell, PEC, for water splitting. The electrodes are semiconductors with different bandgaps and band-edge energies that allow cathodic water reduction and anodic oxidation to O_2. For broad-band semiconductors, photo sensitization with dyes or QDs is paramount to bring the absorption to the visible and NIR spectral regions. Auxiliary catalysts on the electrode surfaces can also improve the kinetics of O_2 and H_2 production.

PECs offer promising paths toward artificial photosynthesis and solar-fuel technologies. Water splitting has been a principal target of this quest (Fig. 15).[749–751] Photoreduction of water to hydrogen or kinetically stable hydrides opens routes not only for the production of other (carbon) solar fuels (from CO_2 reduction), but also for new synthetic chemistry, in general. Similar to natural photosynthesis, on the anodic side of such PEC designs, water serves as a sacrificial electron donor to produce O_2, while suppressing the formation of H_2O_2 and ROS (Fig. 15).[752] As an archetypical material for photoanodes, TiO_2 exists in several polymorphs[753] with rutile and anatase the most common and stable among them. Small-polaron hopping governs the electrical conductivity of TiO_2, which is typical for metal–oxide semiconductors.[206] Rutile polymorph readily forms localized small polarons regardless if it is pristine or has lattice defects. Anatase, on the other hand exhibits small polarons only in samples with defects or vacancies.[754,755] Strong coupling between the sites of e^- polarons in TiO_2 provides adiabatic regime for their hopping. Conversely, the hopping steps for the h^+ polarons in undoped TiO_2 are diabatic, resulting in hole mobilities that are substantially smaller than the electron ones.[206] This feature has made TiO_2 nanostructures the popular choice for anodes of n-type DSSCs.

DSSCs are PECs where the anodic and cathodic electrochemical conversions are coupled in a steady state. That is, after oxidation at the anode, a charge shuttle carries holes to

the cathode where it gets reduced to carry back electrons to the anode. This configuration converts the absorbed light into electrical energy, rather than into chemical fuels, *i.e.*, DSSCs are PV devices. Photoanodes drive the conversion of light to electrical energy in n-type DSSCs. Many of the materials of choice for photoanodes, however, are UV absorbers, which renders them inapplicable for solar-energy conversion. An electron-rich strongly absorbing dye, adsorbed on the surface of the photoanode material, therefore, acts as a photosensitizer driving efficient PET into the CB of the broad-band of the semiconductor. Photosensitizers based on ruthenium complexes have driven the development of the field. In the 2010s, porphyrin photosensitizers composed of only earth-abundant elements led to the development of DSSCs with the highest power conversion efficiencies.[756,757]

The liquid-mediated electric contact in such junctions permits significant freedoms for the geometry of the electrodes. DSSCs comprises an anode with highly porous morphology that not only provides a huge surface area for adsorbing monolayers of sensitizer, but also causes significant light scattering throughout the electrode active layer.[758,759]

The apparent need to utilize the cathode as a photocathode has driven development of p-type DSSCs.[751] In analogy with the n-type devices, metal–oxide semiconductors mediating high mobility of h^+ polarons, such as NiO,[206] are the principal building blocks for the photocathodes.[751,760] In this case, electron-deficient dyes are essential for undergoing efficient PHT into the VB of the semiconductor.[761–763]

Transitioning from DSSCs to PECs for production of solar fuels (Fig. 15) poses another key challenge: the good photosensitizers are usually terrible catalysts, and *vice versa*. In addition to sensitizing the broad-band semiconductor materials of the electrodes, it is essential to electronically couple to them catalysts for multielectron oxidation and reduction. This requirement places high demands on the metamaterials research for the development of robust multiscale architectures for photoelectrodes. Indeed, materials that strongly absorb visible and NIR light, and provide the needed potentials for driving the chemical conversions on the electrode surfaces, eliminate the need for sensitizers (Fig. 15).

Avoiding the use of liquids, bulk-heterojunction (BHJ) PV devices comprise blends of electron-donor and electron-acceptor solid materials.[764] The intertwining donor and acceptor phases in BHJs ensure: (1) a large contact area between the two phases, across which the initial photoinduced CT occurs; and (2) a decrease in the required distances for exciton migration to a CT interface.[765–767] The continuity of each phase provides electrical contact between the CT interface and the electrodes of the device.[768]

While PV devises mediate the conversion of light radiation into electrical energy, light-emitting diodes (LEDs) convert electrical currents into light.[769–772] Furthermore, at a molecular level, CT strongly impacts the optical properties of the systems.[52,773] In LEDs, CR produces excited states that deactivate radiatively. Nowadays, organic light-emitting diodes (OLEDs) are the mainstream in display technologies. Each new cell phone touts the latest in display technologies. The 30 year development from laboratory research to mass production is truly phenomenal.[774–776] Some of the latest developments encompass a variety of emitters that exhibit phosphorescence and thermally activated delayed fluorescence.[777] Hierarchical ultrastructures found in fireflies offer guidelines for bioinspired designs of OLED.[778] DNA bases can serve as hole-injection and hole-transport media in such devices. Specifically, comparison between adenine- and uracil-containing polymers shows that OLEDs containing the former exhibit improved thermal and redox stability, as well as solvent resistance due to increased cross-linking in the organic media.[779] Biomimetic brightness-enhancement layers reduce the reflection at the interfaces leading to improvements in the illumination efficiency of LEDs.[780]

The dominating common theme in molecular electronics is the focus on two-terminal devices. That is, the molecules serve as ''wires,'' rectifiers, light-energy converters, CT catalysts, and light emitters.

How about three-terminal devices, such as transistors, and even molecular integrated circuits? The immense challenges for wiring a molecule to two electrodes make the thoughts about electricals contact at three different points of a nanometre-size objects sound absurd. Nevertheless, the designs of three-terminal molecular devices is already on the way.[781] Furthermore, a third terminal, such as a transistor gate, does not necessarily require a direct electrical contact with the CT media, it just needs to be able to modulate its CTr properties by applying electrical potentials. This way of thinking has made the field-effect transistor (FET) architectures immensely popular in molecular and organic electronics.[782–786]

Light illumination provides another alternative for affecting the CTr properties of molecular and organic devices and it can serve as a ''third terminal'' in a device, which has set the stage for development of photosensors and numerous other optoelectronic devices.[787,788] Another important discovery, which is still in the realm of basic science, encompasses the utility of infrared radiation for affecting selected vibrational modes in the moieties mediating CT, and in this way, modulating the CT and CTr properties of the molecular systems.[789–792]

These examples illustrate how the discoveries in molecular and biological CT drive technological developments that have global impacts on improving our day-today lives. While many technologies are already mature, it is truly important to pursue novel ideas and paradigms that may appear as ''unappealing investment'' because currently they do not seem to have any direct application. Setting new ways of thinking at this point in time, however, is important for the technological impacts decades from now, and such ''long-term investments'' are key for sustainability of progress.

Conclusions

The multifaceted nature of charge transfer makes it vital for sustaining not only life on Earth, but also the modern ways of living. While many aspects of this fundamental process are still in the realm of basic science, the physical chemistry of charge transfer has provided key frameworks for understanding

biological processes and for advancing medicine, electronics and photonics. These advances unequivocally illustrate the global socioeconomic impacts of charge-transfer science.

List of abbreviations

Aa	Antranilamide
ADP	Adenosine diphosphate
ATP	Adenosine triphosphate
BHJ	Bulk-heterojunction
CA	Charge annihilation
CCD	Charge coupled device
CMOS	Complementary metal oxide semiconductor
CNS	Central nervous system
CoA	Coenzyme A
CR	Charge recombination
CS	Charge separation
CSh	Charge shift
CT	Charge transfer
CTr	Charge transport
DBA	Donor–bridge–acceptor
DBS	Deep brain stimulation
DNA	Deoxyribonucleic acid
DSA	Donor–sensitizer–acceptor
DSSC	Dye-sensitized solar cell
EAP	Electroacupuncture
EEG	Electroencephalography
EnT	Energy transfer
EKG	Electrocardiography
ESh	Electron shift
ET	Electron transfer
ETC	Electron-transfer chain
FC	Franck–Condon
FET	Field-effect transistor
G3P	Glyceraldehyde 3-phosphate
HH	Hole hopping
HOMO	Highest occupied molecular orbital
HSh	Hole shift
HT	Hole transfer
ISC	Intersystem crossing
I–V	Current–voltage
LE	Locally excited
LED	Light-emitting diodes
LUMO	Lowest unoccupied molecular orbital
MIM	Metal–insulator–metal
MH	Marcus–Hush
MLJ	Marcus–Levich–Jortner
MO	Molecular orbital
$NADP^+$	Nicotinamide adenine dinucleotide phosphate
NADPH	$NADP^+$ hydride
NIR	Near infrared
OLED	Organic light-emitting diodes
PC	Photocatalyst
PCA	Photoinduced charge annihilation
PCT	Photoinduced charge transfer
PCS	Photoinduced charge separation
PEC	Photoelectrochemical cell
PESh	Photoinduced electron shift
PET	Photoinduced electron transfer
PHT	Photoinduced hole transfer
PHSh	Photoinduced hole shit
PPI	Polyproline type I
PPII	Polyproline type II
PPP	Pentose phosphate pathway
PT	Proton transfer
PV	Photovoltaic
QD	Quantum dot
ROS	Reactive oxygen species
SAM	Self-assembled monolayers
SP	Special pair
STM	Scanning tunneling microscopy
UV	Ultraviolet
VN	Vagus nerve
VNS	Vagus nerve stimulation

Conflicts of interest

There are no conflicts to declare.

Acknowledgements

The U.S.A. National Science Foundation supported this work with a grant CHE 1800602, an AGEP supplement for J. A. Clark, and a GRFP support for J. Tamayo. The National Institutes of Health provided support for M. Morales (grant T34GM062756). We also extend our gratitude to Prof. Frank H. Quina from Instituto de Química da Universidade de São Paulo, São Paulo, Brazil, for the many fruitful discussions.

Notes and references

1 V. I. Vullev, *J. Phys. Chem. Lett.*, 2011, **2**, 503–508.
2 J. B. Derr, J. Tamayo, E. M. Espinoza, J. A. Clark and V. I. Vullev, *Can. J. Chem.*, 2018, **96**, 843–858.
3 A. W. Wood, A. Lajevardipour and R. L. McIntosh, *Int. J. Environ. Res. Public Health*, 2016, **13**, 950.
4 D. T. Pooley, *QJM*, 2010, **103**, 545–554.
5 K. Maeda, K. B. Henbest, F. Cintolesi, I. Kuprov, C. T. Rodgers, P. A. Liddell, D. Gust, C. R. Timmel and P. J. Hore, *Nature*, 2008, **453**, 387–390.
6 H. G. Hiscock, S. Worster, D. R. Kattnig, C. Steers, Y. Jin, D. E. Manolopoulos, H. Mouritsen and P. J. Hore, *Proc. Natl. Acad. Sci. U. S. A.*, 2016, **113**, 4634–4639.
7 U. Eichhoff and P. Hoefer, *Low Temp. Phys.*, 2015, **41**, 62–66.
8 A. Mukherjee, H. C. Davis, P. Ramesh, G. J. Lu and M. G. Shapiro, *Prog. Nucl. Magn. Reson. Spectrosc.*, 2017, **102–103**, 32–42.
9 M. Krzeszewski, E. M. Espinoza, C. Cervinka, J. B. Derr, J. A. Clark, D. Borchardt, G. J. O. Beran, D. T. Gryko and V. I. Vullev, *Angew. Chem., Int. Ed.*, 2018, **57**, 12365–12369.

10 D. Bao, S. Upadhyayula, J. M. Larsen, B. Xia, B. Georgieva, V. Nunez, E. M. Espinoza, J. D. Hartman, M. Wurch, A. Chang, C.-K. Lin, J. Larkin, K. Vasquez, G. J. O. Beran and V. I. Vullev, *J. Am. Chem. Soc.*, 2014, **136**, 12966–12973.
11 N. Lane, J. F. Allen and W. Martin, *BioEssays*, 2010, **32**, 271–280.
12 P. K. Jayaswal, V. Dogra, A. Shanker, T. R. Sharma and N. K. Singh, *PLoS One*, 2017, **12**, e0184276.
13 R. F. Service, *Science*, 2019, **366**, 292.
14 D. A. McCormick, in *From Molecules to Networks. An Introduction to Cellular and Molecular Neuroscience*, ed. J. H. Byrne, R. Heidelberger and M. N. Waxham, Elsevier Ltd., 3rd edn, 2014, pp. 351–376.
15 L. R. Dalton, P. A. Sullivan, D. H. Bale and B. C. Bricht, *Solid-State Electron.*, 2007, **51**, 1263–1277.
16 C. Groves, *Rep. Prog. Phys.*, 2017, **80**, 026502.
17 J. J. Warren, J. R. Winkler and H. B. Gray, *Coord. Chem. Rev.*, 2013, **257**, 165–170.
18 A. Operamolla, R. Ragni, F. Milano, R. R. Tangorra, A. Antonucci, A. Agostiano, M. Trotta and G. Farinola, *J. Mater. Chem. C*, 2015, **3**, 6471–6478.
19 R. Braakman, *Free Radical Biol. Med.*, 2019, **140**, 172–187.
20 G. J. Schut, O. Zadvornyy, C.-H. Wu, J. W. Peters, E. S. Boyd and M. W. W. Adams, *Biochim. Biophys. Acta, Bioenerg.*, 2016, **1857**, 958–970.
21 D. Shevela, L. O. Bjorn and Govindjee, in *Natural and Artificial Photosynthesis*, ed. R. Razeghifard, John Wiley & Sons, Inc., 2013, pp. 13–63.
22 L. O. Bjoern and Govindjee, *Curr. Sci.*, 2009, **96**, 1466–1474.
23 C. Koerner, *Nova Acta Leopold.*, 2004, **91**, 287–303.
24 G. Ciamician, *Science*, 1912, **36**, 385–394.
25 H. B. Gray, *Nat. Chem.*, 2009, **1**, 7.
26 K. W. J. Barnham, M. Mazzer and B. Clive, *Nat. Mater.*, 2006, **5**, 161–164.
27 R. Y. Guo, J. K. Gu, S. Zong, M. Wu and M. J. Yang, *Biomed. J.*, 2018, **41**, 9–20.
28 R. Z. Zhao, S. Jiang, L. Zhang and Z. B. Yu, *Int. J. Mol. Med.*, 2019, **44**, 3–15.
29 A. Serov, M. Padilla, A. J. Roy, P. Atanassov, T. Sakamoto, K. Asazawa and H. Tanaka, *Angew. Chem., Int. Ed.*, 2014, **53**, 10336–10339.
30 A. Kirubakaran, S. Jain and R. K. Nema, *Renewable Sustainable Energy Rev.*, 2009, **13**, 2430–2440.
31 E. D. Wachsman and K. T. Lee, *Science*, 2011, **334**, 935–939.
32 J. Tollefson, *Nature*, 2010, **464**, 1262–1264.
33 K. Rabaey and R. A. Rozendal, *Nat. Rev. Microbiol.*, 2010, **8**, 706–716.
34 H. A. Gasteiger and N. M. Markovic, *Science*, 2009, **324**, 48–49.
35 D. Bao, B. Millare, W. Xia, B. G. Steyer, A. A. Gerasimenko, A. Ferreira, A. Contreras and V. I. Vullev, *J. Phys. Chem. A*, 2009, **113**, 1259–1267.
36 D. Rehm and A. Weller, *Isr. J. Chem.*, 1970, **8**, 259–271.
37 D. Bao, S. Ramu, A. Contreras, S. Upadhyayula, J. M. Vasquez, G. Beran and V. I. Vullev, *J. Phys. Chem. B*, 2010, **114**, 14467–14479.
38 M. J. Bird, T. Iyoda, N. Bonura, J. Bakalis, A. J. Ledbetter and J. R. Miller, *J. Electroanal. Chem.*, 2017, **804**, 107–115.
39 G. E. Adams, I. R. Flockhart, C. E. Smithen, I. J. Stratford, P. Wardman and M. E. Watts, *Radiat. Res.*, 2012, **178**, AV183–AV189.
40 S. Goldstein, *J. Phys. Chem. A*, 2011, **115**, 8928–8932.
41 B. G. Ershov, E. Janata and A. V. Gordeeva, *Russ. Chem. Bull.*, 2008, **57**, 1821–1826.
42 K. Kobayashi, *Chem. Rev.*, 2019, **119**, 4413–4462.
43 V. I. Vullev and G. Jones, II, *J. Appl. Sci.*, 2005, **5**, 517–526.
44 S. Upadhyayula, V. Nunez, E. M. Espinoza, J. M. Larsen, D. Bao, D. Shi, J. T. Mac, B. Anvari and V. I. Vullev, *Chem. Sci.*, 2015, **6**, 2237–2251.
45 D. C. Grills, D. E. Polyansky and E. Fujita, *ChemSusChem*, 2017, **10**, 4359–4373.
46 P. Wardman and E. D. Clarke, *J. Chem. Soc., Faraday Trans.*, 1976, **72**, 1377–1390.
47 J. M. Larsen, E. M. Espinoza, J. D. Hartman, C.-K. Lin, M. Wurch, P. Maheshwari, R. K. Kaushal, M. J. Marsella, G. J. O. Beran and V. I. Vullev, *Pure Appl. Chem.*, 2015, **87**, 779–792.
48 J. M. Larsen, E. M. Espinoza and V. I. Vullev, *J. Photonics Energy*, 2015, **5**, 055598 (pp. 055591–055514).
49 E. M. Espinoza, B. Xia, N. Darabedian, J. M. Larsen, V. Nunez, D. Bao, J. T. Mac, F. Botero, M. Wurch, F. Zhou and V. I. Vullev, *Eur. J. Org. Chem.*, 2016, 343–356.
50 A. Purc, E. M. Espinoza, R. Nazir, J. J. Romero, K. Skonieczny, A. Jeżewski, J. M. Larsen, D. T. Gryko and V. I. Vullev, *J. Am. Chem. Soc.*, 2016, **138**, 12826–12832.
51 E. M. Espinoza, J. A. Clark, J. B. Derr, D. Bao, B. Georgieva, F. H. Quina and V. I. Vullev, *ACS Omega*, 2018, **3**, 12857–12867.
52 H. G. Ryu, M. F. Mayther, J. Tamayo, C. Azarias, E. M. Espinoza, M. Banasiewicz, L. G. Lukasiewicz, Y. M. Poronik, A. Jezewski, J. Clark, J. B. Derr, K. H. Ahn, D. T. Gryko, D. Jacquemin and V. I. Vullev, *J. Phys. Chem. C*, 2018, **122**, 13424–13434.
53 E. M. Espinoza, J. A. Clark, J. Soliman, J. B. Derr, M. Morales and V. I. Vullev, *J. Electrochem. Soc.*, 2019, **166**, H3175–H3187.
54 M. Born, *Z. Phys.*, 1920, **1**, 45–48.
55 L. Onsager, *J. Am. Chem. Soc.*, 1936, **58**, 1486–1493.
56 T. T. Duignan, D. F. Parsons and B. W. Ninham, *J. Phys. Chem. B*, 2013, **117**, 9412–9420.
57 J. G. Kirkwood, *J. Chem. Phys.*, 1934, **2**, 351–361.
58 A. Dejaegere and M. Karplus, *J. Phys. Chem.*, 1996, **100**, 11148–11164.
59 A. Namiki, N. Nakashima and K. Yoshihara, *J. Chem. Phys.*, 1979, **71**, 925–930.
60 S. M. Bonesi and R. Erra-Balsells, *J. Chem. Soc., Perkin Trans. 2*, 2000, 1583–1595.
61 G. A. Zalesskaya, E. G. Sambor and N. N. Belyi, *J. Appl. Spectrosc.*, 2003, **70**, 391–398.
62 T. Förster, *Discuss. Faraday Soc.*, 1959, **No. 27**, 7–17.
63 D. L. Dexter, *J. Chem. Phys.*, 1953, **21**, 836–850.
64 S. Treiling, C. Förster, F. Reichenauer, L. M. Carrella, E. Rentschler, K. Heinze, C. Wang, U. Resch-Genger,

C. Wang, J. Kalmbach, M. Seitz, P. Boden, M. Gerhards, J. P. Harris and C. Reber, *Angew. Chem., Int. Ed.*, 2019, **58**, 18075–18085.
65 C. Mongin, S. Garakyaraghi, N. Razgoniaeva, M. Zamkov and F. N. Castellano, *Science*, 2016, **351**, 369–372.
66 T. W. Schmidt and F. N. Castellano, *J. Phys. Chem. Lett.*, 2014, **5**, 4062–4072.
67 V. Gray, K. Moth-Poulsen, B. Albinsson and M. Abrahamsson, *Coord. Chem. Rev.*, 2018, **362**, 54–71.
68 Z. Huang and M. Lee Tang, *J. Phys. Chem. Lett.*, 2018, **9**, 6198–6206.
69 V. Gray, P. Xia, Z. Huang, E. Moses, A. Fast, D. A. Fishman, V. I. Vullev, M. Abrahamsson, K. Moth-Poulsen and M. Lee Tang, *Chem. Sci.*, 2017, **8**, 5488–5496.
70 P. Xia, Z. Huang, X. Li, J. J. Romero, V. I. Vullev, G. S. H. Pau and M. L. Tang, *Chem. Commun.*, 2017, **53**, 1241–1244.
71 Z. Huang, P. Xia, N. Megerdich, D. A. Fishman, V. I. Vullev and M. L. Tang, *ACS Photonics*, 2018, **5**, 3089–3096.
72 L. Huang, E. Kakadiaris, T. Vaneckova, K. Huang, M. Vaculovicova and G. Han, *Biomaterials*, 2019, **201**, 77–86.
73 J. Zhou, Q. Liu, W. Feng, Y. Sun and F. Li, *Chem. Rev.*, 2015, **115**, 395–465.
74 R. A. Marcus, *J. Chem. Phys.*, 1956, **24**, 966–978.
75 R. A. Marcus, *J. Chem. Phys.*, 1956, **24**, 979–989.
76 R. A. Marcus, *J. Chem. Phys.*, 1957, **26**, 867–871.
77 R. A. Marcus, *J. Chem. Phys.*, 1957, **26**, 872–877.
78 R. A. Marcus, *Annu. Rev. Phys. Chem.*, 1964, **15**, 155–196.
79 R. A. Marcus, *Rev. Mod. Phys.*, 1993, **65**, 599–610.
80 R. A. Marcus and N. Sutin, *Biochim. Biophys. Acta*, 1985, **811**, 265–322.
81 S. I. Pekar, *Zh. Eksp. Teor. Fiz.*, 1946, **16**, 341–348.
82 R. A. Marcus, *Angew. Chem., Int. Ed. Engl.*, 1993, **32**, 1111–1121.
83 N. S. Hush, *J. Chem. Phys.*, 1958, **28**, 962–972.
84 N. S. Hush, *Trans. Faraday Soc.*, 1961, **57**, 557–580.
85 V. G. Levich and R. R. Dogonadze, *Dokl. Akad. Nauk SSSR*, 1959, **124**, 123–126.
86 V. G. Levich and R. R. Dogonadze, *Dokl. Akad. Nauk SSSR*, 1960, **133**, 158–161.
87 R. R. Dogonadze, *Dokl. Akad. Nauk SSSR*, 1960, **133**, 1368–1371.
88 R. R. Dogonadze, *Dokl. Akad. Nauk SSSR*, 1962, **142**, 1108–1111.
89 V. G. Levich, R. R. Dogonadze and A. M. Kuznetsov, *Dokl. Akad. Nauk SSSR*, 1968, **179**, 137–140.
90 V. G. Levich, R. R. Dogonadze, E. D. German, A. M. Kuznetsov and Y. I. Kharkats, *Electrochim. Acta*, 1970, **15**, 353–367.
91 R. Kubo and Y. Toyozawa, *Prog. Theor. Phys.*, 1955, **13**, 160–182.
92 E. J. Piechota and G. J. Meyer, *J. Chem. Educ.*, 2019, **96**, 2450–2466.
93 S. Gelinas, A. Rao, A. Kumar, S. L. Smith, A. W. Chin, J. Clark, T. S. van der Poll, G. C. Bazan and R. H. Friend, *Science*, 2014, **343**, 512–516.
94 S. M. Falke, C. A. Rozzi, D. Brida, M. Maiuri, M. Amato, E. Sommer, A. De Sio, A. Rubio, G. Cerullo, E. Molinari and C. Lienau, *Science*, 2014, **344**, 1001–1005.
95 J. Jortner, *J. Chem. Phys.*, 1976, **64**, 4860–4867.
96 M. Bixon and J. Jortner, *J. Phys. Chem.*, 1991, **95**, 1941–1944.
97 J. L. Bredas, D. Beljonne, V. Coropceanu and J. Cornil, *Chem. Rev.*, 2004, **104**, 4971–5003.
98 G. Pourtois, D. Beljonne, J. Cornil, M. A. Ratner and J. L. Bredas, *J. Am. Chem. Soc.*, 2002, **124**, 4436–4447.
99 N. P. Redmore, I. V. Rubtsov and M. J. Therien, *J. Am. Chem. Soc.*, 2003, **125**, 8769–8778.
100 S. Di Motta, M. Siracusa and F. Negri, *J. Phys. Chem. C*, 2011, **115**, 20754–20764.
101 S. Chaudhuri, S. Hedstrom, D. D. Mendez-Hernandez, H. P. Hendrickson, K. A. Jung, J. Ho, V. S. Batista, S. Hedstrom, D. D. Mendez-Hernandez and J. Ho, *J. Chem. Theory Comput.*, 2017, **13**, 6000–6009.
102 N. E. Gruhn, D. A. da Silva, T. G. Bill, M. Malagoli, V. Coropceanu, A. Kahn and J. L. Bredas, *J. Am. Chem. Soc.*, 2002, **124**, 7918–7919.
103 H. Eyring, *J. Chem. Phys.*, 1935, **3**, 107–115.
104 M. G. Evans and M. Polanyi, *Trans. Faraday Soc.*, 1935, **31**, 0875–0893.
105 G. Jones, II, D. Yan, J. Hu, J. Wan, B. Xia and V. I. Vullev, *J. Phys. Chem. B*, 2007, **111**, 6921–6929.
106 J. Hu, B. Xia, D. Bao, A. Ferreira, J. Wan, G. Jones and V. I. Vullev, *J. Phys. Chem. A*, 2009, **113**, 3096–3107.
107 H. Yoshida and M. Ogasawara, *J. Radioanal. Nucl. Chem.*, 1986, **101**, 339–348.
108 N. Liang, J. R. Miller and G. L. Closs, *J. Am. Chem. Soc.*, 1990, **112**, 5353–5354.
109 P. Piotrowiak and J. R. Miller, *J. Phys. Chem.*, 1993, **97**, 13052–13060.
110 K. Ushida, Y. Yoshida, T. Kozawa, S. Tagawa and A. Kira, *J. Phys. Chem. A*, 1999, **103**, 4680–4689.
111 R. A. Marcus, *J. Chem. Phys.*, 1965, **43**, 2654–2657.
112 J. V. Beitz and J. R. Miller, *J. Chem. Phys.*, 1979, **71**, 4579–4595.
113 J. R. Miller, L. T. Calcaterra and G. L. Closs, *J. Am. Chem. Soc.*, 1984, **106**, 3047–3049.
114 J. R. Miller, J. V. Beitz and R. K. Huddleston, *J. Am. Chem. Soc.*, 1984, **106**, 5057–5068.
115 M. R. Wasielewski, M. P. Niemczyk, W. A. Svec and E. B. Pewitt, *J. Am. Chem. Soc.*, 1985, **107**, 1080–1082.
116 T. J. Penfold, E. Gindensperger, C. Daniel and C. M. Marian, *Chem. Rev.*, 2018, **118**, 6975–7025.
117 S. E. Braslavsky, *Pure Appl. Chem.*, 2007, **79**, 293–465.
118 I. R. Gould, J. E. Moser, B. Armitage, S. Farid, J. L. Goodman and M. S. Herman, *J. Am. Chem. Soc.*, 1989, **111**, 1917–1919.
119 T. M. McCleskey, J. R. Winkler and H. B. Gray, *J. Am. Chem. Soc.*, 1992, **114**, 6935–6937.
120 I. R. Gould, D. Noukakis, L. Gomezjahn, J. L. Goodman and S. Farid, *J. Am. Chem. Soc.*, 1993, **115**, 4405–4406.
121 C. Turro, J. M. Zaleski, Y. M. Karabatsos and D. G. Nocera, *J. Am. Chem. Soc.*, 1996, **118**, 6060–6067.
122 D. M. Guldi and K. D. Asmus, *J. Am. Chem. Soc.*, 1997, **119**, 5744–5745.
123 D. M. Guldi and K. D. Asmus, *J. Am. Chem. Soc.*, 1997, **119**, 9588.

124 G. Ruiz, F. RodriguezNieto, E. Wolcan and M. R. Feliz, *J. Photochem. Photobiol., A*, 1997, **107**, 47–54.
125 S. Canonica, B. Hellrung and J. Wirz, *J. Phys. Chem. A*, 2000, **104**, 1226–1232.
126 S. Fukuzumi, K. Ohkubo, H. Imahori and D. M. Guldi, *Chem. – Eur. J.*, 2003, **9**, 1585–1593.
127 R. A. Holroyd and J. R. Miller, *J. Phys. Chem. B*, 2019, **123**, 9206–9211.
128 J. Hong, O. A. Kharenko, J. Fan, F. Xie, A. K. Petros, B. R. Gibney and M. Y. Ogawa, *Angew. Chem., Int. Ed.*, 2006, **45**, 6137–6140.
129 G. A. Mines, M. J. Bjerrum, M. G. Hill, D. R. Casimiro, I. J. Chang, J. R. Winkler and H. B. Gray, *J. Am. Chem. Soc.*, 1996, **118**, 1961–1965.
130 I. R. Gould, R. Moody and S. Farid, *J. Am. Chem. Soc.*, 1988, **110**, 7242–7244.
131 H. Makita and G. Hastings, *Proc. Natl. Acad. Sci. U. S. A.*, 2017, **114**, 9267–9272.
132 E. M. Espinoza, D. Bao, M. Krzeszewski, D. T. Gryko and V. I. Vullev, *Int. J. Chem. Kinet.*, 2019, **51**, 657–668.
133 M. Kuss-Petermann and O. S. Wenger, *Phys. Chem. Chem. Phys.*, 2016, **18**, 18657–18664.
134 J. R. Winkler and H. B. Gray, *Chem. Rev.*, 1992, **92**, 369–379.
135 H. B. Gray and J. R. Winkler, *Q. Rev. Biophys.*, 2003, **36**, 341–372.
136 N. A. Romero and D. A. Nicewicz, *Chem. Rev.*, 2016, **116**, 10075–10166.
137 C. K. Prier, D. A. Rankic and D. W. C. MacMillan, *Chem. Rev.*, 2013, **113**, 5322–5363.
138 K. Goliszewska, K. Rybicka-Jasińska, J. A. Clark, V. I. Vullev and D. Gryko, *ACS Catal.*, 2020, **10**, 5920–5927.
139 M. D. Newton, *Coord. Chem. Rev.*, 2003, **238**, 167–185.
140 H. Mcconnell, *J. Chem. Phys.*, 1961, **35**, 508–515.
141 B. P. Paulson, J. R. Miller, W. X. Gan and G. Closs, *J. Am. Chem. Soc.*, 2005, **127**, 4860–4868.
142 O. S. Wenger, *Acc. Chem. Res.*, 2011, **44**, 25–35.
143 H. B. Gray and J. R. Winkler, *Proc. Natl. Acad. Sci. U. S. A.*, 2005, **102**, 3534–3539.
144 J. F. O'Donnell and C. K. Mann, *J. Electroanal. Chem. Interfacial Electrochem.*, 1967, **13**, 157–162.
145 C. C. Moser, C. C. Page, R. Farid and P. L. Dutton, *J. Bioenerg. Biomembr.*, 1995, **27**, 263–274.
146 D. N. Beratan, J. N. Onuchic, J. R. Winkler and H. B. Gray, *Science*, 1992, **258**, 1740–1741.
147 J. N. Betts, D. N. Beratan and J. N. Onuchic, *J. Am. Chem. Soc.*, 1992, **114**, 4043–4046.
148 C. C. Page, C. C. Moser, X. Chen and P. L. Dutton, *Nature*, 1999, **402**, 47–52.
149 C. C. Page, C. C. Moser and P. L. Dutton, *Curr. Opin. Chem. Biol.*, 2003, **7**, 551–556.
150 D. N. Beratan, J. N. Betts and J. N. Onuchic, *Science*, 1991, **252**, 1285–1288.
151 M. L. Tan, I. Balabin and J. N. Onuchic, *Biophys. J.*, 2004, **86**, 1813–1819.
152 J. N. Onuchic and D. N. Beratan, *J. Am. Chem. Soc.*, 1987, **109**, 6771–6778.
153 S. S. Skourtis, D. N. Beratan and D. H. Waldeck, *Procedia Chem.*, 2011, **3**, 99–104.
154 T. R. Prytkova, I. V. Kurnikov and D. N. Beratan, *Science*, 2007, **315**, 622–625.
155 I. A. Balabin and J. N. Onuchic, *Science*, 2000, **290**, 114–117.
156 G. I. Likhtenshtein, *J. Photochem. Photobiol., A*, 1996, **96**, 79–92.
157 S. J. Jang and M. D. Newton, *J. Chem. Phys.*, 2005, **122**, 024501.
158 S. S. Skourtis, I. A. Balabin, T. Kawatsu and D. N. Beratan, *Proc. Natl. Acad. Sci. U. S. A.*, 2005, **102**, 3552–3557.
159 W. W. Zhang, Y. Zhao and W. Z. Liang, *Sci. China: Chem.*, 2011, **54**, 707–714.
160 M. G. Mavros, D. Hait and T. Van Voorhis, *J. Chem. Phys.*, 2016, **145**, 214105.
161 D. N. Beratan, C. R. Liu, A. Migliore, N. F. Polizzi, S. S. Skourtis, P. Zhang and Y. Q. Zhang, *Acc. Chem. Res.*, 2015, **48**, 474–481.
162 Y. Q. Zhang, C. R. Liu, A. Balaeff, S. S. Skourtis and D. N. Beratan, *Proc. Natl. Acad. Sci. U. S. A.*, 2014, **111**, 10049–10054.
163 J. Jortner, M. Bixon, T. Langenbacher and M. E. Michel-Beyerle, *Proc. Natl. Acad. Sci. U. S. A.*, 1998, **95**, 12759–12765.
164 F. C. Grozema, Y. A. Berlin and L. D. A. Siebbeles, *J. Am. Chem. Soc.*, 2000, **122**, 10903–10909.
165 B. Giese, J. Amaudrut, A. K. Köhler, M. Spormann and S. Wessely, *Nature*, 2001, **412**, 318–320.
166 Y. A. Berlin, A. L. Burin and M. A. Ratner, *J. Am. Chem. Soc.*, 2001, **123**, 260–268.
167 M. Bixon and J. Jortner, *J. Am. Chem. Soc.*, 2001, **123**, 12556–12567.
168 C. Lambert, G. Nöll and J. Schelter, *Nat. Mater.*, 2002, **1**, 69–73.
169 G. R. Hutchison, M. A. Ratner and T. J. Marks, *J. Am. Chem. Soc.*, 2005, **127**, 16866–16881.
170 M. J. Tauber, R. F. Kelley, J. M. Giaimo, B. Rybtchinski and M. R. Wasielewski, *J. Am. Chem. Soc.*, 2006, **128**, 1782–1783.
171 K. Susumu, P. R. Frail, P. J. Angiolillo and M. J. Therien, *J. Am. Chem. Soc.*, 2006, **128**, 8380–8381.
172 C. Shih, A. K. Museth, M. Abrahamsson, A. M. Blanco-Rodriguez, A. J. Di Bilio, J. Sudhamsu, B. R. Crane, K. L. Ronayne, M. Towrie, A. Vlcek, Jr., J. H. Richards, J. R. Winkler and H. B. Gray, *Science*, 2008, **320**, 1760–1762.
173 M. Cordes and B. Giese, *Chem. Soc. Rev.*, 2009, **38**, 892–901.
174 R. Venkatramani, S. Keinan, A. Balaeff and D. N. Beratan, *Coord. Chem. Rev.*, 2011, **255**, 635–648.
175 X. S. Li, N. Markandeya, G. Jonusauskas, N. D. McClenaghan, V. Maurizot, S. A. Denisov and I. Huc, *J. Am. Chem. Soc.*, 2016, **138**, 13568–13578.
176 S. D. Kang and G. J. Snyder, *Nat. Mater.*, 2017, **16**, 252–257.
177 A. Mendez-Ardoy, N. Markandeya, X. Li, Y.-T. Tsai, G. Pecastaings, T. Buffeteau, V. Maurizot, L. Muccioli, F. Castet, I. Huc and D. M. Bassani, *Chem. Sci.*, 2017, **8**, 7251–7257.
178 T. Brittain, *Protein Pept. Lett.*, 2008, **15**, 556–561.
179 G. Lenaz and M. L. Genova, *Am. J. Physiol.*, 2007, **292**, C1221–C1239.

180 E. Odella, S. J. Mora, B. L. Wadsworth, M. T. Huynh, J. J. Goings, P. A. Liddell, T. L. Groy, M. Gervaldo, L. E. Sereno, D. Gust, T. A. Moore, G. F. Moore, S. Hammes-Schiffer and A. L. Moore, *J. Am. Chem. Soc.*, 2018, **140**, 15450–15460.
181 E. Odella, B. L. Wadsworth, S. J. Mora, J. J. Goings, M. T. Huynh, D. Gust, T. A. Moore, G. F. Moore, S. Hammes-Schiffer and A. L. Moore, *J. Am. Chem. Soc.*, 2019, **141**, 14057–14061.
182 S. Hammes-Schiffer, *J. Am. Chem. Soc.*, 2015, **137**, 8860–8871.
183 S. Hammes-Schiffer, *Energy Environ. Sci.*, 2012, **5**, 7696–7703.
184 V. R. I. Kaila, *J. R. Soc., Interface*, 2018, **15**, 20170916.
185 S. Hammes-Schiffer, *Acc. Chem. Res.*, 2009, **42**, 1881–1889.
186 G. SteinbergYfrach, P. A. Liddell, S. C. Hung, A. L. Moore, D. Gust and T. A. Moore, *Nature*, 1997, **385**, 239–241.
187 G. Steinberg-Yfrach, J. L. Rigaud, E. N. Durantini, A. L. Moore, D. Gust and T. A. Moore, *Nature*, 1998, **392**, 479–482.
188 I. M. Bennett, H. M. V. Farfano, F. Bogani, A. Primak, P. A. Liddell, L. Otero, L. Sereno, J. J. Silber, A. L. Moore, T. A. Moore and D. Gust, *Nature*, 2002, **420**, 398–401.
189 S. D. Straight, G. Kodis, Y. Terazono, M. Hambourger, T. A. Moore, A. L. Moore and D. Gust, *Nat. Nanotechnol.*, 2008, **3**, 280–283.
190 J. Liu, X. Huang, F. Wang and W. Hong, *Acc. Chem. Res.*, 2019, **52**, 151–160.
191 M. A. Awais, Z. Cai, N. Zhang and L. Yu, *Chem. – Eur. J.*, 2018, **24**, 17180–17187.
192 A. Syed and J. A. Tainer, *ACS Cent. Sci.*, 2019, **5**, 7–9.
193 R. Zhuravel, A. Stern, N. Fardian-Melamed, G. Eidelshtein, L. Katrivas, D. Rotem, A. B. Kotlyar and D. Porath, *Adv. Mater.*, 2018, **30**, 1706984.
194 D. Vuillaume, *ChemPlusChem*, 2019, **84**, 1215–1221.
195 S. L. Rudge and D. S. Kosov, *J. Chem. Phys.*, 2019, **151**, 034107.
196 J. Juhaniewicz, J. Pawlowski and S. Sek, *Isr. J. Chem.*, 2015, **55**, 645–660.
197 V. Mujica and M. A. Ratner, *Chem. Phys.*, 2001, **264**, 365–370.
198 M. A. Rampi and G. M. Whitesides, *Chem. Phys.*, 2002, **281**, 373–391.
199 R. Härtle and M. Thoss, *Phys. Rev. B: Condens. Matter Mater. Phys.*, 2011, **83**, 115414.
200 J. O. Thomas, B. Limburg, J. K. Sowa, K. Willick, J. Baugh, G. A. D. Briggs, E. M. Gauger, H. L. Anderson and J. A. Mol, *Nat. Commun.*, 2019, **10**, 4628.
201 Q. Arnoux, A. Boucly, V. Barth, R. Benbalagh, A. Cossaro, L. Floreano, M. Silly, F. Sirotti, E. Derat, S. Carniato, F. Bournel, J.-J. Gallet, D. Fichou, L. Tortech and F. Rochet, *ACS Appl. Mater. Interfaces*, 2017, **9**, 30992–31004.
202 T. H. Schloemer, A. Sellinger, J. A. Christians, J. M. Luther, A. Sellinger, J. A. Christians and A. Sellinger, *Chem. Sci.*, 2019, **10**, 1904–1935.
203 C. Rodriguez-Seco, L. Cabau, A. Vidal-Ferran and E. Palomares, *Acc. Chem. Res.*, 2018, **51**, 869–880.
204 F. D. Lewis, R. M. Young and M. R. Wasielewski, *Acc. Chem. Res.*, 2018, **51**, 1746–1754.
205 M. A. Harris, A. K. Mishra, R. M. Young, K. E. Brown, M. R. Wasielewski and F. D. Lewis, *J. Am. Chem. Soc.*, 2016, **138**, 5491–5494.
206 I. G. Austin and N. F. Mott, *Adv. Phys.*, 1969, **18**, 41–102.
207 M. Scheele, *Z. Phys. Chem.*, 2015, **229**, 167–178.
208 D. Meggiolaro, F. Ambrosio, E. Mosconi, A. Mahata and F. De Angelis, *Adv. Energy Mater.*, 2020, **10**, 1902748.
209 Y. Natanzon, A. Azulay and Y. Amouyal, *Isr. J. Chem.*, 2020, DOI: 10.1002/ijch.201900101.
210 L. Landau, *Phys. Z. Sowjetunion*, 1933, **3**, 664–665.
211 S. I. Pekar, *Исследования по электроррой теории кристаллов (Studies on the Electron Theory of Crystals)*, Gosudarstvennoe Izdatel'stvo Tekh.-Teoret. Lit., 1951.
212 N. A. Deskins and M. Dupuis, *Phys. Rev. B: Condens. Matter Mater. Phys.*, 2007, **75**, 195212.
213 A. Yildiz, S. B. Lisesivdin, M. Kasap and D. Mardare, *Phys. B*, 2009, **404**, 1423–1426.
214 N. A. Deskins and M. Dupuis, *J. Phys. Chem. C*, 2009, **113**, 346–358.
215 R. A. Marcus, *Discuss. Faraday Soc.*, 1960, 21–31.
216 S. Yomosa, *Suppl. Prog. Theor. Phys.*, 1967, 249–263.
217 S. G. Boxer, *Annu. Rev. Biophys. Biophys. Chem.*, 1990, **19**, 267–299.
218 S. Tanaka and R. A. Marcus, *J. Phys. Chem. B*, 1997, **101**, 5031–5045.
219 M. A. Steffen, K. Q. Lao and S. G. Boxer, *Science*, 1994, **264**, 810–816.
220 E. Galoppini and M. A. Fox, *J. Am. Chem. Soc.*, 1996, **118**, 2299–2300.
221 M. A. Fox and E. Galoppini, *J. Am. Chem. Soc.*, 1997, **119**, 5277–5285.
222 A. Knorr, E. Galoppini and M. A. Fox, *J. Phys. Org. Chem.*, 1997, **10**, 484–498.
223 D. J. Lockhart and P. S. Kim, *Science*, 1992, **257**, 947–951.
224 R. Singh, *J. Electrost.*, 2014, **72**, 322–329.
225 F.-S. Guo, A. K. Bar and R. A. Layfield, *Chem. Rev.*, 2019, **119**, 8479–8505.
226 O. Cador, B. Le Guennic, L. Ouahab and F. Pointillart, *Eur. J. Inorg. Chem.*, 2020, 148–164.
227 A. Wada, *J. Chem. Phys.*, 1958, **29**, 674–675.
228 A. Wada, *J. Chem. Phys.*, 1959, **30**, 328–329.
229 A. Wada, *J. Chem. Phys.*, 1959, **31**, 495–500.
230 W. G. J. Hol, P. T. Van Duijnen and H. J. C. Berendsen, *Nature*, 1978, **273**, 443–446.
231 Y.-G. K. Shin, M. D. Newton and S. S. Isied, *J. Am. Chem. Soc.*, 2003, **125**, 3722–3732.
232 J. W. Hovick and J. C. Poler, *J. Chem. Educ.*, 2005, **82**, 889.
233 A. Wada, *Adv. Biophys.*, 1976, **9**, 1–63.
234 S. Yamabe and K. Morokuma, *J. Am. Chem. Soc.*, 1975, **97**, 4458–4465.
235 M. Kuemin, S. Schweizer, C. Ochsenfeld and H. Wennemers, *J. Am. Chem. Soc.*, 2009, **131**, 15474–15482.
236 T. J. El-Baba, D. R. Fuller, D. E. Clemmer, D. A. Hales and D. H. Russell, *J. Am. Soc. Mass Spectrom*, 2019, **30**, 77–84.
237 W. G. J. Hol, *Prog. Biophys. Mol. Biol.*, 1985, **45**, 149–195.

238 D. A. Doyle, J. M. Cabral, R. A. Pfuetzner, A. Kuo, J. M. Gulbis, S. L. Cohen, B. T. Chait and R. MacKinnon, *Science*, 1998, **280**, 69–77.
239 R. Dutzler, E. B. Campbell, M. Cadene, B. T. Chait and R. MacKinnon, *Nature*, 2002, **415**, 287–294.
240 H. Wang, L. P. McIntosh and B. J. Graves, *J. Biol. Chem.*, 2002, **277**, 2225–2233.
241 S. De, M. Okon, B. J. Graves and L. P. McIntosh, *J. Mol. Biol.*, 2016, **428**, 1515–1530.
242 S. D. Fried, S. Bagchi and S. G. Boxer, *Science*, 2014, **346**, 1510–1514.
243 D. s. M. M. Jaradat, *Amino Acids*, 2018, **50**, 39–68.
244 R. Behrendt, P. White and J. Offer, *J. Pept. Sci.*, 2016, **22**, 4–27.
245 P. R. Hansen and A. Oddo, *Methods Mol. Biol.*, 2015, **1348**, 33–50.
246 J. M. Palomo, *RSC Adv.*, 2014, **4**, 32658–32672.
247 V. Maede, S. Els-Heindl and A. G. Beck-Sickinger, *Beilstein J. Org. Chem.*, 2014, **10**, 1197–1212, 1116 pp.
248 K. J. Jensen, *Methods Mol. Biol.*, 2013, **1047**, 1–21.
249 S. Yasutomi, T. Morita, Y. Imanishi and S. Kimura, *Science*, 2004, **304**, 1944–1947.
250 C. Shlizerman, A. Atanassov, I. Berkovich, G. Ashkenasy and N. Ashkenasy, *J. Am. Chem. Soc.*, 2010, **132**, 5070–5076.
251 J. A. Gao, P. Muller, M. Wang, S. Eckhardt, M. Lauz, K. M. Fromm and B. Giese, *Angew. Chem., Int. Ed.*, 2011, **50**, 1926–1930.
252 L. Garbuio, S. Antonello, I. Guryanov, Y. Li, M. Ruzzi, N. J. Turro and F. Maran, *J. Am. Chem. Soc.*, 2012, **134**, 10628–10637.
253 M. Lauz, S. Eckhardt, K. M. Fromm and B. Giese, *Phys. Chem. Chem. Phys.*, 2012, **14**, 13785–13788.
254 I. Swierszcz, P. Skurski and J. Simons, *J. Phys. Chem. A*, 2012, **116**, 1828–1837.
255 O. Cramariuc, P. J. Aittala and T. I. Hukka, *J. Mol. Model.*, 2013, **19**, 697–704.
256 I. Anusiewicz, P. Skurski and J. Simons, *J. Phys. Chem. B*, 2014, **118**, 7892–7901.
257 J. Wang, P. E. Videla and V. S. Batista, *Protein Sci.*, 2017, **26**, 1692–1697.
258 Y. Chen, J. Viereck, R. Harmer, S. Rangan, R. A. Bartynski and E. Galoppini, *J. Am. Chem. Soc.*, 2020, **142**, 3489–3498.
259 A. Vilan, A. Shanzer and D. Cahen, *Nature*, 2000, **404**, 166–168.
260 Y. Selzer and D. Cahen, *Adv. Mater.*, 2001, **13**, 508–511.
261 A. M. Munro, B. Zacher, A. Graham and N. R. Armstrong, *ACS Appl. Mater. Interfaces*, 2010, **2**, 863–869.
262 N. Kedem, S. Blumstengel, F. Henneberger, H. Cohen, G. Hodes and D. Cahen, *Phys. Chem. Chem. Phys.*, 2014, **16**, 8310–8319.
263 P. R. Brown, D. Kim, R. R. Lunt, N. Zhao, M. G. Bawendi, J. C. Grossman and V. Bulovic, *ACS Nano*, 2014, **8**, 5863–5872.
264 M. Jesper, M. Alt, J. Schinke, S. Hillebrandt, I. Angelova, V. Rohnacher, A. Pucci, U. Lemmer, W. Jaegermann, W. Kowalsky, T. Glaser, E. Mankel, R. Lovrincic, F. Golling, M. Hamburger and U. H. F. Bunz, *Langmuir*, 2015, **31**, 10303–10309.
265 P. K. Santra, A. F. Palmstrom, J. T. Tanskanen, N. Yang and S. F. Bent, *J. Phys. Chem. C*, 2015, **119**, 2996–3005.
266 J. Nieto-Pescador, B. Abraham, J. J. Li, A. Batarseh, R. A. Bartynski, E. Galoppini and L. Gundlach, *J. Phys. Chem. C*, 2016, **120**, 48–55.
267 K. T. Ngo, J. Rochford, H. Fan, A. Batarseh, K. Chitre, S. Rangan, R. A. Bartynski and E. Galoppini, *Faraday Discuss.*, 2015, **185**, 497–506.
268 M. I. Nugraha, H. Matsui, S. Z. Bisri, M. Sytnyk, W. Heiss, M. A. Loi and J. Takeya, *APL Mater.*, 2016, **4**, 116105.
269 D. M. Kroupa, M. Voros, N. P. Brawand, B. W. McNichols, E. M. Miller, J. Gu, A. J. Nozik, A. Sellinger, G. Galli and M. C. Beard, *Nat. Commun.*, 2017, **8**, 15257.
270 D. M. Kroupa, M. Voros, N. P. Brawand, N. Bronstein, B. W. McNichols, C. V. Castaneda, A. J. Nozik, A. Sellinger, G. Galli and M. C. Beard, *J. Phys. Chem. Lett.*, 2018, **9**, 3425–3433.
271 F. Rabanal, B. R. Gibney, W. F. DeGrado, C. C. Moser and P. L. Dutton, *Inorg. Chim. Acta*, 1996, **243**, 213–218.
272 M. W. Mutz, G. L. McLendon, J. F. Wishart, E. R. Gaillard and A. F. Corin, *Proc. Natl. Acad. Sci. U. S. A.*, 1996, **93**, 9521–9526.
273 M. W. Mutz, J. F. Wishart and G. L. McLendon, *Adv. Chem. Ser.*, 1998, **254**, 145–159.
274 G. Jones, II, V. Vullev, E. H. Braswell and D. Zhu, *J. Am. Chem. Soc.*, 2000, **122**, 388–389.
275 A. Y. Kornilova, J. F. Wishart, W. Xiao, R. C. Lasey, A. Fedorova, Y.-K. Shin and M. Y. Ogawa, *J. Am. Chem. Soc.*, 2000, **122**, 7999–8006.
276 G. Jones, II and V. I. Vullev, *Org. Lett.*, 2002, **4**, 4001–4004.
277 V. I. Vullev and G. Jones, II, *Res. Chem. Intermed.*, 2002, **28**, 795–815.
278 L. Cristian, P. Piotrowiak and R. S. Farid, *J. Am. Chem. Soc.*, 2003, **125**, 11814–11815.
279 G. Jones, II, X. Zhou and V. I. Vullev, *Photochem. Photobiol. Sci.*, 2003, **2**, 1080–1087.
280 S. A. Serron, W. S. Aldridge, C. N. Fleming, R. M. Danell, M. H. Baik, M. Sykora, D. M. Dattelbaum and T. J. Meyer, *J. Am. Chem. Soc.*, 2004, **126**, 14506–14514.
281 M. H. V. Huynh, D. M. Dattelbaum and T. J. Meyer, *Coord. Chem. Rev.*, 2005, **249**, 457–483.
282 P. B. Harbury, T. Zhang, P. S. Kim and T. Alber, *Science*, 1993, **262**, 1401–1407.
283 D. E. Robertson, R. S. Farid, C. C. Moser, J. L. Urbauer, S. E. Mulholland, R. Pidikiti, J. D. Lear, A. J. Wand, W. F. DeGrado and P. L. Dutton, *Nature*, 1994, **368**, 425–432.
284 S. Kimura, *Org. Biomol. Chem.*, 2008, **6**, 1143–1148.
285 G. Jones, II and V. I. Vullev, *Org. Lett.*, 2001, **3**, 2457–2460.
286 G. Jones, II and V. I. Vullev, *J. Phys. Chem. A*, 2001, **105**, 6402–6406.
287 C. T. Choma, J. D. Lear, M. J. Nelson, P. L. Dutton, D. E. Robertson and W. F. DeGrado, *J. Am. Chem. Soc.*, 1994, **116**, 856–865.
288 F. Rabanal, W. F. DeGrado and P. L. Dutton, *J. Am. Chem. Soc.*, 1996, **118**, 473–474.

289 G. V. Kozlov and M. Y. Ogawa, *J. Am. Chem. Soc.*, 1997, **119**, 8377–8378.
290 V. I. Vullev and G. Jones, *Tetrahedron Lett.*, 2002, **43**, 8611–8615.
291 A. Fedorova, A. Chaudhari and M. Y. Ogawa, *J. Am. Chem. Soc.*, 2003, **125**, 357–362.
292 L. Liu, J. Hong and M. Y. Ogawa, *J. Am. Chem. Soc.*, 2004, **126**, 50–51.
293 M. Boncheva and H. Vogel, *Biophys. J.*, 1997, **73**, 1056–1072.
294 K. Kitagawa, T. Morita and S. Kimura, *J. Phys. Chem. B*, 2005, **109**, 13906–13911.
295 S. Sek, K. Swiatek and A. Misicka, *J. Phys. Chem. B*, 2005, **109**, 23121–23124.
296 S. Sek, A. Misicka, K. Swiatek and E. Maicka, *J. Phys. Chem. B*, 2006, **110**, 19671–19677.
297 H. Uji, K. Tanaka and S. Kimura, *J. Phys. Chem. C*, 2016, **120**, 3684–3689.
298 H. Uji, Y. Yatsunami and S. Kimura, *J. Phys. Chem. C*, 2015, **119**, 8054–8061.
299 T. Kaindl, K. Adlkofer, T. Morita, J. Umemura, O. Konovalov, S. Kimura and M. Tanaka, *J. Phys. Chem. C*, 2010, **114**, 22677–22683.
300 K. Kitagawa, T. Morita and S. Kimura, *Langmuir*, 2005, **21**, 10624–10631.
301 T. Morita, K. Yanagisawa and S. Kimura, *Polym. J.*, 2008, **40**, 700–709.
302 S. Okamoto, T. Morita and S. Kimura, *Langmuir*, 2009, **25**, 3297–3304.
303 H. Uji, T. Ito, M. Matsumoto and S. Kimura, *J. Phys. Chem. A*, 2016, **120**, 1190–1196.
304 G. Jones, II, L. N. Lu, V. Vullev, D. Gosztola, S. Greenfield and M. Wasielewski, *Bioorg. Med. Chem. Lett.*, 1995, **5**, 2385–2390.
305 K. Kawai and T. Majima, *Acc. Chem. Res.*, 2013, **46**, 2616–2625.
306 M. K. Ashraf, R. R. Pandey, R. K. Lake, B. Millare, A. A. Gerasimenko, D. Bao and V. I. Vullev, *Biotechnol. Prog.*, 2009, **25**, 915–922.
307 B. Xia, D. Bao, S. Upadhyayula, G. Jones and V. I. Vullev, *J. Org. Chem.*, 2013, **78**, 1994–2004.
308 E. M. Espinoza, J. M. Larsen and V. I. Vullev, *J. Phys. Chem. Lett.*, 2016, **7**, 758–764.
309 E. M. Espinoza, J. M. Larsen and V. I. Vullev, *ECS Trans.*, 2015, **66**, 1–9.
310 J. M. Larsen-Clinton, E. M. Espinoza, M. F. Mayther, J. Clark, C. Tao, D. Bao, C. M. Larino, M. Wurch, S. Lara and V. I. Vullev, *Phys. Chem. Chem. Phys.*, 2017, **19**, 7871–7876.
311 E. M. Espinoza, J. M. Larsen-Clinton, M. Krzeszewski, N. Darabedian, D. T. Gryko and V. I. Vullev, *Pure Appl. Chem.*, 2017, **89**, 1777–1797.
312 E. M. Espinoza and V. I. Vullev, *ECS Trans.*, 2017, **77**, 1517–1523.
313 K. Skonieczny, E. M. Espinoza, J. B. Derr, M. Morales, J. M. Clinton, B. Xia and V. I. Vullev, *Pure Appl. Chem.*, 2020, **92**, 275–299.
314 J. B. Derr, J. A. Clark, M. Morales, E. M. Espinoza, S. Vadhin and V. I. Vullev, *RSC Adv.*, 2020, **10**, 24419–24424.
315 S. Upadhyayula, D. Bao, B. Millare, S. S. Sylvia, K. M. M. Habib, K. Ashraf, A. Ferreira, S. Bishop, R. Bonderer, S. Baqai, X. Jing, M. Penchev, M. Ozkan, C. S. Ozkan, R. K. Lake and V. I. Vullev, *J. Phys. Chem. B*, 2011, **115**, 9473–9490.
316 J. Wan, A. Ferreira, W. Xia, C. H. Chow, K. Takechi, P. V. Kamat, G. Jones and V. I. Vullev, *J. Photochem. Photobiol., A*, 2008, **197**, 364–374.
317 E. Kaiser, V. C. Galvis and U. Armbruster, *Biochem. J.*, 2019, **476**, 2725–2741.
318 E. L. Harrison, L. Arce Cubas, J. E. Gray and C. Hepworth, *Plant J.*, 2020, **101**, 768–779.
319 S. Al-Attar and S. de Vries, *Coord. Chem. Rev.*, 2013, **257**, 64–80.
320 E. A. Schon and N. A. Dencher, *Cell Metab.*, 2009, **9**, 1–3.
321 C. T. Straub, B. M. Zeldes, G. J. Schut, M. W. W. Adams and R. M. Kelly, *Curr. Opin. Biotechnol*, 2017, **45**, 104–112.
322 M. Basen and V. Mueller, *Extremophiles*, 2017, **21**, 15–26.
323 E. R. Donati, C. Castro and M. S. Urbieta, *World J. Microbiol. Biotechnol.*, 2016, **32**, 1–8.
324 J. De Vrieze, D. Smet, J. Klok, J. Colsen, L. T. Angenent and S. E. Vlaeminck, *Bioresour. Technol.*, 2016, **218**, 1237–1245.
325 M. Keller, A. Loder, M. Basen, J. Izquierdo, R. M. Kelly and M. W. W. Adams, *Biofuels*, 2014, **5**, 499–515.
326 D. I. Arnon, *Photosynth. Res.*, 1991, **29**, 117–131.
327 R. Pascal and L. Boiteau, *Philos. Trans. R. Soc., B*, 2011, **366**, 2949–2958.
328 H. C. Hesse, M. Schimpe, D. Kucevic and A. Jossen, *Energies*, 2017, **10**, 2107.
329 W. D. Zeng, Y. M. Cao, Y. Bai, Y. H. Wang, Y. S. Shi, M. Zhang, F. F. Wang, C. Y. Pan and P. Wang, *Chem. Mater.*, 2010, **22**, 1915–1925.
330 T. T. Zhu and M. Dittrich, *Front. Bioeng. Biotechnol.*, 2016, **4**, 4.
331 M. P. Johnson, *Essays Biochem.*, 2016, **60**, 255–273.
332 J. Beld, D. J. Lee and M. D. Burkart, *Mol. BioSyst.*, 2015, **11**, 38–59.
333 S. Zhang, Q. Fan, R. Xia and T. J. Meyer, *Acc. Chem. Res.*, 2020, **53**, 255–264.
334 J. O. Taylor, Y. Wang and F. Hartl, *ChemCatChem*, 2020, **12**, 386–393.
335 U. O. Nwabara, E. R. Cofell, S. Verma, E. Negro and P. J. A. Kenis, *ChemSusChem*, 2020, **13**, 855–875.
336 R. Kas, K. Yang, D. Bohra, R. Kortlever, T. Burdyny and W. A. Smith, *Chem. Sci.*, 2020, **11**, 1738–1749.
337 M. Moura de Salles Pupo and R. Kortlever, *ChemPhysChem*, 2019, **20**, 2926–2935.
338 J. Chen, M. McGraw and E. Y. X. Chen, *ChemSusChem*, 2019, **12**, 4543–4569.
339 J. L. White, M. F. Baruch, J. E. Pander, III, Y. Hu, I. C. Fortmeyer, J. E. Park, T. Zhang, K. Liao, J. Gu, Y. Yan, T. W. Shaw, E. Abelev and A. B. Bocarsly, *Chem. Rev.*, 2015, **115**, 12888–12935.
340 G. Ghadimkhani, N. R. de Tacconi, W. Chanmanee, C. Janaky and K. Rajeshwar, *Chem. Commun.*, 2013, **49**, 1297–1299.

341 A. M. Appel, J. E. Bercaw, A. B. Bocarsly, H. Dobbek, D. L. DuBois, M. Dupuis, J. G. Ferry, E. Fujita, R. Hille, P. J. A. Kenis, C. A. Kerfeld, R. H. Morris, C. H. F. Peden, A. R. Portis, S. W. Ragsdale, T. B. Rauchfuss, J. N. H. Reek, L. C. Seefeldt, R. K. Thauer and G. L. Waldrop, *Chem. Rev.*, 2013, **113**, 6621–6658.
342 C. Iniguez, S. Capo-Bauca, U. Niinemets, H. Stoll, P. Aguilo-Nicolau and J. Galmes, *Plant J.*, 2020, **101**, 897–918.
343 M. Sarewicz and A. Osyczka, *Physiol. Rev.*, 2015, **95**, 219–243.
344 Q. Qu, F. Zeng, X. Liu, Q. J. Wang and F. Deng, *Cell Death Dis.*, 2016, **7**, e2226.
345 C. T. Rodgers and P. J. Hore, *Proc. Natl. Acad. Sci. U. S. A.*, 2009, **106**, 353–360.
346 C. Kerpal, S. Richert, J. G. Storey, S. Pillai, P. A. Liddell, D. Gust, S. R. Mackenzie, P. J. Hore and C. R. Timmel, *Nat. Commun.*, 2019, **10**, 3707.
347 S. Hayashi, E. Taikhorshid and K. Schulten, *Biophys. J.*, 2009, **96**, 403–416.
348 D. C. Cao, J. Pokorny, V. C. Smith and A. J. Zele, *Vision Res.*, 2008, **48**, 2586–2592.
349 A. Vogt, Y. Guo, S. P. Tsunoda, S. Kateriya, M. Elstner and P. Hegemann, *Sci. Rep.*, 2015, **5**, 16450.
350 R. Fudim, M. Szczepek, J. Vierock, A. Vogt, A. Schmidt, G. Kleinau, P. Fischer, F. Bartl, P. Scheerer and P. Hegemann, *Sci. Signaling*, 2019, **12**, eaau5948.
351 L. A. Kadir, M. Stacey and R. Barrett-Jolley, *Front. Physiol.*, 2018, **9**, 1661.
352 G. J. Kress and S. Mennerick, *Neuroscience*, 2009, **158**, 211–222.
353 D. R. Lovley and E. J. P. Phillips, *Appl. Environ. Microbiol.*, 1986, **52**, 751–757.
354 D. R. Lovley and E. J. P. Phillips, *Appl. Environ. Microbiol.*, 1986, **51**, 683–689.
355 D. R. Lovley and E. J. P. Phillips, *Appl. Environ. Microbiol.*, 1987, **53**, 1536–1540.
356 D. R. Lovley and E. J. P. Phillips, *Appl. Environ. Microbiol.*, 1988, **54**, 1472–1480.
357 E. E. Roden and D. R. Lovley, *Geomicrobiol. J.*, 1993, **11**, 49–56.
358 D. R. Lovley, S. J. Giovannoni, D. C. White, J. E. Champine, E. J. P. Phillips, Y. A. Gorby and S. Goodwin, *Arch. Microbiol.*, 1993, **159**, 336–344.
359 E. E. Roden and D. R. Lovley, *Appl. Environ. Microbiol.*, 1993, **59**, 734–742.
360 F. Caccavo, Jr., D. J. Lonergan, D. R. Lovley, M. Davis, J. F. Stolz and M. J. McInerney, *Appl. Environ. Microbiol.*, 1994, **60**, 3752–3759.
361 D. R. Lovley and E. J. P. Phillips, *Appl. Environ. Microbiol.*, 1994, **60**, 2394–2399.
362 C. R. Myers and K. H. Nealson, *Science*, 1988, **240**, 1319–1321.
363 K. Venkateswaran, D. P. Moser, M. E. Dollhopf, D. P. Lies, D. A. Saffarini, B. J. MacGregor, D. B. Ringelberg, D. C. White, M. Nishijima, H. Sano, J. Burghardt, E. Stackebrandt and K. H. Nealson, *Int. J. Syst. Bacteriol.*, 1999, **49**, 705–724.
364 K. A. Perry, J. E. Kostka, G. W. Luther, III and K. H. Nealson, *Science*, 1993, **259**, 801–803.
365 M. E. Dollhopf, K. H. Nealson, D. M. Simon and G. W. Luther, *Mar. Chem.*, 2000, **70**, 171–180.
366 A. D. Anbar, Y. Duan, T. W. Lyons, G. L. Arnold, B. Kendall, R. A. Creaser, A. J. Kaufman, G. W. Gordon, C. Scott, J. Garvin and R. Buick, *Science*, 2007, **317**, 1903–1906.
367 J. H. Quastel, M. Stephenson and M. D. Whetham, *Biochem. J.*, 1925, **19**, 304–317.
368 R. L. Starkey and H. O. Halvorson, *Soil Sci.*, 1927, **24**, 381–402.
369 J. L. Roberts, *Soil Sci.*, 1947, **63**, 135–140.
370 S. M. Bromfield, *J. Gen. Microbiol.*, 1954, **11**, 1–6.
371 K. Richter, M. Schicklberger and J. Gescher, *Appl. Environ. Microbiol.*, 2012, **78**, 913–921.
372 L. Shi, T. C. Squier, J. M. Zachara and J. K. Fredrickson, *Mol. Microbiol.*, 2007, **65**, 12–20.
373 D. R. Lovley, D. E. Holmes and K. P. Nevin, *Adv. Microb. Physiol.*, 2004, **49**, 219–286.
374 K. H. Nealson and D. Saffarini, *Annu. Rev. Microbiol.*, 1994, **48**, 311–343.
375 N. S. Malvankar, S. E. Yalcin, M. T. Tuominen and D. R. Lovley, *Nat. Nanotechnol.*, 2014, **9**, 1012–1017.
376 M. Y. El-Naggar, G. Wanger, K. M. Leung, T. D. Yuzvinsky, G. Southam, J. Yang, W. M. Lau, K. H. Nealson and Y. A. Gorby, *Proc. Natl. Acad. Sci. U. S. A.*, 2010, **107**, 18127–18131.
377 K. M. Leung, G. Wanger, M. Y. El-Naggar, Y. Gorby, G. Southam, W. M. Lau and J. Yang, *Nano Lett.*, 2013, **13**, 2407–2411.
378 Z. M. Summers, H. E. Fogarty, C. Leang, A. E. Franks, N. S. Malvankar and D. R. Lovley, *Science*, 2010, **330**, 1413–1415.
379 D. R. Lovley, *Annu. Rev. Microbiol.*, 2017, **71**, 643–664.
380 P. T. Ha, S. R. Lindemann, L. Shi, A. C. Dohnalkova, J. K. Fredrickson, M. T. Madigan and H. Beyenal, *Nat. Commun.*, 2017, **8**, 13924.
381 D. L. Cologgi, S. Lampa-Pastirk, A. M. Speers, S. D. Kelly and G. Reguera, *Proc. Natl. Acad. Sci. U. S. A.*, 2011, **108**, 15248–15252.
382 D. R. Lovley and E. J. P. Phillips, *Appl. Environ. Microbiol.*, 1992, **58**, 850–856.
383 M. D. Tucker, L. L. Barton and B. M. Thomson, *Appl. Microbiol. Biotechnol.*, 1996, **46**, 74–77.
384 N. F. Polizzi, S. S. Skourtis and D. N. Beratan, *Faraday Discuss.*, 2012, **155**, 43–62.
385 M. Breuer, K. M. Rosso, J. Blumberger and J. N. Butt, *J. R. Soc., Interface*, 2015, **12**, 20141117.
386 J. R. Winkler and H. B. Gray, *Q. Rev. Biophys.*, 2015, **48**, 411–420.
387 S. Pirbadian, S. E. Barchinger, K. M. Leung, H. S. Byun, Y. Jangir, R. A. Bouhenni, S. B. Reed, M. F. Romine, D. A. Saffarini, L. Shi, Y. A. Gorby, J. H. Golbeck and M. Y. El-Naggar, *Proc. Natl. Acad. Sci. U. S. A.*, 2014, **111**, 12883–12888.
388 P. Subramanian, S. Pirbadian, M. Y. El-Naggar and G. J. Jensen, *Proc. Natl. Acad. Sci. U. S. A.*, 2018, **115**, E3246–E3255.

389 W. E. Brownell, F. Qian and B. Anvari, *Biophys. J.*, 2010, **99**, 845–852.
390 N. Khatibzadeh, S. Gupta, B. Farrell, W. E. Brownell and B. Anvari, *Soft Matter*, 2012, **8**, 8350–8360.
391 H. von Canstein, J. Ogawa, S. Shimizu and J. R. Lloyd, *Appl. Environ. Microbiol.*, 2008, **74**, 615–623.
392 N. J. Kotloski and J. A. Gralnick, *mBio*, 2013, **4**(1), e00553–12.
393 A. Okamoto, S. Kalathil, X. Deng, K. Hashimoto, R. Nakamura and K. H. Nealson, *Sci. Rep.*, 2014, **4**, 5628.
394 G. Reguera, K. D. McCarthy, T. Mehta, J. S. Nicoll, M. T. Tuominen and D. R. Lovley, *Nature*, 2005, **435**, 1098–1101.
395 N. S. Malvankar, M. Vargas, K. P. Nevin, A. E. Franks, C. Leang, B. C. Kim, K. Inoue, T. Mester, S. F. Covalla, J. P. Johnson, V. M. Rotello, M. T. Tuominen and D. R. Lovley, *Nat. Nanotechnol.*, 2011, **6**, 573–579.
396 J. P. Veazey, G. Reguera and S. H. Tessmer, *Phys. Rev. E: Stat., Nonlinear, Soft Matter Phys.*, 2011, **84**, 060901.
397 X. Y. Ru, P. Zhang and D. N. Beratan, *J. Phys. Chem. B*, 2019, **123**, 5035–5047.
398 R. J. Steidl, S. Lampa-Pastirk and G. Reguera, *Nat. Commun.*, 2016, **7**, 12217.
399 M. Vargas, N. S. Malvankar, P. L. Tremblay, C. Leang, J. A. Smith, P. Patel, O. Synoeyenbos-West, K. P. Nevin and D. R. Lovley, *mBio*, 2013, **4**, e00105.
400 K. Xiao, N. S. Malvankar, C. J. Shu, E. Martz, D. R. Lovley and X. Sun, *Sci. Rep.*, 2016, **6**, 23385.
401 I. V. Kurnikov, G. S. M. Tong, M. Madrid and D. N. Beratan, *J. Phys. Chem. B*, 2002, **106**, 7–10.
402 D. J. F. Walker, E. Martz, D. E. Holmes, Z. M. Zhou, S. S. Nonnenmann and D. R. Lovley, *mBio*, 2019, **10**, e00579–19.
403 N. Poweleit, P. Ge, H. H. Nguyen, R. R. O. Loo, R. P. Gunsalus and Z. H. Zhou, *Nat. Microbiol.*, 2017, **2**, 16222.
404 N. L. Ing, R. K. Spencer, S. H. Luong, H. D. Nguyen and A. I. Hochbaum, *ACS Nano*, 2018, **12**, 2652–2661.
405 N. L. Ing, M. Y. El-Naggar and A. I. Hochbaum, *J. Phys. Chem. B*, 2018, **122**, 10403–10423.
406 F. J. T. Staal, M. T. Anderson, G. E. J. Staal, L. A. Herzenberg and C. Gitler, *Proc. Natl. Acad. Sci. U. S. A.*, 1994, **91**, 3619–3622.
407 K. Belarbi, E. Cuvelier, A. Destee, B. Gressier and M. C. Chartier-Harlin, *Mol. Neurodegener.*, 2017, **12**, 84, DOI: 10.1186/s13024-017-0225-5.
408 N. Durand and P. Storz, *Expert Rev. Anticancer Ther.*, 2017, **17**, 19–31.
409 G. Y. Liou and P. Storz, *Free Radical Res.*, 2010, **44**, 479–496.
410 P. Storz, *Front. Biosci., Landmark Ed.*, 2005, **10**, 1881–1896.
411 T. Shiibashi and T. Iida, *Dev. Comp. Immunol.*, 2001, **25**, 461–465.
412 N. Saha and H. K. Goswami, *Hum. Hered.*, 1987, **37**, 273–277.
413 K. C. Patra and N. Hay, *Trends Biochem. Sci.*, 2014, **39**, 347–354.
414 A. Marti, J. J. Perez and J. Madrenas, *Gen. Physiol. Biophys.*, 2018, **37**, 71–82.
415 G. A. Light, J. L. Hsu, M. H. Hsieh, K. Meyer-Gomes, J. Sprock, N. R. Swerdlow and D. L. Braff, *Biol. Psychiatry*, 2006, **60**, 1231–1240.
416 S. Rush and D. A. Driscoll, *IEEE Trans. Biomed. Eng.*, 1969, **16**, 15–22.
417 R. E. Dustman, R. Y. Emmerson, R. O. Ruhling, D. E. Shearer, L. A. Steinhaus, S. C. Johnson, H. W. Bonekat and J. W. Shigeoka, *Neurobiol. Aging*, 1990, **11**, 193–200.
418 R. E. Dustman, D. E. Shearer and R. Y. Emmerson, *Prog. Neurobiol.*, 1993, **41**, 369–401.
419 M. Desco, J. A. Hernandez, A. Santos and M. Brammer, *Hum. Brain Mapp.*, 2001, **14**, 16–27.
420 J. N. Weiss, P. S. Chen, Z. L. Qu, H. S. Karagueuzian, S. F. Lin and A. Garfinkel, *J. Cardiovasc. Electrophysiol.*, 2002, **13**, 292–295.
421 J. N. Weiss, Z. L. Qu, P. S. Chen, S. F. Lin, H. S. Karagueuzian, H. Hayashi, A. Garfinkel and A. Karma, *Circulation*, 2005, **112**, 1232–1240.
422 O. Kavehei, T. J. Hamilton, N. D. Truong and A. Nikpour, *Trends Pharmacol. Sci.*, 2019, **40**, 735–746.
423 S. R. Bornstein and S. Ben-Haim, *Horm. Metab. Res.*, 2015, **47**, 401–403.
424 G. Sinha, *Nat. Biotechnol.*, 2015, **33**, 226.
425 F. J. Rawson, *Ther. Delivery*, 2015, **6**, 5–8.
426 J. Banerjee, P. D. Ghatak, S. Roy, S. Khanna, C. Hemann, B. Deng, A. Das, J. L. Zweier, D. Wozniak and C. K. Sen, *PLoS One*, 2015, **10**, e0119531.
427 S. Reardon, *Nature*, 2014, **511**, 18.
428 K. Famm, B. Litt, K. J. Tracey, E. S. Boyden and M. Slaoui, *Nature*, 2013, **496**, 159–161.
429 G. Sinha, *Nat. Med.*, 2013, **19**, 654.
430 R. E. Alexander, *J. Am. Dent. Assoc., JADA*, 1973, **86**, 813–816.
431 T. Matsumoto and B. A. Levy, *PA Med.*, 1974, **77**, 30–36.
432 F.-m. Yang, L. Yao, S.-j. Wang, Y. Guo, Z.-f. Xu, C.-H. Zhang, K. Zhang, Y.-x. Fang and Y.-y. Liu, *Chin. J. Integr. Med.*, 2020, **26**, 310–320.
433 S. S. Chavan and K. J. Tracey, *Nat. Med.*, 2014, **20**, 239–241.
434 P. V. Peplow and G. D. Baxter, *RSC Drug Discovery Ser.*, 2013, **31**, 313–338.
435 Z. Liu, Y. Ding and Y. S. Zeng, *Curr. Med. Chem.*, 2011, **18**, 5165–5171.
436 B. R. Cassileth, J. Gubili and Y. K. Simon, *Nat. Rev. Urol.*, 2009, **6**, 228–233.
437 E. Ernst, *Nat. Clin. Pract. Rheumatol.*, 2006, **2**, 74–80.
438 J. S. Han and L. Terenius, *Annu. Rev. Pharmacol. Toxicol.*, 1982, **22**, 193–220.
439 G. Chen, *Am. J. Chin. Med.*, 1975, **3**, 27–34.
440 M. Baruscotti, A. Barbuti and A. Bucchi, *J. Mol. Cell. Cardiol.*, 2010, **48**, 55–64.
441 A. Bucchi, C. Piantoni, A. Barbuti, D. DiFrancesco and M. Baruscotti, *Channelopathies Heart Dis.*, 2018, 97–126.
442 N. J. Chandler, I. D. Greener, J. O. Tellez, S. Inada, H. Musa, P. Molenaar, D. DiFrancesco, M. Baruscotti, R. Longhi, R. H. Anderson, R. Billeter, V. Sharma, D. C. Sigg, M. R. Boyett and H. Dobrzynski, *Circulation*, 2009, **119**, 1562–1575.
443 S. C. Schachter and C. B. Saper, *Epilepsia*, 1998, **39**, 677–686.
444 D. K. Naritoku, W. J. Terry and R. H. Helfert, *Epilepsy Res.*, 1995, **22**, 53–62.

445 R. L. Johnson and C. G. Wilson, *J. Inflammation Res.*, 2018, **11**, 203–213.
446 K. D. Williams, R. Johnson, S. Moore and C. G. Wilson, *J. Invest. Med.*, 2019, **67**, 154.
447 S. C. Schachter, *Vagus and trigeminal nerve stimulation*, 2016.
448 R. Torres-Rosas, G. Yehia, G. Pena, P. Mishra, M. D. Thompson-Bonilla, M. A. Moreno-Eutimio, L. A. Arriaga-Pizano, A. Isibasi and L. Ulloa, *Nat. Med.*, 2014, **20**, 291–295.
449 G. A. Ulett, S. P. Han and J. S. Han, *Biol. Psychiatry*, 1998, **44**, 129–138.
450 Y. Long, H. Wei, J. Li, G. Yao, B. Yu, D. L. Ni, A. L. F. Gibson, X. L. Lan, Y. D. Jiang, W. B. Cai and X. D. Wang, *ACS Nano*, 2018, **12**, 12533–12540.
451 J. Guridi, M. C. Rodriguez-Oroz and J. A. Obeso, *Deep Brain Stimulation in Neurological and Psychiatric Disorders*, 2008, pp. 277–289.
452 R. Kumar, A. E. Lang, M. C. Rodriguez-Oroz, A. M. Lozano, P. Limousin, P. Pollak, A. L. Benabid, J. Guridi, E. Ramos, C. van der Linden, A. Vandewalle, J. Caemaert, E. Lannoo, D. van den Abbeele, G. Vingerhoets, M. Wolters and J. A. Obeso, *Neurology*, 2000, **55**, S34–S39.
453 J. A. Obeso, J. Guridi, M. C. Rodriguez-Oroz, Y. Agid, P. Bejjani, A. M. Bonnet, A. E. Lang, A. M. Lozano, R. Kumar, A. Benabid, P. Pollack, P. Krack, S. Rehncrona, R. Ekberg, M. Grabowski, A. Albanese, M. Scerrati, E. Moro, W. Koller, S. B. Wilkinson, R. Pahwa, J. Volkmann, N. Allert, H. J. Freund, J. Kulisevsky, A. Gironell, J. Molet, V. Tronnier, W. Fogel, M. Krause, T. Funk, C. Kern, U. Kestenbach, R. Iansek, J. Rosenfeld, A. Churchyard, D. O'Sullivan, M. Pell, R. Markus, A. Bayes, R. Blesa, B. Oliver, C. W. Olanow, I. M. Germano, M. Brin, J. Jankovic, R. G. Grossman, W. G. Ondo, J. L. Vitek, R. A. E. Bakay, M. R. DeLong, E. Tolosa, J. Rumia, F. Valldeoriola, A. Benabid, A. Albanese, M. R. DeLong, A. M. Lang, A. Lozano, J. A. Obeso, C. W. Olanow, P. Pollack, W. C. Koller, J. Vitek, S. Wilkinson and D.-B. S. Parkinsons, *N. Engl. J. Med.*, 2001, **345**, 956–963.
454 X. Tao, A. Lee, W. Limapichat, D. A. Dougherty and R. MacKinnon, *Science*, 2010, **328**, 67–73.
455 T. W. Berger, M. Baudry, R. D. Brinton, J. S. Liaw, V. Z. Marmarelis, A. Y. Park, B. J. Sheu and A. R. Tanguay, *Proc. IEEE*, 2001, **89**, 993–1012.
456 M. C. Rodriguez-Oroz, I. D. Zamarbide, J. Guridi and J. A. Obeso, *Neurology*, 2001, **56**, A273–A274.
457 S. M. Zhang, S. Yuan, L. P. Huang, X. X. Zheng, Z. H. Wu, K. D. Xu and G. Pan, *Sci. Rep.*, 2019, **9**, 1321.
458 S. K. Talwar, S. H. Xu, E. S. Hawley, S. A. Weiss, K. A. Moxon and J. K. Chapin, *Nature*, 2002, **417**, 37–38.
459 S. Yun, C. S. Koh, J. Jeong, J. Seo, S. H. Ahn, G. J. Choi, S. Shim, J. Shin, H. H. Jung, J. W. Chang and S. J. Kim, *Electronics*, 2019, **8**, 706.
460 A. Lavazza, *Front. Hum. Neurosci.*, 2016, **10**, 262.
461 J. Carlsson, N. W. Paul, M. Dann, J. Neuzner and D. Pfeiffer, *Dtsch. Arzteblatt Int.*, 2012, **109**, 535–541.
462 J. Nelson, R. A. McKinley, L. McIntire, C. Goodyear, A. Kreiner, C. Phillips and L. Monforton, *Front. Hum. Neurosci.*, 2016, **10**, 589.
463 N. Yin, G. Z. Xu, Q. X. Yang, J. Zhao, X. W. Yang, J. Q. Jin, W. N. Fu and M. G. Sun, *IEEE Trans. Magn.*, 2012, **48**, 723–726.
464 P. X. Gao, J. H. Song, J. Liu and Z. L. Wang, *Adv. Mater.*, 2007, **19**, 67–72.
465 J. Navas, T. Bove, J. A. Cobos, F. Nuno and K. Brebol, IEEE Miniaturised Battery Charger Using Piezoelectric Transformers, Anaheim, CA, 2001.
466 M. R. Sarker, S. H. M. Ali, M. Othman and S. Islam, *Designing a Battery-Less Piezoelectric based Energy Harvesting Interface Circuit with 300 mV Startup Voltage*, Univ Kebangsaan Malaysia (UKM), Bangi, Malaysia, 2012.
467 C. S. Chao, P. C. Huang, M. K. Chen and L. S. Jang, *Sens. Actuators, A*, 2011, **168**, 313–319.
468 L. S. Jang and W. H. Kan, *Biomed. Microdevices*, 2007, **9**, 619–626.
469 S. Almubarak, H. Nethercott, M. Freeberg, C. Beaudon, A. Jha, W. Jackson, R. Marcucio, T. Miclau, K. Healy and C. Bahney, *Bone*, 2016, **83**, 197–209.
470 E. Katz and P. Bollella, *Isr. J. Chem.*, 2020, DOI: 10.1002/ijch.202000045.
471 S. Shleev, *ChemPlusChem*, 2017, **82**, 522–539.
472 M. Rasmussen, R. E. Ritzmann, I. Lee, A. J. Pollack and D. Scherson, *J. Am. Chem. Soc.*, 2012, **134**, 1458–1460.
473 L. Halamkova, J. Halamek, V. Bocharova, A. Szczupak, L. Alfonta and E. Katz, *J. Am. Chem. Soc.*, 2012, **134**, 5040–5043.
474 A. Zebda, S. Cosnier, J. P. Alcaraz, M. Holzinger, A. Le Goff, C. Gondran, F. Boucher, F. Giroud, K. Gorgy, H. Lamraoui and P. Cinquin, *Sci. Rep.*, 2013, **3**, 1516.
475 M. Southcott, K. MacVittie, J. Halamek, L. Halamkova, W. D. Jemison, R. Lobel and E. Katz, *Phys. Chem. Chem. Phys.*, 2013, **15**, 6278–6283.
476 M. V. Schaefer, R. M. Handler and M. M. Scherer, *Geochem. Trans.*, 2017, **18**, 7.
477 M. Sander, T. B. Hofstetter and C. A. Gorski, *Environ. Sci. Technol.*, 2015, **49**, 5862–5878.
478 S. C. Ying, B. D. Kocar and S. Fendorf, *Geochim. Cosmochim. Acta*, 2012, **96**, 294–303.
479 C. Z. Wu, W. Xie, M. Zhang, L. F. Bai, J. L. Yang and Y. Xie, *Chem. – Eur. J.*, 2009, **15**, 492–500.
480 S. V. Yanina and K. M. Rosso, *Science*, 2008, **320**, 218–222.
481 S. Kasai, Y. Sugiura, A. Prasad, K. Y. Inoue, T. Sato, T. Honmo, A. Kumar, P. Pospisil, K. Ino, Y. Hashi, Y. Furubayashi, M. Matsudaira, A. Suda, R. Kunikata and T. Matsue, *Sci. Rep.*, 2019, **9**, 1–10.
482 K. Ogata, M. Hatakeyama, Y. Sakamoto and S. Nakamura, *J. Phys. Chem. B*, 2019, **123**, 6444–6452.
483 W. W. Fischer, J. Hemp and J. E. Johnson, *Annu. Rev. Earth Planet. Sci.*, 2016, **44**, 647–683.
484 J. E. Johnson, S. M. Webb, K. Thomas, S. Ono, J. L. Kirschvink and W. W. Fischer, *Proc. Natl. Acad. Sci. U. S. A.*, 2013, **110**, 11238–11243.
485 F. Rappaport and B. A. Diner, *Coord. Chem. Rev.*, 2008, **252**, 259–272.
486 J. Raymond and R. E. Blankenship, *Coord. Chem. Rev.*, 2008, **252**, 377–383.

487 C. W. Hoganson and G. T. Tabcock, *Science*, 1997, **277**, 1953–1956.
488 V. K. Yachandra, K. Sauer and M. P. Klein, *Chem. Rev.*, 1996, **96**, 2927–2950.
489 K. Wieghardt, *Angew. Chem., Int. Ed. Engl.*, 1994, **106**, 725–728.
490 R. N. Deguzman, A. Awaluddin, Y. F. Shen, Z. R. Tian, S. L. Suib, S. Ching and C. L. Oyoung, *Chem. Mater.*, 1995, **7**, 1286–1292.
491 W. M. Telford, L. P. Geldart and R. E. Sheriff, *Applied Geophysics*, Cambridge University Press, 2nd edn, 1990, pp. 283–292.
492 S. E. Fosdick, K. N. Knust, K. Scida and R. M. Crooks, *Angew. Chem., Int. Ed.*, 2013, **52**, 10438–10456.
493 X. Zhang, Q. Zhai, H. Xing, J. Li and E. Wang, *ACS Sens.*, 2017, **2**, 320–326.
494 A. Gamero-Quijano, A. F. Molina-Osorio, P. Peljo and M. D. Scanlon, *Phys. Chem. Chem. Phys.*, 2019, **21**, 9627–9640.
495 A. J. Frierdich, M. Helgeson, C. S. Liu, C. M. Wang, K. M. Rosso and M. M. Scherer, *Environ. Sci. Technol.*, 2015, **49**, 8479–8486.
496 O. Shekhah, W. Ranke, A. Schuele, G. Kolios and R. Schloegl, *Angew. Chem., Int. Ed.*, 2003, **42**, 5760–5763.
497 G. Picasso Escobar, A. Quintilla Beroy, M. P. Pina Iritia and J. Herguido Huerta, *Chem. Eng. J.*, 2004, **102**, 107–117.
498 M. d. S. Ramos, M. d. S. Santos, L. P. Gomes, A. Albornoz and M. d. C. Rangel, *Appl. Catal., A*, 2008, **341**, 12–17.
499 J. Moir, N. Soheilnia, P. O'Brien, A. Jelle, C. M. Grozea, D. Faulkner, M. G. Helander and G. A. Ozin, *ACS Nano*, 2013, **7**, 4261–4274.
500 I. M. Abdrafikova, G. P. Kayukova, S. M. Petrov, A. I. Ramazanova, R. Z. Musin and V. I. Morozov, *Pet. Chem.*, 2015, **55**, 104–111.
501 J. F. Lopes, J. C. M. Silva, M. T. M. Cruz, J. W. d. M. Carneiro and W. B. De Almeida, *RSC Adv.*, 2016, **6**, 40408–40417.
502 H. Shui, H. Jiao, F. He, T. Shui, X. Wang, H. Zhou, C. Pan, Z. Wang, Z. Lei, S. Ren, S. Kang and C. C. Xu, *Energy Fuels*, 2018, **32**, 3022–3030.
503 M. da Costa Borges Soares, F. F. Barbosa, M. A. M. Torres, A. Valentini, A. dos Reis Albuquerque, J. R. Sambrano, S. B. C. Pergher, N. Essayem and T. P. Braga, *Catal. Sci. Technol.*, 2019, **9**, 2469–2484.
504 S. C. Ying, B. D. Kocar, S. D. Griffis and S. Fendorf, *Environ. Sci. Technol.*, 2011, **45**, 5572–5579.
505 R. P. Mock, M. V. Schaefer, J. L. Pacheco, L. Lake, I. Lee and S. C. Ying, *ACS Earth Space Chem.*, 2019, **3**, 550–561.
506 C. Liu, J. J. Gallagher, K. K. Sakimoto, E. M. Nichols, C. J. Chang, M. C. Y. Chang and P. D. Yang, *Nano Lett.*, 2015, **15**, 3634–3639.
507 D. R. Bond and D. R. Lovley, *Appl. Environ. Microbiol.*, 2003, **69**, 1548–1555.
508 Y. Kawamata and P. S. Baran, *Joule*, 2020, **4**, 701–704.
509 C. Kingston, M. D. Palkowitz, Y. Takahira, J. C. Vantourout, B. K. Peters, Y. Kawamata and P. S. Baran, *Acc. Chem. Res.*, 2020, **53**, 72–83.
510 E. Laborda, M. C. Henstridge, C. Batchelor-McAuley and R. G. Compton, *Chem. Soc. Rev.*, 2013, **42**, 4894–4905.
511 A. V. Listratova, N. Sbei and L. G. Voskressensky, *Eur. J. Org. Chem.*, 2020, 2012–2027.
512 M. C. Leech and K. Lam, *Acc. Chem. Res.*, 2020, **53**, 121–134.
513 Y. Yuan and A. Lei, *Nat. Commun.*, 2020, **11**, 802.
514 L. Hu, Z. Xing and X. Feng, *ACS Energy Lett.*, 2020, **5**, 430–436.
515 P. Xiong and H.-C. Xu, *Acc. Chem. Res.*, 2019, **52**, 3339–3350.
516 J. Lin, J. Zhong, D. Bao, J. Reiber-Kyle, W. Wang, V. Vullev, M. Ozkan and C. S. Ozkan, *J. Nanosci. Nanotechnol.*, 2012, **12**, 1770–1775.
517 W. Wang, S. Guo, M. Penchev, J. Zhong, J. Lin, D. Bao, V. Vullev, M. Ozkan and C. S. Ozkan, *J. Nanosci. Nanotechnol.*, 2012, **12**, 6913–6920.
518 M. Wang, B. Feng, H. Li and H. X. Li, *Chem*, 2019, **5**, 805–837.
519 P. Trogadas and M. O. Coppens, *Chem. Soc. Rev.*, 2020, **49**, 3107–3141.
520 A. Lattes, *Actual. Chim.*, 2012, **367–368**, 8–18.
521 J. Fournier, *Actual. Chim.*, 2005, **283**, 47–53.
522 B. Alkotaini, S. Abdellaoui, K. Hasan, M. Grattieri, T. Quah, R. Cai, M. Y. Yuan and S. D. Minteer, *ACS Sustainable Chem. Eng.*, 2018, **6**, 4909–4915.
523 D. P. Hickey, E. M. Gaffney and S. D. Minteer, *Top. Curr. Chem.*, 2018, **376**, 43.
524 S. D. Minteer, *Int. Mater. Rev.*, 2018, **63**, 241–256.
525 R. R. Wu, C. L. Ma and Z. G. Zhu, *Curr. Opin. Electrochem.*, 2020, **19**, 1–7.
526 S. Kalathil, K. P. Katuri, A. S. Alazmi, S. Pedireddy, N. Kornienko, P. M. F. J. Costa and P. E. Saikaly, *Chem. Mater.*, 2019, **31**, 3686–3693.
527 M. Peng, Y. Qiao, M. Luo, M. Wang, S. Chu, Y. Zhao, P. Liu, J. Liu and Y. Tan, *ACS Appl. Mater. Interfaces*, 2019, **11**, 40062–40068.
528 W. Sun and Q. Sun, *Acc. Chem. Res.*, 2019, **52**, 2370–2381.
529 V. Nuñez and I. Vullev Valentine, in *Encyclopedia of Surface and Colloid Science*, ed. P. Somasundaran, CRCnetBASE, Taylor & Francis Group, 3rd edn, 2015, pp. 1–22.
530 G. Sinawang, M. Osaki, Y. Takashima, H. Yamaguchi and A. Harada, *Chem. Commun.*, 2020, **56**, 4381–4395.
531 D. Xia, P. Wang, X. Ji, N. M. Khashab, J. L. Sessler and F. Huang, *Chem. Rev.*, 2020, **120**, 6070–6123.
532 H. J. Sim, H. Kim, Y. Jang, G. M. Spinks, S. Gambhir, D. L. Officer, G. G. Wallace and S. J. Kim, *ACS Appl. Mater. Interfaces*, 2019, **11**, 46026–46033.
533 B. Akkopru-Akgun, S. Trolier-McKinstry and M. T. Lanagan, *J. Am. Ceram. Soc.*, 2015, **98**, 3270–3279.
534 M. W. Kanan and D. G. Nocera, *Science*, 2008, **321**, 1072–1075.
535 Y. Liu and P. Atanassov, *Curr. Opin. Electrochem.*, 2020, **19**, 175–183.
536 V. Svoboda and P. Atanassov, in *Enzymatic Fuel Cells. From Fundamentals to Applications*, ed. H. R. Luckarift, P. Atanassov and G. R. Johnson, John Wiley & Sons, Inc., 2014, pp. 337–360.
537 G. Strack, R. Nichols, P. Atanassov, H. R. Luckarift and G. R. Johnson, *Methods Mol. Biol.*, 2013, **1051**, 217–228.

538 J. Lilloja, E. Kibena-Poldsepp, A. Sarapuu, M. Kodali, Y. Chen, T. Asset, M. Kaarik, M. Merisalu, P. Paiste, J. Aruvali, A. Treshchalov, M. Rahn, J. Leis, V. Sammelselg, S. Holdcroft, P. Atanassov and K. Tammeveski, *ACS Appl. Energy Mater.*, 2020, **3**, 5375–5384.
539 T. Mineva, I. Matanovic, P. Atanassov, M.-T. Sougrati, L. Stievano, M. Clemancey, A. Kochem, J.-M. Latour and F. Jaouen, *ACS Catal.*, 2019, **9**, 9359–9371.
540 W. R. Leow, Y. Lum, A. Ozden, Y. Wang, D.-H. Nam, B. Chen, J. Wicks, T.-T. Zhuang, F. Li, D. Sinton and E. H. Sargent, *Science*, 2020, **368**, 1228–1233.
541 J. C. Siu, N. Fu and S. Lin, *Acc. Chem. Res.*, 2020, **53**, 547–560.
542 P. T. Smith, S. Weng and C. J. Chang, *Inorg. Chem.*, 2020, **59**, 9270–9278.
543 F. Wang and S. S. Stahl, *Acc. Chem. Res.*, 2020, **53**, 561–574.
544 B. D. McCloskey and D. Addison, *ACS Catal.*, 2017, **7**, 772–778.
545 M. H. Shaw, J. Twilton and D. W. C. MacMillan, *J. Org. Chem.*, 2016, **81**, 6898–6926.
546 A. J. Bard, R. Memming and B. Miller, *Pure Appl. Chem.*, 1991, **63**, 569–596.
547 F. E. Osterloh, *ACS Energy Lett.*, 2017, **2**, 445–453.
548 L. Buzzetti, G. E. M. Crisenza and P. Melchiorre, *Angew. Chem., Int. Ed.*, 2019, **58**, 3730–3747.
549 J. W. Tucker and C. R. J. Stephenson, *J. Org. Chem.*, 2012, **77**, 1617–1622.
550 Y. X. Fang, Y. W. Ma, M. F. Zheng, P. J. Yang, A. M. Asiri and X. C. Wang, *Coord. Chem. Rev.*, 2018, **373**, 83–115.
551 E. Amouyal, *Sol. Energy Mater. Sol. Cells*, 1995, **38**, 249–276.
552 B. Y. Wang, W. Chen, Y. F. Song, G. H. Li, W. Wei, J. H. Fang and Y. H. Sun, *Catal. Today*, 2018, **311**, 23–39.
553 M. Reckenthäler and A. G. Griesbeck, *Adv. Synth. Catal.*, 2013, **355**, 2727–2744.
554 X. Zhang, K. P. Rakesh, L. Ravindar and H. L. Qin, *Green Chem.*, 2018, **20**, 4790–4833.
555 T. Ghosh, T. Slanina and B. König, *Chem. Sci.*, 2015, **6**, 2027–2034.
556 M. Fagnoni, D. Dondi, D. Ravelli and A. Albini, *Chem. Rev.*, 2007, **107**, 2725–2756.
557 C. S. Wang, P. H. Dixneuf and J. F. Soule, *Chem. Rev.*, 2018, **118**, 7532–7585.
558 J. Xie, H. M. Jin and A. S. K. Hashmi, *Chem. Soc. Rev.*, 2017, **46**, 5193–5203.
559 Y. T. Zhao and W. J. Xia, *Chem. Soc. Rev.*, 2018, **47**, 2591–2608.
560 J. Zhu, W. C. Yang, X. D. Wang and L. Wu, *Adv. Synth. Catal.*, 2018, **360**, 386–400.
561 L. Revathi, L. Ravindar, W. Y. Fang, K. P. Rakesh and H. L. Qin, *Adv. Synth. Catal.*, 2018, **360**, 4652–4698.
562 Q. X. Qin, H. Jiang, Z. T. Hu, D. Ren and S. Y. Yu, *Chem. Rec.*, 2017, **17**, 754–774.
563 B. M. Hockin, C. F. Li, N. Robertson and E. Zysman-Colman, *Catal. Sci. Technol.*, 2019, **9**, 889–915.
564 K. Rybicka-Jasińska, W. Q. Shan, K. Zawada, K. M. Kadish and D. Gryko, *J. Am. Chem. Soc.*, 2016, **138**, 15451–15458.
565 M. Ethirajan, Y. H. Chen, P. Joshi and R. K. Pandey, *Chem. Soc. Rev.*, 2011, **40**, 340–362.
566 L. L. Li and E. W. G. Diau, *Chem. Soc. Rev.*, 2013, **42**, 291–304.
567 M. K. Panda, K. Ladomenou and A. G. Coutsolelos, *Coord. Chem. Rev.*, 2012, **256**, 2601–2627.
568 K. Gruber, B. Puffer and B. Kräutler, *Chem. Soc. Rev.*, 2011, **40**, 4346–4363.
569 C. Brenig, L. Prieto, R. Oetterli and F. Zelder, *Angew. Chem., Int. Ed.*, 2018, **57**, 16308–16312.
570 A. J. Wierzba, A. Wincenciuk, M. Karczewski, V. I. Vullev and D. Gryko, *Chem. – Eur. J.*, 2018, **24**, 10344–10356.
571 M. Jost, J. Fernandez-Zapata, M. C. Polanco, J. M. Ortiz-Guerrero, P. Y. T. Chen, G. Kang, S. Padmanabhan, M. Elias-Arnanz and C. L. Drennan, *Nature*, 2015, **526**, 536–541.
572 J. M. Ortiz-Guerrero, M. C. Polanco, F. J. Murillo, S. Padmanabhan and M. Elias-Arnanz, *Proc. Natl. Acad. Sci. U. S. A.*, 2011, **108**, 7565–7570.
573 A. Al Mamun, M. J. Toda, P. Lodowski and P. M. Kozlowski, *J. Phys. Chem. B*, 2019, **123**, 2585–2598.
574 M. Giedyk, K. Goliszewska and D. Gryko, *Chem. Soc. Rev.*, 2015, **44**, 3391–3404.
575 M. Giedyk, J. Turkowska, S. Lepak, M. Marculewicz, K. O. Proinsias and D. Gryko, *Org. Lett.*, 2017, **19**, 2670–2673.
576 H. Tian, H. Shimakoshi, K. Imamura, Y. Shiota, K. Yoshizawa and Y. Hisaeda, *Chem. Commun.*, 2017, **53**, 9478–9481.
577 M. Ociepa, O. Baka, J. Narodowiec and D. Gryko, *Adv. Synth. Catal.*, 2017, **359**, 3560–3565.
578 K. o. Proinsias, A. Jackowska, K. Radzewicz, M. Giedyk and D. Gryko, *Org. Lett.*, 2018, **20**, 296–299.
579 M. Ociepa, A. J. Wierzba, J. Turkowska and D. Gryko, *J. Am. Chem. Soc.*, 2020, **142**, 5355–5361.
580 R. Keese, H. Siegenthaler, R. Luginbuhl, M. A. Rashid and M. Schnippering, *ECS Trans.*, 2007, **2**, 27–33.
581 F. J. Widner, A. D. Lawrence, E. Deery, D. Heldt, S. Frank, K. Gruber, K. Wurst, M. J. Warren and B. Kraeutler, *Angew. Chem., Int. Ed.*, 2016, **55**, 11281–11286.
582 S. Dey and J. Zhao, *J. Phys. Chem. Lett.*, 2016, **7**, 2921–2929.
583 S. Palato, H. Seiler, H. Baker, C. Sonnichsen, P. Brosseau and P. Kambhampati, *J. Chem. Phys.*, 2020, **152**, 104710.
584 V. Krivenkov, P. Samokhvalov, D. Dyagileva, A. Karaulov and I. Nabiev, *ACS Photonics*, 2020, **7**, 831–836.
585 S. Mandal and N. V. Tkachenko, *J. Phys. Chem. Lett.*, 2019, **10**, 2775–2781.
586 X.-B. Li, C.-H. Tung and L.-Z. Wu, *Angew. Chem., Int. Ed.*, 2019, **58**, 10804–10811.
587 J. Huang, K. L. Mulfort, P. Du and L. X. Chen, *J. Am. Chem. Soc.*, 2012, **134**, 16472–16475.
588 A. Fujishima and K. Honda, *Nature*, 1972, **238**, 37–38.
589 N. Hoffmann, *Aust. J. Chem.*, 2015, **68**, 1621–1639.
590 L. E. Oi, M.-Y. Choo, H. V. Lee, H. C. Ong, S. B. Abd Hamid and J. C. Juan, *RSC Adv.*, 2016, **6**, 108741–108754.
591 Q. Liu and J. Wang, *Sol. Energy*, 2019, **184**, 454–465.
592 M. Shakeel Ahmad, A. K. Pandey and N. Abd Rahim, *Renewable Sustainable Energy Rev.*, 2017, **77**, 89–108.

593 C. Huang, X.-B. Li, C.-H. Tung and L.-Z. Wu, *Chem. – Eur. J.*, 2018, **24**, 11530–11534.
594 Y. Jiang, C. Wang, C. R. Rogers, M. S. Kodaimati and E. A. Weiss, *Nat. Chem.*, 2019, **11**, 1034–1040.
595 L. Amirav and A. P. Alivisatos, *J. Am. Chem. Soc.*, 2013, **135**, 13049–13053.
596 M. Saliba, J.-P. Correa-Baena, M. Grätzel, A. Hagfeldt and A. Abate, *Angew. Chem., Int. Ed.*, 2018, **57**, 2554–2569.
597 K. Wang, H. P. Lu, X. L. Zhu, Y. X. Lin, M. C. Beard, Y. Yan and X. H. Chen, *ACS Energy Lett.*, 2020, **5**, 566–571.
598 H. W. Huang, B. Pradhan, J. Hofkens, M. B. J. Roeffaers and J. A. Steele, *ACS Energy Lett.*, 2020, **5**, 1107–1123.
599 M. Ha, J.-H. Kim, M. You, Q. Li, C. Fan and J.-M. Nam, *Chem. Rev.*, 2019, **119**, 12208–12278.
600 A. Gellé, T. Jin, L. de la Garza, G. D. Price, L. V. Besteiro and A. Moores, *Chem. Rev.*, 2020, **120**, 986–1041.
601 D. C. Ratchford, *ASC Nano*, 2019, **13**, 13610–13614.
602 J. Albero, Y. Peng and H. Garcia, *ACS Catal.*, 2020, **10**, 5734–5749.
603 S. Li, P. Miao, Y. Zhang, J. Wu, B. Zhang, Y. Du, X. Han, J. Sun and P. Xu, *Adv. Mater.*, 2020, DOI: 10.1002/adma.202000086.
604 W. Li, J. Miao, T. Peng, H. Lv, J.-G. Wang, K. Li, Y. Zhu and D. Li, *Nano Lett.*, 2020, **20**, 2507–2513.
605 J. Schneider and D. W. Bahnemann, *J. Phys. Chem. Lett.*, 2013, **4**, 3479–3483.
606 J. Hu, J. Wang, T. H. Nguyen and N. Zheng, *Beilstein J. Org. Chem.*, 2013, **9**, 1977–2001.
607 C. Carbonell and A. B. Braunschweig, *Acc. Chem. Res.*, 2017, **50**, 190–198.
608 J. C. Colmenares, R. S. Varma and V. Nair, *Chem. Soc. Rev.*, 2017, **46**, 6675–6686.
609 S. Das and V. C. Srivastava, *Photochem. Photobiol. Sci.*, 2016, **15**, 714–730.
610 V. Nuñez, S. Upadhyayula, B. Millare, J. M. Larsen, A. Hadian, S. Shin, P. Vandrangi, S. Gupta, H. Xu, A. P. Lin, G. Y. Georgiev and V. I. Vullev, *Anal. Chem.*, 2013, **85**, 4567–4577.
611 K. Chau, B. Millare, A. Lin, S. Upadhyayula, V. Nuñez, H. Xu and V. I. Vullev, *Microfluid. Nanofluid.*, 2011, **10**, 907–917.
612 M. S. Thomas, B. Millare, J. M. Clift, D. Bao, C. Hong and V. I. Vullev, *Ann. Biomed. Eng.*, 2010, **38**, 21–32.
613 M. S. Thomas, J. M. Clift, B. Millare and V. I. Vullev, *Langmuir*, 2010, **26**, 2951–2957.
614 B. Millare, M. Thomas, A. Ferreira, H. Xu, M. Holesinger and V. I. Vullev, *Langmuir*, 2008, **24**, 13218–13224.
615 C. Hong, D. Bao, M. S. Thomas, J. M. Clift and V. I. Vullev, *Langmuir*, 2008, **24**, 8439–8442.
616 V. I. Vullev, J. Wan, V. Heinrich, P. Landsman, P. E. Bower, B. Xia, B. Millare and G. Jones, II, *J. Am. Chem. Soc.*, 2006, **128**, 16062–16072.
617 B. T. Mayers, D. V. Vezenov, V. I. Vullev and G. M. Whitesides, *Anal. Chem.*, 2005, **77**, 1310–1316.
618 F. Wang and S. S. Stahl, *Angew. Chem., Int. Ed.*, 2019, **58**, 6385–6390.
619 Y. Yu, P. Guo, J.-S. Zhong, Y. Yuan and K.-Y. Ye, *Org. Chem. Front.*, 2020, **7**, 131–135.
620 C. Joachim, J. K. Gimzewski and A. Aviram, *Nature*, 2000, **408**, 541–548.
621 B. Mann and H. Kuhn, *J. Appl. Phys.*, 1971, **42**, 4398–4405.
622 E. E. Polymeropoulos and J. Sagiv, *J. Chem. Phys.*, 1978, **69**, 1836–1847.
623 R. Frisenda, A. J. Molina-Mendoza, T. Mueller, A. Castellanos-Gomez and H. S. J. van der Zant, *Chem. Soc. Rev.*, 2018, **47**, 3339–3358.
624 A. Aviram and M. A. Ratner, *Chem. Phys. Lett.*, 1974, **29**, 277–283.
625 M. A. Reed, C. Zhou, C. J. Muller, T. P. Burgin and J. M. Tour, *Science*, 1997, **278**, 252–254.
626 B. Q. Xu and N. J. J. Tao, *Science*, 2003, **301**, 1221–1223.
627 J. Park, A. N. Pasupathy, J. I. Goldsmith, C. Chang, Y. Yaish, J. R. Petta, M. Rinkoski, J. P. Sethna, H. D. Abruna, P. L. McEuen and D. C. Ralph, *Nature*, 2002, **417**, 722–725.
628 A. Nitzan and M. A. Ratner, *Science*, 2003, **300**, 1384–1389.
629 N. J. Tao, *Nat. Nanotechnol.*, 2006, **1**, 173–181.
630 S. V. Aradhya and L. Venkataraman, *Nat. Nanotechnol.*, 2013, **8**, 399–410.
631 N. Prokopuk and K. A. Son, *J. Phys.: Condens. Matter*, 2008, **20**, 374116.
632 R. Frisenda, D. Stefani and H. S. J. van der Zant, *Acc. Chem. Res.*, 2018, **51**, 1359–1367.
633 O. Azzaroni, M. Mir, M. Alvarez, L. Tiefenauer and W. Knoll, *Langmuir*, 2008, **24**, 2878–2883.
634 G. S. Bang, H. Chang, J. R. Koo, T. Lee, R. C. Advincula and H. Lee, *Small*, 2008, **4**, 1399–1405.
635 S. Grunder, D. M. Torres, C. Marquardt, A. Blaszczyk, R. Krupke and M. Mayor, *Eur. J. Org. Chem.*, 2011, 478–496.
636 W. Ho, *J. Chem. Phys.*, 2002, **117**, 11033–11061.
637 G. Binning, H. Rohrer, C. Gerber and E. Weibel, *Phys. Rev. Lett.*, 1982, **49**, 57–61.
638 A. Vilan, D. Aswal and D. Cahen, *Chem. Rev.*, 2017, **117**, 4248–4286.
639 E. Pensa, E. Cortes, G. Corthey, P. Carro, C. Vericat, M. H. Fonticelli, G. Benitez, A. A. Rubert and R. C. Salvarezza, *Acc. Chem. Res.*, 2012, **45**, 1183–1192.
640 R. Frisenda, S. Tarkuc, E. Galan, M. L. Perrin, R. Eelkema, F. C. Grozema and H. S. J. van der Zant, *Beilstein J. Nanotechnol.*, 2015, **6**, 1558–1567.
641 P. E. Laibinis, G. M. Whitesides, D. L. Allara, Y. T. Tao, A. N. Parikh and R. G. Nuzzo, *J. Am. Chem. Soc.*, 1991, **113**, 7152–7167.
642 R. G. Nuzzo, B. R. Zegarski and L. H. Dubois, *J. Am. Chem. Soc.*, 1987, **109**, 733–740.
643 W. J. Liang, M. P. Shores, M. Bockrath, J. R. Long and H. Park, *Nature*, 2002, **417**, 725–729.
644 X. F. Guo, J. P. Small, J. E. Klare, Y. L. Wang, M. S. Purewal, I. W. Tam, B. H. Hong, R. Caldwell, L. M. Huang, S. O'Brien, J. M. Yan, R. Breslow, S. J. Wind, J. Hone, P. Kim and C. Nuckolls, *Science*, 2006, **311**, 356–359.
645 H. Wang, E. R. McNellis, S. Kinge, M. Bonn and E. Canovas, *Nano Lett.*, 2013, **13**, 5311–5315.
646 L. A. Ponomarenko, F. Schedin, M. I. Katsnelson, R. Yang, E. W. Hill, K. S. Novoselov and A. K. Geim, *Science*, 2008, **320**, 356–358.

647 C. S. Lent, B. Isaksen and M. Lieberman, *J. Am. Chem. Soc.*, 2003, **125**, 1056–1063.
648 J. Valdiviezo and J. L. Palma, *J. Phys. Chem. C*, 2018, **122**, 2053–2063.
649 Y. Cui, C. J. Xia, Y. H. Su, B. Q. Zhang, A. M. Chen, A. Y. Yang, T. T. Zhang and Y. Liu, *Acta Phys. Sin.*, 2018, **67**, 118501, DOI: 10.7498/aps.67.20180088.
650 G. Lovat, B. Choi, D. W. Paley, M. L. Steigerwald, L. Venkataraman and X. Roy, *Nat. Nanotechnol.*, 2017, **12**, 1050–1055.
651 V. Linko, J. Leppiniemi, S. T. Paasonen, V. P. Hytonen and J. J. Toppari, *Nanotechnology*, 2011, **22**, 275610.
652 H. Cohen, C. Nogues, R. Naaman and D. Porath, *Proc. Natl. Acad. Sci. U. S. A.*, 2005, **102**, 11589–11593.
653 M. Taniguchi and T. Kawai, *Phys. E*, 2006, **33**, 1–12.
654 K. Wang, *J. Funct. Biomater.*, 2018, **9**, 8.
655 A. Rakitin, P. Aich, C. Papadopoulos, Y. Kobzar, A. S. Vedeneev, J. S. Lee and J. M. Xu, *Phys. Rev. Lett.*, 2001, **86**, 3670–3673.
656 Z. Z. Huang, F. Pu, D. Hu, C. Y. Wang, J. S. Ren and X. G. Qu, *Chem. – Eur. J.*, 2011, **17**, 3774–3780.
657 F. D. Lewis, *Isr. J. Chem.*, 2013, **53**, 350–365.
658 E. C. M. Tse, T. J. Zwang, S. Bedoya and J. K. Barton, *ACS Cent. Sci.*, 2019, **5**, 65–72.
659 D. Porath, G. Cuniberti and R. Di Felice, *Long-Range Charge Transfer in DNA II*, 2004, vol. 237, pp. 183–227.
660 B. X. Shen, M. A. Kostiainen and V. Linko, *Langmuir*, 2018, **34**, 14911–14920.
661 C. J. Murphy, M. R. Arkin, N. D. Ghatlia, S. Bossmann, N. J. Turro and J. K. Barton, *Proc. Natl. Acad. Sci. U. S. A.*, 1994, **91**, 5315–5319.
662 D. B. Hall, R. E. Holmlin and J. K. Barton, *Nature*, 1996, **382**, 731–735.
663 M. R. Arkin, E. D. A. Stemp, R. E. Holmlin, J. K. Barton, A. Hormann, E. J. C. Olson and P. F. Barbara, *Science*, 1996, **273**, 475–480.
664 R. E. Holmlin, P. J. Dandliker and J. K. Barton, *Angew. Chem., Int. Ed. Engl.*, 1997, **36**, 2715–2730.
665 C. L. Guo, K. Wang, E. Zerah-Harush, J. Hamill, B. Wang, Y. Dubi and B. Q. Xu, *Nat. Chem.*, 2016, **8**, 484–490.
666 H. Cohen, C. Nogues, R. Naaman and D. Porath, *Proc. Natl. Acad. Sci. U. S. A.*, 2005, **102**, 11589–11593.
667 J. Hihath, B. Q. Xu, P. M. Zhang and N. J. Tao, *Proc. Natl. Acad. Sci. U. S. A.*, 2005, **102**, 16979–16983.
668 C. G. Heden and A. Rupprecht, *Acta Chem. Scand.*, 1966, **20**, 583–585.
669 H. W. Fink and C. Schonenberger, *Nature*, 1999, **398**, 407–410.
670 M. G. Debije, M. T. Milano and W. A. Bernhard, *Angew. Chem., Int. Ed.*, 1999, **38**, 2752–2756.
671 A. Y. Kasumov, M. Kociak, S. Gueron, B. Reulet, V. T. Volkov, D. V. Klinov and H. Bouchiat, *Science*, 2001, **291**, 280–282.
672 D. N. Beratan, S. Priyadarshy and S. M. Risser, *Chem. Biol.*, 1997, **4**, 3–8.
673 M. P. Ruiz, A. C. Aragones, N. Camarero, J. G. Vilhena, M. Ortega, L. A. Zotti, R. Perez, J. C. Cuevas, P. Gorostiza and I. Diez-Perez, *J. Am. Chem. Soc.*, 2017, **139**, 15337–15346.
674 J. M. Artes, I. Diez-Perez and P. Gorostiza, *Nano Lett.*, 2012, **12**, 2679–2684.
675 J. Kolay, S. Bera, T. Rakshit and R. Mukhopadhyay, *Langmuir*, 2018, **34**, 3126–3135.
676 J. A. Fereiro, G. Porat, T. Bendikov, I. Pecht, M. Sheves and D. Cahen, *J. Am. Chem. Soc.*, 2018, **140**, 13317–13326.
677 Y. A. Zhao, B. Ashcroft, P. M. Zhang, H. Liu, S. M. Sen, W. Song, J. Im, B. Gyarfas, S. Manna, S. Biswas, C. Borges and S. Lindsay, *Nat. Nanotechnol.*, 2014, **9**, 466–473.
678 M. Ortega, J. G. Vilhena, L. A. Zotti, I. Diez-Perez, J. C. Cuevas and R. Perez, *Biomolecules*, 2019, **9**, 611.
679 J. A. Fereiro, B. Kayser, C. Romero-Muniz, A. Vilan, D. A. Dolgikh, R. V. Chertkova, J. C. Cuevas, L. A. Zotti, I. Pecht, M. Sheves and D. Cahen, *Angew. Chem., Int. Ed.*, 2019, **58**, 11852–11859.
680 C. L. Guo, X. Yu, S. Refaely-Abramson, L. Sepunaru, T. Bendikov, I. Pecht, L. Kronik, A. Vilan, M. Sheves and D. Cahen, *Proc. Natl. Acad. Sci. U. S. A.*, 2016, **113**, 10785–10790.
681 A. R. Champagne, A. N. Pasupathy and D. C. Ralph, *Nano Lett.*, 2005, **5**, 305–308.
682 G. B. Fields and R. L. Noble, *Int. J. Pept. Protein Res.*, 1990, **35**, 161–214.
683 R. P. Cheng, S. H. Gellman and W. F. DeGrado, *Chem. Rev.*, 2001, **101**, 3219–3232.
684 C. Montalbetti and V. Falque, *Tetrahedron*, 2005, **61**, 10827–10852.
685 M. A. Gallop, R. W. Barrett, W. J. Dower, S. P. A. Fodor and E. M. Gordon, *J. Med. Chem.*, 1994, **37**, 1233–1251.
686 A. L. Gui, E. Luais, J. R. Peterson and J. J. Gooding, *ACS Appl. Mater. Interfaces*, 2013, **5**, 4827–4835.
687 X. W. Fu, Y. Wang, W. H. Zhong and G. Z. Cao, *ACS Omega*, 2017, **2**, 1679–1686.
688 J. T. Mac, V. Nuñez, J. M. Burns, Y. A. Guerrero, V. I. Vullev and B. Anvari, *Biomed. Opt. Express*, 2016, **7**, 1311–1322.
689 S. Gupta, M. R. Chatni, A. L. N. Rao, V. I. Vullev, L. V. Wang and B. Anvari, *Nanoscale*, 2013, **5**, 1772–1776.
690 B. Bahmani, S. Gupta, S. Upadhyayula, V. I. Vullev and B. Anvari, *J. Biomed. Opt.*, 2011, **16**, 051303.
691 B. Bahmani, Y. Guerrero, D. Bacon, V. Kundra, V. I. Vullev and B. Anvari, *Lasers Surg. Med.*, 2014, **46**, 582–592.
692 B. Bahmani, C. Y. Lytle, A. M. Walker, S. Gupta, V. I. Vullev and B. Anvari, *Int. J. Nanomed.*, 2013, **8**, 1609–1620.
693 S. Sankaranarayanan, R. Singh and V. R. Bhethanabotla, *J. Appl. Phys.*, 2010, **108**, 104507.
694 N. J. Ronkainen, H. B. Halsall and W. R. Heineman, *Chem. Soc. Rev.*, 2010, **39**, 1747–1763.
695 J. J. Davis, B. Peters, W. Xi and D. Axford, *Curr. Nanosci.*, 2008, **4**, 62–70.
696 H. Choi and C. C. M. Mody, *Soc. Stud. Sci.*, 2009, **39**, 11–50.
697 H. W. Bahng, A. Hagfeldt and J. E. Moser, *J. Phys. Chem. C*, 2018, **122**, 19359–19369.
698 H. W. Bahng, A. Hagfeldt and J. E. Moser, *J. Phys. Chem. C*, 2018, **122**, 19348–19358.

699 K. Slowinski, H. K. Y. Fong and M. Majda, *J. Am. Chem. Soc.*, 1999, **121**, 7257–7261.
700 K. Slowinski and M. Majda, *J. Electroanal. Chem.*, 2000, **491**, 139–147.
701 M. Galperin, A. Nitzan, S. Sek and M. Majda, *J. Electroanal. Chem.*, 2003, **550**, 337–350.
702 E. Tran, A. E. Cohen, R. W. Murray, M. A. Rampi and G. M. Whitesides, *J. Am. Chem. Soc.*, 2009, **131**, 2141–2150.
703 M. Hegner, P. Wagner and G. Semenza, *Surf. Sci.*, 1993, **291**, 39–46.
704 E. A. Weiss, R. C. Chiechi, G. K. Kaufman, J. K. Kriebel, Z. F. Li, M. Duati, M. A. Rampi and G. M. Whitesides, *J. Am. Chem. Soc.*, 2007, **129**, 4336–4349.
705 E. V. Agina, I. A. Usov, O. V. Borshchev, J. B. Wang, A. Mourran, M. A. Shcherbina, A. V. Bakirov, S. Grigorian, M. Moller, S. N. Chvalun and S. A. Ponomarenko, *Langmuir*, 2012, **28**, 16186–16195.
706 F. Gholamrezaie, S. G. J. Mathijssen, E. C. P. Smits, T. C. T. Geuns, P. A. van Hal, S. A. Ponomarenko, H. G. Flesch, R. Resel, E. Cantatore, P. W. M. Blom and D. M. de Leeuw, *Nano Lett.*, 2010, **10**, 1998–2002.
707 E. Mikayelyan, A. V. Bakirov, M. A. Shcherbina, S. N. Chvalun, S. A. Ponomarenko and S. Grigorian, *RSC Adv.*, 2015, **5**, 1319–1322.
708 A. S. Sizov, D. S. Anisimov, E. V. Agina, O. V. Borshchey, A. V. Bakirov, M. A. Shcherbina, S. Grigorian, V. V. Bruevich, S. N. Chvalun, D. Y. Paraschuk and S. A. Ponomarenko, *Langmuir*, 2014, **30**, 15327–15334.
709 M. Takenaga, S. Jo, M. Graupe and T. R. Lee, *J. Colloid Interface Sci.*, 2008, **320**, 264–267.
710 M. Liu, N. A. Amro and G. Y. Liu, *Annu. Rev. Phys. Chem.*, 2008, **59**, 367–386.
711 J. C. Love, L. A. Estroff, J. K. Kriebel, R. G. Nuzzo and G. M. Whitesides, *Chem. Rev.*, 2005, **105**, 1103–1169.
712 H. Wang, S. F. Chen, L. Y. Li and S. Y. Jiang, *Langmuir*, 2005, **21**, 2633–2636.
713 M. Cerruti, S. Fissolo, C. Carraro, C. Ricciardi, A. Majumdar and R. Maboudian, *Langmuir*, 2008, **24**, 10646–10653.
714 S. C. Chang, I. Chao and Y. T. Tao, *J. Am. Chem. Soc.*, 1994, **116**, 6792–6805.
715 E. Katz, A. Riklin and I. Willner, *J. Electroanal. Chem.*, 1993, **354**, 129–144.
716 P. E. Laibinis, M. A. Fox, J. P. Folkers and G. M. Whitesides, *Langmuir*, 1991, **7**, 3167–3173.
717 J. A. M. Sondaghuethorst, C. Schonenberger and L. G. J. Fokkink, *J. Phys. Chem.*, 1994, **98**, 6826–6834.
718 J. Lukkari, M. Meretoja, I. Kartio, K. Laajalehto, M. Rajamaki, M. Lindstrom and J. Kankare, *Langmuir*, 1999, **15**, 3529–3537.
719 G. Heimel, L. Romaner, E. Zojer and J. L. Bredas, *Acc. Chem. Res.*, 2008, **41**, 721–729.
720 A. Operamolla, A. Punzi and G. M. Farinola, *Asian J. Org. Chem.*, 2017, **6**, 120–138.
721 E. A. Weiss, R. C. Chiechi, G. K. Kaufman, J. K. Kriebel, Z. F. Li, M. Duati, M. A. Rampi and G. M. Whitesides, *J. Am. Chem. Soc.*, 2007, **129**, 4336–4349.
722 J. G. Kushmerick, D. B. Holt, S. K. Pollack, M. A. Ratner, J. C. Yang, T. L. Schull, J. Naciri, M. H. Moore and R. Shashidhar, *J. Am. Chem. Soc.*, 2002, **124**, 10654–10655.
723 J. G. Kushmerick, D. B. Holt, J. C. Yang, J. Naciri, M. H. Moore and R. Shashidhar, *Phys. Rev. Lett.*, 2002, **89**, 086802.
724 A. S. Blum, J. G. Kushmerick, D. P. Long, C. H. Patterson, J. C. Yang, J. C. Henderson, Y. Yao, J. M. Tour, R. Shashidhar and B. R. Ratna, *Nat. Mater.*, 2005, **4**, 167–172.
725 J. G. Kushmerick, D. L. Allara, T. E. Mallouk and T. S. Mayer, *MRS Bull.*, 2004, **29**, 396–402.
726 G. S. Liu, Y. W. Xu, Y. F. Kong, L. Wang, J. Wang, X. Xie, Y. H. Luo and B. R. Yang, *ACS Appl. Mater. Interfaces*, 2018, **10**, 37699–37708.
727 H. Min, P. L. Girard-Lauriault, T. Gross, A. Lippitz, P. Dietrich and W. E. S. Unger, *Anal. Bioanal. Chem.*, 2012, **403**, 613–623.
728 B. Panjwani and S. K. Sinha, *J. Mech. Behav. Biomed. Mater.*, 2012, **15**, 103–111.
729 A. Nanci, J. D. Wuest, L. Peru, P. Brunet, V. Sharma, S. Zalzal and M. D. McKee, *J. Biomed. Mater. Res.*, 1998, **40**, 324–335.
730 F. Luderer and U. Walschus, *Immobilisation of DNA on Chips I*, 2005, vol. 260, pp. 37–56.
731 J. Wan, M. S. Thomas, S. Guthrie and V. I. Vullev, *Ann. Biomed. Eng.*, 2009, **37**, 1190–1205.
732 M. R. Linford, P. Fenter, P. M. Eisenberger and C. E. D. Chidsey, *J. Am. Chem. Soc.*, 1995, **117**, 3145–3155.
733 M. Grandbois, M. Beyer, M. Rief, H. Clausen-Schaumann and H. E. Gaub, *Science*, 1999, **283**, 1727–1730.
734 M. R. Linford, P. Fenter, P. M. Eisenberger and C. E. D. Chidsey, *J. Am. Chem. Soc.*, 1995, **117**, 3145–3155.
735 T. Ito, M. Namba, P. Buhlmann and Y. Umezawa, *Langmuir*, 1997, **13**, 4323–4332.
736 J. Y. M. Yang and C. W. Frank, in *Organic Thin Films: Structure and Applications*, ed. C. W. Frank, 1998, vol. 695, pp. 67–80.
737 D. Appelhans, D. Ferse, H. J. P. Adler, W. Plieth, A. Fikus, K. Grundke, F. J. Schmitt, T. Bayer and B. Adolphi, *Colloids Surf., A*, 2000, **161**, 203–212.
738 S. C. Clear and P. F. Nealey, *Langmuir*, 2001, **17**, 720–732.
739 A. Cadranel, J. T. Margraf, V. Strauss, T. Clark and D. M. Guldi, *Acc. Chem. Res.*, 2019, **52**, 955–963.
740 G. Bottari, M. A. Herranz, L. Wibmer, M. Volland, L. Rodriguez-Perez, D. M. Guldi, A. Hirsch, N. Martin, F. D'Souza and T. Torres, *Chem. Soc. Rev.*, 2017, **46**, 4464–4500.
741 V. Strauss, A. Roth, M. Sekita and D. M. Guldi, *Chem*, 2016, **1**, 531–556.
742 J.-S. Wei, T.-B. Song, P. Zhang, X.-Q. Niu, X.-B. Chen and H.-M. Xiong, *Mater. Chem. Front.*, 2020, **4**, 729–749.
743 M. Ghazinejad, J. R. Kyle, S. Guo, D. Pleskot, D. Bao, V. I. Vullev, M. Ozkan and C. S. Ozkan, *Adv. Funct. Mater.*, 2012, **22**, 4519–4525.
744 A. Beda, C. Villevieille, P.-L. Taberna, P. Simon and C. Matei Ghimbeu, *J. Mater. Chem. A*, 2020, **8**, 5558–5571.
745 N. Kumara, A. Lim, C. M. Lim, M. I. Petra and P. Ekanayake, *Renewable Sustainable Energy Rev.*, 2017, **78**, 301–317.

746 K. Sivula and R. van de Krol, *Nat. Rev. Mater.*, 2016, **1**, 15010.
747 D. G. Nocera, *Acc. Chem. Res.*, 2012, **45**, 767–776.
748 A.-E. Becquerel, *Comptes Rendus*, 1839, **9**, 561–567.
749 M. Grätzel, *Nature*, 2001, **414**, 338–344.
750 M. G. Walter, E. L. Warren, J. R. McKone, S. W. Boettcher, Q. X. Mi, E. A. Santori and N. S. Lewis, *Chem. Rev.*, 2010, **110**, 6446–6473.
751 S. N. Yun, N. Vlachopoulos, A. Qurashi, S. Ahmad and A. Hagfeldt, *Chem. Soc. Rev.*, 2019, **48**, 3705–3722.
752 J. R. Swierk and T. E. Mallouk, *Chem. Soc. Rev.*, 2013, **42**, 2357–2387.
753 M. L. Zhang, T. D. Chen and Y. J. Wang, *RSC Adv.*, 2017, **7**, 52755–52761.
754 M. Setvin, C. Franchini, X. F. Hao, M. Schmid, A. Janotti, M. Kaltak, C. G. Van de Walle, G. Kresse and U. Diebold, *Phys. Rev. Lett.*, 2014, **113**, 086402.
755 M. Setvin, X. F. Hao, B. Daniel, J. Pavelec, Z. Novotny, G. S. Parkinson, M. Schmid, G. Kresse, C. Franchini and U. Diebold, *Angew. Chem., Int. Ed.*, 2014, **53**, 4714–4716.
756 A. Yella, H. W. Lee, H. N. Tsao, C. Y. Yi, A. K. Chandiran, M. K. Nazeeruddin, E. W. G. Diau, C. Y. Yeh, S. M. Zakeeruddin and M. Grätzel, *Science*, 2011, **334**, 629–634.
757 S. Mathew, A. Yella, P. Gao, R. Humphry-Baker, B. F. E. Curchod, N. Ashari-Astani, I. Tavernelli, U. Rothlisberger, M. K. Nazeeruddin and M. Grätzel, *Nat. Chem.*, 2014, **6**, 242–247.
758 K. J. Hwang, J. Y. Park, S. Jin, S. O. Kang and D. W. Cho, *New J. Chem.*, 2014, **38**, 6161–6167.
759 K. J. Hwang, D. W. Park, S. H. Jin, S. O. Kang and D. W. Cho, *Mater. Chem. Phys.*, 2015, **149**, 594–600.
760 H. N. Tian, *Sustainable Energy Fuels*, 2019, **3**, 888–898.
761 T. T. T. Pham, S. K. Saha, D. Provost, Y. Farre, M. Raissi, Y. Pellegrin, E. Blart, S. Vedraine, B. Ratier, D. Aldakov, F. Odobel and J. Boucle, *J. Phys. Chem. C*, 2017, **121**, 129–139.
762 H. El Moll, F. A. Black, C. J. Wood, A. Al-Yasari, A. R. Marri, I. V. Sazanovich, E. A. Gibson and J. Fielden, *Phys. Chem. Chem. Phys.*, 2017, **19**, 18831–18835.
763 M. Wild, J. Griebel, A. Hajduk, D. Friedrich, A. Stark, B. Abel and K. R. Siefermann, *Sci. Rep.*, 2016, **6**, 26263.
764 H. J. Park and L. J. Guo, *Progress in High-Efficient Solution Process Organic Photovoltaic Devices: Fundamentals, Materials, Devices and Fabrication*, 2015, vol. 130, pp. 349–373.
765 H. Lee, C. Park, D. H. Sin, J. H. Park and K. Cho, *Adv. Mater.*, 2018, **30**, 1800453.
766 A. Pivrikas, H. Neugebauer and N. S. Sariciftci, *Sol. Energy*, 2011, **85**, 1226–1237.
767 H. Lu, D. Bao, M. Penchev, M. Ghazinejad, V. I. Vullev, C. S. Ozkan and M. Ozkan, *Adv. Sci. Lett.*, 2010, **3**, 101–109.
768 O. J. Sandberg, A. Sundqvist, M. Nyman and R. Osterbacka, *Phys. Rev. Appl.*, 2016, **5**, 044005.
769 N. H. Kim, J. Jeong and H. Chae, *Appl. Sci. Convergence Technol.*, 2016, **25**, 1–6.
770 P. Petrova and R. Tomova, *Bulg. Chem. Commun.*, 2009, **41**, 211–225.
771 A. L. Rogach, N. Gaponik, J. M. Lupton, C. Bertoni, D. E. Gallardo, S. Dunn, N. L. Pira, M. Paderi, P. Repetto, S. G. Romanov, C. O'Dwyer, C. M. S. Torres and A. Eychmuller, *Angew. Chem., Int. Ed.*, 2008, **47**, 6538–6549.
772 R. Tomova, P. Petrova, A. Buroff and R. Stoycheva-Topalova, *Bulg. Chem. Commun.*, 2007, **39**, 247–259.
773 K. Skonieczny, J. Yoo, J. M. Larsen, E. M. Espinoza, M. Barbasiewicz, V. I. Vullev, C.-H. Lee and D. T. Gryko, *Chem. – Eur. J.*, 2016, **22**, 7485–7496.
774 H. Kaur, S. Sundriyal, V. Pachauri, S. Ingebrandt, K. H. Kim, A. L. Sharma and A. Deep, *Coord. Chem. Rev.*, 2019, **401**, 213077.
775 A. Salehi, X. Y. Fu, D. H. Shin and F. So, *Adv. Funct. Mater.*, 2019, **29**, 1808803.
776 H. Zhu, E. S. Shin, A. Liu, D. Ji, Y. Xu and Y. Y. Noh, *Adv. Funct. Mater.*, 2020, **30**, 1904588.
777 A. Salehi, X. Y. Fu, D. H. Shin and F. So, *Adv. Funct. Mater.*, 2019, **29**, 1808803.
778 J. J. Kim, J. Lee, S. P. Yang, H. G. Kim, H. S. Kweon, S. Yoo and K. H. Jeong, *Nano Lett.*, 2016, **16**, 2994–3000.
779 C. C. Cheng, Y. L. Chu, F. C. Chang, D. J. Lee, Y. C. Yen, J. K. Chen, C. W. Chu and Z. Xin, *Nano Energy*, 2015, **13**, 1–8.
780 C. K. Nien and H. H. Yu, *Mater. Chem. Phys.*, 2019, **227**, 191–199.
781 R. M. Young, A. P. N. Singh, A. K. Thazhathveetil, V. Y. Cho, Y. Q. Zhang, N. Renaud, F. C. Grozema, D. N. Beratan, M. A. Ratner, G. C. Schatz, Y. A. Berlin, F. D. Lewis and M. R. Wasielewski, *J. Am. Chem. Soc.*, 2015, **137**, 5113–5122.
782 C. D. Dimitrakopoulos and P. R. L. Malenfant, *Adv. Mater.*, 2002, **14**, 99–117.
783 B. C. Thompson and J. M. J. Frechet, *Angew. Chem., Int. Ed.*, 2008, **47**, 58–77.
784 V. Coropceanu, J. Cornil, D. A. da Silva, Y. Olivier, R. Silbey and J. L. Bredas, *Chem. Rev.*, 2007, **107**, 926–952.
785 H. Sirringhaus, *Adv. Mater.*, 2005, **17**, 2411–2425.
786 S. Guo, D. Bao, S. Upadhyayula, W. Wang, A. B. Guvenc, J. R. Kyle, H. Hosseinibay, K. N. Bozhilov, V. I. Vullev, C. S. Ozkan and M. Ozkan, *Adv. Funct. Mater.*, 2013, **23**, 5199–5211.
787 F. D'Souza and O. Ito, *Chem. Commun.*, 2009, 4913–4928.
788 H. Zhang, S. Jenatsch, J. De Jonghe, F. Nuesch, R. Steim, A. C. Veron and R. Hany, *Sci. Rep.*, 2015, **5**, 9439.
789 Z. W. Lin, C. M. Lawrence, D. Q. Xiao, V. V. Kireev, S. S. Skourtis, J. L. Sessler, D. N. Beratan and I. V. Rubtsov, *J. Am. Chem. Soc.*, 2009, **131**, 18060–18062.
790 D. Q. Xiao, S. S. Skourtis, I. V. Rubtsov and D. N. Beratan, *Nano Lett.*, 2009, **9**, 1818–1823.
791 Y. K. Yue, T. Grusenmeyer, Z. Ma, P. Zhang, R. H. Schmehl, D. N. Beratan and I. V. Rubtsov, *Dalton Trans.*, 2015, **44**, 8609–8616.
792 Z. Ma, Z. W. Lin, C. Lawrence, I. V. Rubtsov, P. Antoniou, S. S. Skourtis, P. Zhang and D. N. Beratan, *Chem. Sci.*, 2018, **9**, 6395–6405.